

**Photocatalytic Organic Pollutants Degradation in Metal-Organic Frameworks**

Journal:	<i>Energy &amp; Environmental Science</i>
Manuscript ID:	EE-REV-04-2014-001299.R1
Article Type:	Review Article
Date Submitted by the Author:	26-Apr-2014
Complete List of Authors:	Wang, Chong-Chen; Beijing University of Civil Engineering and Architecture, Key Laboratory of Urban Stormwater System and Water Environment (Ministry of Education) Li, Jian-Rong; Beijing University Of Technology, College of Environmental and Energy; Texas A&M University, Chemistry Lv, Xiu-Liang; Beijing University of Technology, Department of Chemistry and Chemical Engineering Zhang, Yan-Qiu; Beijing University of Civil Engineering and Architecture, Beijing Climate Change Response Research and Education Center Guo, Guangsheng; Beijing University of Technology, Department of Chemistry and Chemical Engineering

# Photocatalytic Organic Pollutants Degradation in Metal-Organic Frameworks

Chong-Chen Wang,<sup>a,b</sup> Jian-Rong Li,<sup>b,\*</sup> Xiu-Liang Lv,<sup>b</sup> Yan-Qiu Zhang,<sup>c</sup> Guangsheng Guo<sup>b,\*</sup>

<sup>a</sup> *Key Laboratory of Urban Stormwater System and Water Environment (Ministry of Education),  
Beijing University of Civil Engineering and Architecture, Beijing, 100044, China*

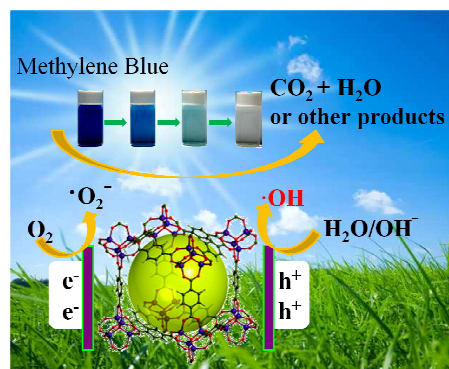
<sup>b</sup> *Department of Chemistry and Chemical Engineering, College of Environmental and Energy  
Engineering, Beijing University of Technology, Beijing 100022, China*

<sup>c</sup> *Beijing Climate Change Response Research and Education Center, Beijing University of Civil  
Engineering and Architecture, Beijing, 100044, China*

\*Corresponding author. E-mail: jrli@bjut.edu.cn

To *Energy & Environmental Science* (review)

## Graphical Abstract



This review summarizes research advances of the photocatalytic organic pollutants degradation in metal-organic frameworks.

**Abstract:** Efficient removal of organic pollutants from the wastewater has become a hot research topic due to its ecological and environmental importance. Traditional water treatment methods such as adsorption, coagulation, and membrane separation suffer from high operating costs, and even generating secondary pollutants. Photocatalysis on semiconductor catalysts (TiO<sub>2</sub>, ZnO, Fe<sub>2</sub>O<sub>3</sub>, CdS, GaP, and ZnS) has demonstrated efficiency in degrading a wide range of organic pollutants into biodegradable or less toxic organic compounds, as well as inorganic CO<sub>2</sub>, H<sub>2</sub>O, NO<sub>3</sub><sup>-</sup>, PO<sub>4</sub><sup>3-</sup>, and halide ions. However, the difficult post-separation, easy agglomeration, and low solar energy conversion efficiency of these inorganic catalysts limit their large scale applications. Exploitation of new catalysts has been attracting great attention in the related research communities. In the past two decades, a class of newly-developed inorganic-organic hybrid porous materials, namely metal-organic frameworks (MOFs) has generated a rapid development due to their versatile applications such as in catalysis and separation. Recent research has showed that these materials, acting as catalysts are quite effective in the photocatalytic degradation of organic pollutants. This review highlights the research progress of MOFs' application in this aspect. The reported examples are collected and analyzed; and the reaction mechanism, the influence of various factors on the catalytic performance, the involved challenges, and the prospect are discussed and estimated. It is clear that MOFs have a bright future in the photocatalysis for pollutants degradation.

**Keywords:** metal-organic frameworks; organic pollutants; photocatalytic degradation; wastewater treatment

## 1. Introduction

Industrial plants generate increasing amounts of wastewater, which often causes severe environmental problems. Wastewaters produced in many industrial processes often contain organic compounds that are toxic and not amenable to direct biological treatment.<sup>1,4</sup> Organic pollutants are huge in types and numbers, including organic dyes, phenols, biphenyls, pesticides, fertilizers, hydrocarbons, plasticizers, detergents, oils, greases, pharmaceuticals, proteins, carbohydrates, and so on.<sup>5</sup> Each type of pollutants has a lot of members. Taking organic dyes for example, there are more than 100,000 commercially available dyes with over  $7 \times 10^5$  t produced annually. These organic dyes are chemically stable and lowly biodegradable in water system, which are potentially harmful to eco-environment.<sup>6,7</sup> One of the greatest environmental concerns with organic dyes is of their absorption and reflection of sunlight entering into water, which further interferes with the growth of bacteria to a level sufficient to biologically degrade impurities in the water.<sup>8</sup> Organic pollutants in wastewater, with high toxicity and hard degradation, have become one of the most serious global environmental issues today. Organic pollutants once released into the aquatic ecosystem can cause various environmental problems, such as clogging sewage treatment plants, adversely affecting on the aquatic biota, and increasing biochemical oxygen.<sup>9,10</sup> Therefore, an effective and economic technique needs to be developed to reduce the concentrations of organic pollutants before releasing the wastewater into the aquatic environment. Currently, industrially available wastewater treatment technologies like adsorption and coagulation merely concentrate or separate these pollutants from water, but not completely “eliminated” or “destroyed” them into biodegradable or less toxic organic compounds, as well as inorganic  $\text{CO}_2$ ,  $\text{H}_2\text{O}$ ,  $\text{NO}_3^-$ ,  $\text{PO}_4^{3-}$  and halide ions.<sup>11</sup> Other water treatment methods such as chemical and membrane technologies usually involve high operating costs, and sometimes generate other toxic secondary pollutants.<sup>12</sup> For example, chlorination has been widely used in disinfection process, where the generated by-products are mutagenic and carcinogenic to human health.<sup>13-16</sup>

Among various physical, chemical, and biological technologies used in the pollution control, the advanced oxidation processes (AOPs), including Fenton reaction, photocatalysis, sonolysis, ozonation, and their combination, are increasingly adopted in the destroy of organic contaminants, due to their high efficiency, simplicity, good reproducibility, and easy handling.<sup>13,17</sup> In general, the AOP involves an in situ generation of highly reactive and nonselective chemical oxidants (i.e.  $\text{H}_2\text{O}_2$ ,  $\bullet\text{OH}$ ,  $\bullet\text{O}_2^-$ ,  $\text{O}_3$ ) to degrade persistent and nonbiodegradable organic substances.<sup>13</sup> The advantage of AOPs is to convert toxic organic compounds into less toxic ones. Under suitable conditions, it is possible to oxidize completely organic molecules to form  $\text{CO}_2$  and  $\text{H}_2\text{O}$ . In AOPs, the heterogeneous photocatalysis by using semiconductor catalysts such as  $\text{TiO}_2$ ,  $\text{ZnO}$ ,  $\text{Fe}_2\text{O}_3$ ,  $\text{CdS}$ ,  $\text{GaP}$ ,

and ZnS has been demonstrated to be highly efficient in degrading a wide range of organic pollutants into easily biodegradable compounds or less toxic molecules, and even eventually mineralizing them into innocuous CO<sub>2</sub> and H<sub>2</sub>O.<sup>13,18-27</sup> The heterogeneous photocatalysis possesses some advantages, which make feasible application in wastewater treatment, including (i) ambient operating temperature and pressure, (ii) complete mineralization of parents and their intermediate compounds without leaving secondary pollution, and (iii) low operating costs.<sup>13</sup> One typical drawback in the photocatalysis is that the usually used semiconductor photocatalysts is not so photo-stable under operation conditions. Usually, the illumination of these catalysts in aqueous media leads to their corrosion, thereby the migration of metal ions into water, and finally the complete dissolution of the solid catalysts. For examples, transition metal sulfides are highly unstable narrow band-gap semiconductors, and the irradiation under light often leads to the dissolution of them. Other metal oxides such as iron oxides with various stoichiometries, silver oxide, and copper oxides also prefer to photo corrosion. Among explored semiconductor photocatalysts TiO<sub>2</sub> is most-popularly used, due to its long durability, low cost, low toxicity, superhydrophilicity, as well as remarkable chemical and photochemical stability.<sup>28-32</sup> However, the application of TiO<sub>2</sub> catalyst for wastewater treatment is also facing a series of technical challenges. Firstly, the post-separation of the TiO<sub>2</sub> catalyst is difficult after the water treatment, which obstructs the practicality in industrial process. Secondly, the fine particle size of the TiO<sub>2</sub>, together with their large surface area-to-volume ratio and high surface energy leads to a strong tendency for the catalyst agglomeration. Finally, the catalyst itself also shows some disadvantageous issues, like low photocurrent quantum yield due to electron-hole recombination and low solar energy utilization efficiency resulting from narrow band gap ( $E_g = 3.2$  eV). Consequently, it is of urgent demand to look for new photocatalysts with improved performances.<sup>13</sup>

Metal-organic frameworks (MOFs), a class of newly-developed inorganic-organic hybrid porous materials, has generated a rapid development due to their diverse and easily tailored structures,<sup>33-38</sup> as well as various potential applications, such as in catalysis,<sup>39-42</sup> separation,<sup>43-48</sup> gas storage,<sup>41, 49-52</sup> carbon dioxide capture,<sup>53-56</sup> and so on.<sup>33-38,43-46,57-60</sup> MOFs are composed of metal-containing nodes connected by organic linkers through strong chemical bonds. Some MOFs behave as semiconductors when exposed into light, implying that they are potentially useful as photocatalysts.<sup>61</sup> Recent research indeed not only demonstrated porous MOFs materials to be a new class of photocatalysts usable in catalytic degradation of organic pollutants under UV/visible/UV-visible irradiation, but also triggered an intense interest in exploring MOFs application as photocatalysts in other aspects.<sup>62-72</sup> Based on the richness of metal-containing nodes and organic bridging linkers, as well as the controllability of synthesis, it is easy to construct MOFs with tailorable capacity to absorb light, and thereby

initiating desirable photocatalytic properties for specific application in organic pollutants degradation. The study of MOFs' application in this topic thus has a bright future even if not being so widely explored to date, in contrast to the conventional photocatalysts of metal oxides and sulfides. Herein, we highlight the research progress of MOFs' application in the photocatalytic degradation of organic pollutants. The reported examples are collected and analyzed, the reaction mechanism and the influence of various factors on the catalytic performances are discussed, as well as the involved challenges and the prospect are estimated.

## 2. The organic pollutants degradation in *d*-block metals based MOFs

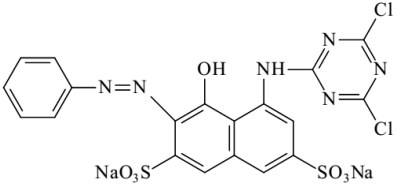
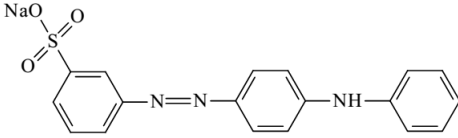
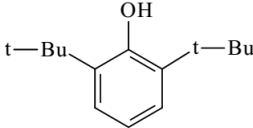
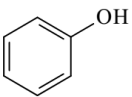
Recently, much effort has been devoted to develop new photocatalytic materials based on MOFs, which is motivated largely by a demand to solve pollution problems, in view of their potential applications in the green degradation of organic pollutants.<sup>74-78</sup> It is clear that MOFs are providing a unique opportunity for exploring new catalysts to achieve good performance towards organic pollutant degradation. Some organic pollutants treated in this review are listed in Table 1.

**Table 1** The structures and natures of some organic pollutants

Dye Name*	Chemical Structures	Ionicity	Size (nm <sup>3</sup> )	Absorption $\lambda_{\max}$ (nm)
Orange G (OG)		Anionic	1.62×0.94×0.29	484
Methyl Orange (MO)		Anionic	1.54×0.48×0.28	467
Alizarin Red S (ARS)		Anionic	1.17×0.57×0.23	428
Congo Red (CR)		Anionic	2.61×0.86×0.39	493

Cresol Red (CRR)		Anionic	1.01×1.13×0.	435
			31	
Cotton Blue (CB)		Anionic	1.98×1.17×0.	595
			34	
Coomassie Brilliant Blue R-250 (CBB)		Anionic	2.23×1.21×0.	555
			41	
Methylene Blue (MB)		Cationic	1.38×0.64×0.	672
		c	21	
Rhodamine Blue L (RBL)		Cationic	1.78×1.12×0.	610
		c	43	

Methyl Violet (MV)		Cationic	1.42×1.01×0.	585
		c	22	
Methyl Red (MR)		Cationic	1.50×0.41×0.	436
		c	23	
Bismarck Brown R (BBR)		Cationic	2.21×0.39×0.	520
		c	20	
Acid Mordant Navy Blue RRN (RRN)		Anionic	2.35×0.87×5.	597
			58	
Rhodamine B (RhB)		Cationic	1.56×1.35×0.	552
		c	42	
Remazol Brilliant Blue R (RBBR)		Anionic	1.57×1.16×0.	591
			53	

Reactive Red X3B (X3B)		Anionic	1.53×1.32×0.	511
			45	
Metanil Yellow (MY)		Anionic	1.62×0.78×0.	414
			30	
2,6-Di-tert-butylphenol (DTBP)		-	1.04×0.81×0.	
			54	
phenol		-	0.65×0.58×0.	270
			28	
thiophene		-	0.74×0.68×0.	-
			28	

In the past decade, *d*-block transition metal MOFs had attracted intense interest not only due to their significant contribution in numerous areas including magnetism,<sup>78</sup> catalysis,<sup>80,81</sup> gas separation,<sup>47</sup> drug delivery<sup>82,83</sup> and the embedding of nanoparticles,<sup>41,84</sup> but also due to their structural diversity and intriguing topologies.<sup>85-87</sup> Some MOFs constructed by transition metals, like Zn(II),<sup>62,63,88,89</sup> Cu(I)/Cu(II),<sup>89,90</sup> Cd(II),<sup>89,90</sup> Co(II)/Co(III),<sup>63,89-94</sup> and Fe(II)/Fe(III)<sup>27,88,89</sup> had been examined as photocatalysts to degrade organic pollutants under UV, visible or UV-vis light. Table 2 lists some of these MOFs which showed good photocatalytic performances on the degradation of organic pollutants.

Table 2 Performances of some MOFs constructed with *d*-block metals as photocatalysts for the degradation of organic pollutants in aqueous media

MOF <sup>a</sup>	$E_g$ (eV)	Irrigation	Organic pollutants	Initial concentration (mg L <sup>-1</sup> )	Time (min)	Degradation efficiency (%)	Ref.
MOF-5	3.40	UV	Phenol	40.0	180	50	68
MOF-5	3.40	UV	DTBP	40.0	180	100	62
(emim) <sub>2</sub> [InK(btec) <sub>1.5</sub> (H <sub>2</sub> O) <sub>2</sub> ]	3.15	UV	MB	5	180	90	96
(emim)[In <sub>3</sub> (μ <sub>3</sub> -OH) <sub>2</sub> (btec) <sub>2</sub> ]:2H <sub>2</sub> O	3.8	UV	MB	5	840	100	97
Zn <sub>3</sub> (btc) <sub>2</sub> (thin film)	-	UV-vis	MB(H <sub>2</sub> O <sub>2</sub> )	10	60	99	98
MIL-88A	2.05	vis	MB(H <sub>2</sub> O <sub>2</sub> )	32	20	100 <sup>d</sup>	99
[Zn <sub>4</sub> (O)(tdc) <sub>3</sub> (4,4'-bimb) <sub>4</sub> ]:5.25H <sub>2</sub> O·CH <sub>3</sub> OH	-	vis	X3B	3.69	540	100 <sup>d</sup>	100
NTU-9	1.74	vis	RhB(H <sub>2</sub> O <sub>2</sub> )	47.9	80	100	101
NTU-9	1.74	vis	MB(H <sub>2</sub> O <sub>2</sub> )	31.9	20	100	101
[Cu <sup>II</sup> (salimcy)](Cu <sup>I</sup> ) <sub>2</sub> ·DMF	-	vis	MB(H <sub>2</sub> O <sub>2</sub> )	12	22	96	102
[Cu <sup>II</sup> (salimcy)](Cu <sup>I</sup> ) <sub>2</sub> ·DMF	-	vis	RhB(H <sub>2</sub> O <sub>2</sub> )	12	50	95	102
[Cu <sup>II</sup> (salimcy)](Cu <sup>I</sup> ) <sub>2</sub> ·DMF	-	vis	MO(H <sub>2</sub> O <sub>2</sub> )	12	55	100	102
Cu(Br-ip)(bitmb)(H <sub>2</sub> O)	-	vis	MY(H <sub>2</sub> O <sub>2</sub> )	3.75	180	89	103
(tpp) <sub>2</sub> [Cd <sub>3</sub> (4,4'-obb) <sub>4</sub> ]	-	vis	MB	3	360	98.5	104
Cu(hfipbb)(2,2'-bpy)(H <sub>2</sub> O) <sub>2</sub>	-	Vis	RhB	9.58	360	95	105
Cu <sub>2</sub> (hfipbb) <sub>2</sub> (4,4'-bpy)(H <sub>2</sub> O)	-	vis	RhB	9.58	360	70	105
(Me <sub>4</sub> N) <sub>6</sub> [Cu <sub>12</sub> (OMe) <sub>6</sub> (pz) <sub>6</sub> (btc) <sub>6</sub> ]:18H <sub>2</sub> O	-	UV	RhB	9.58	320	61	106
(Me <sub>4</sub> N) <sub>6</sub> [Cu <sub>12</sub> (OH) <sub>6</sub> (pz) <sub>6</sub> (btc) <sub>6</sub> ]:21H <sub>2</sub> O	-	UV	RhB	9.58	320	51	106
[Cd(4,4'-bpy)(H <sub>2</sub> O) <sub>2</sub> (S <sub>2</sub> O <sub>3</sub> ) <sub>2</sub> ]:2H <sub>2</sub> O	2.91	UV	MB	25	60	86 <sup>c</sup>	107
Cd <sub>2</sub> (4,4'-bpy) <sub>3</sub> (S <sub>2</sub> O <sub>3</sub> ) <sub>2</sub>	2.75	UV	MB	25	60	84 <sup>c</sup>	107
Cd <sub>2</sub> (4,4'-bpy) <sub>2.5</sub> (S <sub>2</sub> O <sub>3</sub> ) <sub>2</sub>	2.75	UV	MB	25	60	76 <sup>c</sup>	107
[Cd(4,4'-bpy)(H <sub>2</sub> O) <sub>2</sub> (S <sub>2</sub> O <sub>3</sub> ) <sub>2</sub> ]:2H <sub>2</sub> O	2.91	UV	RBL	100	90	90 <sup>c</sup>	107
Cd <sub>2</sub> (4,4'-bpy) <sub>3</sub> (S <sub>2</sub> O <sub>3</sub> ) <sub>2</sub>	2.75	UV	RBL	100	90	85 <sup>c</sup>	107
Cd <sub>2</sub> (4,4'-bpy) <sub>2.5</sub> (S <sub>2</sub> O <sub>3</sub> ) <sub>2</sub>	2.75	UV	RBL	100	90	85 <sup>c</sup>	107
[Cd(4,4'-bpy)(H <sub>2</sub> O) <sub>2</sub> (S <sub>2</sub> O <sub>3</sub> ) <sub>2</sub> ]:2H <sub>2</sub> O	2.91	UV	MV	100	90	99 <sup>c</sup>	107
Cd <sub>2</sub> (4,4'-bpy) <sub>3</sub> (S <sub>2</sub> O <sub>3</sub> ) <sub>2</sub>	2.75	UV	MV	100	90	99 <sup>c</sup>	107

$\text{Cd}_2(4,4'\text{-bpy})_2.5(\text{S}_2\text{O}_3)_2$	2.75	UV	MV	100	90	99 <sup>c</sup>	107
$[\text{Cd}(4,4'\text{-bpy})(\text{H}_2\text{O})_2(\text{S}_2\text{O}_3)] \cdot 2\text{H}_2\text{O}$	2.91	UV	MR	100	90	95 <sup>c</sup>	107
$\text{Cd}_2(4,4'\text{-bpy})_3(\text{S}_2\text{O}_3)_2$	2.75	UV	MR	100	90	95 <sup>c</sup>	107
$\text{Cd}_2(4,4'\text{-bpy})_2.5(\text{S}_2\text{O}_3)_2$	2.75	UV	MR	100	90	95 <sup>c</sup>	107
$[\text{Cd}(3,3'\text{-bpy})(\text{H}_2\text{O})_2(\text{S}_2\text{O}_3)] \cdot 2\text{H}_2\text{O}$	2.91	UV	BBR	100	90	95 <sup>c</sup>	107
$\text{Cd}_2(4,4'\text{-bpy})_3(\text{S}_2\text{O}_3)_2$	2.75	UV	BBR	100	90	97 <sup>c</sup>	107
$\text{Cd}_2(4,4'\text{-bpy})_2.5(\text{S}_2\text{O}_3)_2$	2.75	UV	BBR	100	90	97 <sup>c</sup>	107
$[\text{Cd}(4,4'\text{-bpy})(\text{H}_2\text{O})_2(\text{S}_2\text{O}_3)] \cdot 2\text{H}_2\text{O}$	2.91	sunlight	MB	25	90	70 <sup>c</sup>	107
$\text{Cd}_2(4,4'\text{-bpy})_3(\text{S}_2\text{O}_3)_2$	2.75	sunlight	MB	25	90	68 <sup>c</sup>	107
$\text{Cd}_2(4,4'\text{-bpy})_2.5(\text{S}_2\text{O}_3)_2$	2.75	sunlight	MB	25	90	60 <sup>c</sup>	107
$[\text{Cd}(4,4'\text{-bpy})(\text{H}_2\text{O})_2(\text{S}_2\text{O}_3)] \cdot 2\text{H}_2\text{O}$	2.91	sunlight	RBL	100	90	95 <sup>c</sup>	107
$\text{Cd}_2(4,4'\text{-bpy})_3(\text{S}_2\text{O}_3)_2$	2.75	sunlight	RBL	100	90	78 <sup>c</sup>	107
$\text{Cd}_2(4,4'\text{-bpy})_2.5(\text{S}_2\text{O}_3)_2$	2.75	sunlight	RBL	100	90	75 <sup>c</sup>	107
$[\text{Cd}(4,4'\text{-bpy})(\text{H}_2\text{O})_2(\text{S}_2\text{O}_3)] \cdot 2\text{H}_2\text{O}$	2.91	sunlight	MV	100	90	70 <sup>c</sup>	107
$\text{Cd}_2(4,4'\text{-bpy})_3(\text{S}_2\text{O}_3)_2$	2.75	sunlight	MV	100	90	65 <sup>c</sup>	107
$\text{Cd}_2(4,4'\text{-bpy})_2.5(\text{S}_2\text{O}_3)_2$	2.75	sunlight	MV	100	90	63 <sup>c</sup>	107
$[\text{Cd}(4,4'\text{-bpy})(\text{H}_2\text{O})_2(\text{S}_2\text{O}_3)] \cdot 2\text{H}_2\text{O}$	2.91	sunlight	MR	100	90	75 <sup>c</sup>	107
$\text{Cd}_2(4,4'\text{-bpy})_3(\text{S}_2\text{O}_3)_2$	2.75	sunlight	MR	100	90	68 <sup>c</sup>	107
$\text{Cd}_2(4,4'\text{-bpy})_2.5(\text{S}_2\text{O}_3)_2$	2.75	sunlight	MR	100	90	66 <sup>c</sup>	107
$[\text{Cd}(4,4'\text{-bpy})(\text{H}_2\text{O})_2(\text{S}_2\text{O}_3)] \cdot 2\text{H}_2\text{O}$	2.91	sunlight	BBR	100	90	90 <sup>c</sup>	107
$\text{Cd}_2(4,4'\text{-bpy})_3(\text{S}_2\text{O}_3)_2$	2.75	sunlight	BBR	100	90	85 <sup>c</sup>	107
$\text{Cd}_2(4,4'\text{-bpy})_2.5(\text{S}_2\text{O}_3)_2$	2.75	sunlight	BBR	100	90	84 <sup>c</sup>	107
$\text{Co}_2(\text{tkcomm})(\text{llpd})_2$	1.98	UV	MB	16	90	81	108
$\text{Mn}_2(\text{tkcomm})(\text{llpd})_2$	3.09	UV	MB	16	90	88	108
$\text{Zn}_2(\text{tkcomm})(\text{llpd})_2$	3.26	UV	MB	16	90	78	108
$\text{Cd}_2(\text{tkcomm})(\text{llpd})_2$	3.31	UV	MB	16	90	87	108
$\text{Zn}(1,4\text{-bdc})(\text{dpbpdca})$ - solvents	-	UV	RhB	5.0	810	85 <sup>c</sup>	109
$\text{Cu}_4(\text{dcpcpb})_2(\mu_3\text{-OH})_2(\text{CH}_3\text{OH})_2(\text{H}_2\text{O})$	3.49	UV	MB	16	90	64	110
$\text{Co}_2(\text{dcpcpb})(\mu_3\text{-OH})(\text{H}_2\text{O})_2$	2.96	UV	MB	16	90	73	110
$\text{Cu}_4(\text{dcpcpb})_2(\mu_3\text{-OH})_2(\text{CH}_3\text{OH})_2(\text{H}_2\text{O})$	3.49	UV	RhB	4.79	90	19	110

$\text{Co}_2(\text{dcpcpb})(\mu_3\text{-OH})(\text{H}_2\text{O})_2$	2.96	UV	RhB	4.79	90	79	110
$\text{Mn}_2(\text{ptp})_{4/3}(\text{pbcpp})_2$	-	UV	MO	5.6	90	40	111
$[\text{Cu}_5(\text{H}_2\text{tmbtmp})_2(\text{btb})_2(\text{OH})_2] \cdot 3\text{H}_2\text{O}$	-	UV	MB	10	120	59	112
$\text{Cd}(\text{tdc})(\text{bix})(\text{H}_2\text{O})$	3.31	UV	MO	20	150	90	113
$\text{Gd}(\text{H}_2\text{O})_3\text{Co}(2,3\text{-pdc})$	-	UV	RBBR	100	90	88 <sup>c</sup>	114
$\text{Pb}_2(\text{ttt}(\text{ox})_{1/2})(\text{H}_2\text{O})$	3.33	UV	MO	6.6	150	13	115
$\text{Pb}_3(\text{ttt})_2(\text{H}_2\text{O})_2$	3.32	UV	MO	6.6	150	13.7	115
$\text{Cd}(\text{npdyda})(\text{H}_2\text{O})_2$	4.4	UV	MO	4.9	60	60 <sup>c</sup>	116
$\text{Pb}(\text{npdyda})(\text{DMF})$	4.3	UV	MO	4.9	60	60 <sup>c</sup>	116
$\text{Cd}(\text{npdyda})(\text{phen})$	3.8	UV	MO	4.9	60	80 <sup>c</sup>	116
$\text{Cd}_5(\text{npdyda})_5(2,2'\text{-bpy})_2$	5.0	UV	MO	4.9	60	42 <sup>c</sup>	116
$\text{Zn}(\text{NH}_2\text{bdc})(\text{bix}) \cdot (\text{DMF})_2$	-	visible	X3B	3.69	540	98 <sup>c</sup>	117
$[\text{Cu}_3(4\text{-bpah})_4(1,3,5\text{-btc})_2] \cdot 8\text{H}_2\text{O}$	-	UV	MB	10	240	50 <sup>c</sup>	118
$[\text{Cu}_3(4\text{-bpah})_3(1,2\text{-bdc})_3(\text{H}_2\text{O})_2] \cdot 4\text{H}_2\text{O}$	-	UV	MB	10	240	53 <sup>c</sup>	118
$\text{Cu}(4\text{-bpah})(1,3\text{-bdc})(\text{H}_2\text{O})$	-	UV	MB	10	240	54 <sup>c</sup>	118
$\text{Co}(4\text{-bpah})(1,3\text{-bdc})(\text{H}_2\text{O})$	-	UV	MB	10	240	25 <sup>c</sup>	118
$\text{Ni}(4\text{-bpah})(1,3\text{-bdc})(\text{H}_2\text{O})$	-	UV	MB	10	240	55 <sup>c</sup>	118
$\text{Zn}(4\text{-bpah})(1,3\text{-bdc})(\text{H}_2\text{O})$	-	UV	MB	10	240	55 <sup>c</sup>	118
$\text{Cd}(4\text{-bpah})(1,3\text{-bdc})$	-	UV	MB	10	240	40 <sup>c</sup>	118
$[\text{Cd}(3\text{-bpah})(1,3\text{-bdc})] \cdot \text{H}_2\text{O}$	-	UV	MB	10	240	65 <sup>c</sup>	118
$[\text{Cu}_2(3\text{-bpah})(1,3\text{-bdc})_2] \cdot \text{H}_2\text{O}$	-	UV	MB	10	240	68 <sup>c</sup>	118
$\text{Ag}_7(4,4'\text{-tmbpt})(\text{Hcb-iso-p})_2(\text{cb-iso-p})(\text{H}_2\text{O})$	3.36	UV	MB	17.6	90	73	119
$[\text{NaCd}_3(4,4'\text{-tmbpt})(\text{cb-iso-p})_2(\text{OH})] \cdot \text{H}_2\text{O}$	3.44	UV	MB	17.6	90	65	119
$[\text{Cd}_3(3,4'\text{-tmbpt})_2(\text{cb-iso-p})_2(\text{H}_2\text{O})] \cdot 1.5\text{H}_2\text{O}$	3.50	UV	MB	17.6	90	54	119
$[\text{Zn}_4(\text{dpcpbe})_2(\mu_3\text{-OH})_2(\text{H}_2\text{O})_{1.5}] \cdot 2\text{H}_2\text{O}$	3.49	UV	MB	3.2	90	32	120
$\text{Zn}_5\text{Na}(\text{dpcpbe})_2(\mu_3\text{-OH})_4(\text{CH}_3\text{CH}_2\text{O})(\text{H}_2\text{O})_2$	3.53	UV	MB	3.2	90	31	120
$[\text{Cd}_4(\text{dpcpbe})_2(\text{bime})_{0.5}(\mu_3\text{-OH})_2(\text{H}_2\text{O})_{1.5}] \cdot 2\text{H}_2\text{O}$	3.52	UV	MB	3.2	90	29	120
$\text{Zn}_4(\text{dpcpbe})_2(\text{bet})_{0.5}(\mu_3\text{-OH})_2(\text{H}_2\text{O})$	3.46	UV	MB	3.2	90	32	120
$\text{Cu}_6(\mu_3\text{-O})(\mu_3\text{-OH})(\text{pz})_6(\text{btc})$	-	UV	RhB	9.58	105	98	121
$\text{Cd}_2(\text{bpe})_3(\text{H}_2\text{O})_4(\text{S}_2\text{O}_3)_2$	2.53	UV	MR	100	90	50 <sup>c</sup>	122

$\text{Cd}_2(\text{bpe})_3(\text{H}_2\text{O})_4(\text{S}_2\text{O}_3)_2$	2.53	UV	RBL	100	90	55 °C	122
$\text{Cd}(\text{bpe})\text{S}_2\text{O}_3$	2.53	UV	MR	100	90	60 °C	122
$\text{Cd}(\text{bpe})\text{S}_2\text{O}_3$	2.53	UV	RBL	100	90	62 °C	122
$[\text{Co}_2(\text{tkcomm})(\text{tkiymm})] \cdot 4.25\text{H}_2\text{O}$	3.78	UV	MB	17.6	75	95	123
$[\text{Co}_2(\text{tkcomm})(\text{tkiymm})] \cdot 4.25\text{H}_2\text{O}$	3.78	vis	MB	3.51	300	49.6	123
$[\text{Co}_2(\text{tkcomm})(\text{tkiymm})] \cdot 4.25\text{H}_2\text{O}$	3.78	UV	RhB	9.58	600	66	123
$[\text{Co}_2(\text{tkcomm})(\text{tkiymm})] \cdot 4.25\text{H}_2\text{O}$	3.78	UV	X3B	3.69	600	56.7	123
$[\text{Ni}(\text{sdb})(\text{bitmb})(\text{H}_2\text{O})] \cdot \text{H}_2\text{O}$	2.12	UV	MY(H <sub>2</sub> O <sub>2</sub> )	3.75	180	43.7	124
$[\text{Cd}(\text{sdb})(\text{bitmb})(\text{H}_2\text{O})] \cdot (\text{THF})(\text{H}_2\text{O})$	3.89	UV	MY(H <sub>2</sub> O <sub>2</sub> )	3.75	180	24.7	124
$[\text{Zn}_2(\text{sdb})_2(\text{bitmb})] \cdot (\text{THF})_2$	4.08	UV	MY(H <sub>2</sub> O <sub>2</sub> )	3.75	180	51.9	124
$\text{Co}_2(\text{sdb})_2(\text{bitmb})$	2.11	UV	MY(H <sub>2</sub> O <sub>2</sub> )	3.75	180	82.3	124
$[\text{Cu}_3(3\text{-dpsea})(1,3,5\text{-btc})_2(\text{H}_2\text{O})_5] \cdot 4\text{H}_2\text{O}$	-	UV	MB	17.6	120	56	125
$[\text{Cu}(3\text{-dpyh})_{0.5}(1,4\text{-ndc})] \cdot \text{H}_2\text{O}$	-	UV	MB	17.6	120	67	125
$\text{Cu}(\text{ptz})(\text{I})^{\text{b}}$	1.65	vis	MB(H <sub>2</sub> O <sub>2</sub> )	18.7	24	98	126
$\text{Cu}(\text{ptz})(\text{I})^{\text{b}}$	1.65	vis	RhB(H <sub>2</sub> O <sub>2</sub> )	18.7	35	100	126
$\text{Cu}(\text{ptz})(\text{I})^{\text{b}}$	1.65	vis	MO(H <sub>2</sub> O <sub>2</sub> )	18.7	45	95	126
$\text{Cu}(\text{ptz})(\text{II})^{\text{b}}$	2.24	vis	MB(H <sub>2</sub> O <sub>2</sub> )	18.7	24	85 °C	126
$\text{Cu}(\text{ptz})(\text{II})^{\text{b}}$	2.24	vis	RhB(H <sub>2</sub> O <sub>2</sub> )	18.7	35	70 °C	126
$\text{Cu}(\text{ptz})(\text{II})^{\text{b}}$	2.24	vis	MO(H <sub>2</sub> O <sub>2</sub> )	18.7	45	70 °C	126
MIL-53(Fe)	2.72	UV-vis	MB	140	40	11	27
MIL-53(Fe)	2.72	vis	MB	140	40	30	27
MIL-53(Fe)	2.72	UV-vis	MB(H <sub>2</sub> O <sub>2</sub> )	140	20	99	27
MIL-53(Fe)	2.72	vis	MB(H <sub>2</sub> O <sub>2</sub> )	140	20	20	27
MIL-53(Al)	3.87	UV-vis	MB	140	60	30	27
MIL-53(Cr)	3.20	UV-vis	MB	140	60	32	27
Cu/ZIF-67	1.95	vis	MO	16.35	25	100	91
$[\text{Co}_2(4,4'\text{-bpy})](4,4'\text{-obb})_2$	3.11	UV	OG	100	100	90 °C	63
$[\text{Co}_2(4,4'\text{-bpy})](4,4'\text{-obb})_2$	3.11	UV	RhB	100	100	62 °C	63
$[\text{Co}_2(4,4'\text{-bpy})](4,4'\text{-obb})_2$	3.11	UV	RBBR	100	100	100 °C	63
$[\text{Co}_2(4,4'\text{-bpy})](4,4'\text{-obb})_2$	3.11	UV	MB	100	100	85 °C	63

$[\text{Ni}_2(4,4'\text{-bpy})(4,4'\text{-obb})_2 \cdot 2\text{H}_2\text{O}]$	3.89	UV	OG	100	100	85 °c	63
$[\text{Ni}_2(4,4'\text{-bpy})(4,4'\text{-obb})_2 \cdot 2\text{H}_2\text{O}]$	3.89	UV	RhB	100	100	47 °c	63
$[\text{Ni}_2(4,4'\text{-bpy})(4,4'\text{-obb})_2 \cdot 2\text{H}_2\text{O}]$	3.89	UV	RBBR	100	100	95 °c	63
$[\text{Ni}_2(4,4'\text{-bpy})(4,4'\text{-obb})_2 \cdot 2\text{H}_2\text{O}]$	3.89	UV	MB	100	100	80 °c	63
$[\text{Zn}_2(4,4'\text{-bpy})(4,4'\text{-obb})_2]$	4.02	UV	OG	100	100	70 °c	63
$[\text{Zn}_2(4,4'\text{-bpy})(4,4'\text{-obb})_2]$	4.02	UV	RhB	100	100	43 °c	63
$[\text{Zn}_2(4,4'\text{-bpy})(4,4'\text{-obb})_2]$	4.02	UV	RBBR	100	100	80 °c	63
$[\text{Zn}_2(4,4'\text{-bpy})(4,4'\text{-obb})_2]$	4.02	UV	MB	100	100	72 °c	63
Cu(dm-bim)	2.49	vis	MB	18.7	20	96	90
Cu(dm-bim)	2.49	vis	RhB	18.7	34	100	90
Cu(dm-bim)	2.49	vis	MO	18.7	45	95	90
$[\text{Zn}_4\text{O}(2,6\text{-ndc})_3(\text{DMF})_{1.5}(\text{H}_2\text{O})_{0.5}] \cdot 4\text{DMF} \cdot 7.5\text{H}_2\text{O}$	2.85	UV-vis	MO	20	120	65 °c	93
$[\text{Zn}_4\text{O}(2,6\text{-ndc})_3(\text{DMF})_{1.5}(\text{H}_2\text{O})_{0.5}] \cdot 4\text{DMF} \cdot 7.5\text{H}_2\text{O}$	2.85	vis	MO	20	120	45 °c	93
$[\text{Mn}_3(\text{btc})_2(4,4'\text{-bimb})_2] \cdot 4\text{H}_2\text{O}$	4.04	UV	X3B	3.69	600	65 °c	94
$[\text{Mn}_3(\text{btc})_2(\text{bimb})_2] \cdot 4\text{H}_2\text{O}$	4.04	vis	X3B	3.69	600	15 °c	94
$[\text{Co}_3(\text{btc})_2(\text{bimb})_2] \cdot 4\text{H}_2\text{O}$	3.72	UV	X3B	3.69	600	100	94
$[\text{Co}_3(\text{btc})_2(\text{bimb})_2] \cdot 4\text{H}_2\text{O}$	3.72	vis	X3B	3.69	600	70 °c	94
$[\text{Zn}_4(2\text{-mim})_6\text{WO}_4] \cdot 1.5\text{DMF}$ (HZIF-1W)	2.2	vis	$\text{MO}(\text{H}_2\text{O}_2)$	16.35	120	24.5	127
$[\text{Zn}_4(2\text{-mim})_6\text{MoO}_4] \cdot 2\text{DMF}$ (HZIF-1Mo)	1.32	vis	$\text{MO}(\text{H}_2\text{O}_2)$	16.35	120	81.6	127
$\text{Fe}_3\text{O}_4@/\text{MIL-100}(\text{Fe})$	-	UV-vis	MB	40	100	35	89
$\text{Fe}_3\text{O}_4@/\text{MIL-100}(\text{Fe})$	-	UV-vis	$\text{MB}(\text{H}_2\text{O}_2)$	40	100	99	89
$\text{Fe}_3\text{O}_4@/\text{MIL-100}(\text{Fe})$	-	vis	MB	40	20	20	89
$\text{Fe}_3\text{O}_4@/\text{MIL-100}(\text{Fe})$	-	vis	$\text{MB}(\text{H}_2\text{O}_2)$	40	200	99.77	89
MIL-53(Fe)	2.7	vis	RhB	10	50	62.1	88
MIL-53(Fe)	2.7	vis	$\text{RhB}(\text{H}_2\text{O}_2)$	10	50	100	88
$(\text{Me}_3\text{Sn})_4\text{Fe}(\text{CN})_6$	-	UV	MB	17.6	30	92	92
$[\text{Co}_2(1,4\text{-bdc})(\text{nep})_2] \cdot 4\text{H}_2\text{O}$	-	vis	OG	45.2	300	67.59	128
$[\text{Co}_2(1,4\text{-bdc})(\text{nep})_2] \cdot 4\text{H}_2\text{O}$	-	vis	RhB	47.9	300	67.52	128
$[\text{Co}_2(1,4\text{-bdc})(\text{nep})_2] \cdot 4\text{H}_2\text{O}$	-	vis	MB	35.1	300	62.75	128
$[\text{Co}_2(1,4\text{-bdc})(\text{nep})_2] \cdot 4\text{H}_2\text{O}$	-	vis	MV	40.8	300	33.29	128

$[\text{Ni}_2(4,4'\text{-bimb})_3(\text{H}_2\text{O})_6] \cdot (\text{aobtc}) \cdot (\text{DMF})_2 \cdot (\text{H}_2\text{O})_2$		vis	X3B	3.69	540	70 °C	129
$[\text{Cd}(3,3',4,4'\text{-bptcH}_2)(\text{H}_2\text{O})] \cdot (\text{bimb})$		vis	X3B	3.69	540	50 °C	129
$[\text{Cu}(3\text{-dpye})(3\text{-npa})(\text{H}_2\text{O})] \cdot 3\text{H}_2\text{O}$	-	UV	MB	10	240	70 °C	130
$\text{Cu}(3\text{-dpye})_{0.5}(5\text{-aip})(\text{H}_2\text{O})$	-	UV	MB	10	240	70 °C	130
$[\text{Cu}(3\text{-dpye})(1,3\text{-bdc})] \cdot 3\text{H}_2\text{O}$	-	UV	MB	10	240	80 °C	130
$\text{Cu}_3(3\text{-dpye})(1,2\text{-bdc})_2(\mu_2\text{-OH})_2$	-	UV	MB	10	240	64 °C	130
$\text{Cu}_3(3\text{-dpyb})(1,2\text{-bdc})_2(\mu_2\text{-OH})_2$	-	UV	MB	10	240	66 °C	130
$[\text{Cu}(3\text{-dpyh})_{0.5}(1,2\text{-bdc})] \cdot \text{H}_2\text{O}$	-	UV	MB	10	240	83 °C	130
$\text{Cu}(3\text{-dpyh})_{0.5}(5\text{-aip})(\text{H}_2\text{O})$	-	UV	MB	10	240	66 °C	130
$[\text{Co}(3\text{-dpyh})(5\text{-Hip})(\text{H}_2\text{O})_3] \cdot \text{H}_2\text{O}$	-	UV	MB	10	240	52	131
$[\text{Co}(3\text{-dpyh})(5\text{-nip})] \cdot \text{H}_2\text{O}$	-	UV	MB	10	240	39	131
$[\text{Co}(3\text{-dpyh})(5\text{-mip})] \cdot \text{H}_2\text{O}$	-	UV	MB	10	240	34	131
$[\text{Co}(3\text{-dpyh})_{0.5}(5\text{-aip})(\text{H}_2\text{O})] \cdot 2\text{H}_2\text{O}$	-	UV	MB	10	240	47	131
$\text{Co}(\text{btec})_{0.5}(4,4'\text{-bimb})$	2.68	vis	X3B	3.69	540	80 °C	95
$\text{Ni}(\text{btec})_{0.5}(\text{bimb})$	2.63	vis	X3B	3.69	540	80 °C	95
$\text{Cd}(\text{btec})_{0.5}(\text{bimb})_{0.5}$	2.32	vis	X3B	3.69	540	90 °C	95
$\text{Cd}(3\text{-NO}_2\text{-bdc})(\text{bbi})$	-	vis	X3B	3.69	540	60	132
$\text{Co}(3\text{-NO}_2\text{-bdc})(\text{bbi})$	-	vis	X3B	3.69	540	80	132
$\text{Cu}(3\text{-dpyh})(3\text{-nph})(\text{H}_2\text{O})_2$	-	UV	MB	10	120	73	133
$\text{Ni}(3\text{-dpyh})(3\text{-nph})(\text{H}_2\text{O})_2$	-	UV	MB	10	120	73	133
$\text{Co}(3\text{-dpyh})(3\text{-nph})(\text{H}_2\text{O})_2$	-	UV	MB	10	120	85	133
$[\text{Cu}_9(\text{OH})_6(\text{bte})_2(\text{sip})_4(\text{H}_2\text{O})_3] \cdot 6\text{H}_2\text{O}$	-	UV	$\text{MO}(\text{H}_2\text{O}_2)$	10	280	76.1	134
$\text{Cd}(\text{nddda})(\text{H}_2\text{O})_2$	4.4	UV	MO	2.15	60	60 °C	116
$\text{Pb}(\text{nddda})(\text{DMF})$	4.3	UV	MO	2.15	60	62 °C	116
$\text{Cd}(\text{nddda})(\text{phen})$	3.8	UV	MO	2.15	60	81 °C	116
$\text{Cd}_5(\text{nddda})_5(2,2'\text{-bpy})_2$	5.0	UV	MO	2.15	60	45 °C	116
$\text{Cu}_2(\text{btec})(\text{btx})_{1.5}$		vis	$\text{MO}(\text{H}_2\text{O}_2)$	10	95	96.1	135
$\text{Co}_2(\text{bip})_2(\text{H}_2\text{O})$	-	UV	MB	10	180	79	136
$[\text{Co}(\text{bip})(\text{phen})(\text{H}_2\text{O})] \cdot \text{H}_2\text{O}$	-	UV	MB	10	180	42	136
$[\text{Co}_2(1,4\text{-biyb})_2(2\text{-emsn})_2(\text{H}_2\text{O})] \cdot \text{H}_2\text{O}$	-	UV	MB	10	180	64	137

Cd(1,4-biyb)(2-cmsn)(H <sub>2</sub> O)	-	UV	MB	10	180	37	137
[Zn(1,4-biyb)(2-cmsn)]·2H <sub>2</sub> O	-	UV	MB	10	180	54	137
Cd(1,4-biyb)(adtz)(H <sub>2</sub> O)	-	UV	MB	10	180	72	137
[Zn(1,4-biyb)(adtz)]·H <sub>2</sub> O	-	UV	MB	10	180	62	137
[Ag <sub>2</sub> (pdbmb) <sub>2</sub> (CF <sub>3</sub> SO <sub>3</sub> ) <sub>2</sub> ]·H <sub>2</sub> O	3.03	UV-vis	MB	1000	540	90	138
Fe <sub>2</sub> (bhbdh)	-	vis	RhB(H <sub>2</sub> O <sub>2</sub> )	0.2	15	90	139
Fe <sub>2</sub> (bhbdh)	-	vis	MB(H <sub>2</sub> O <sub>2</sub> )	0.13	15	90	139
[Ag <sub>4</sub> (4,4'-bpy) <sub>4</sub> (ap) <sub>2</sub> ]·11H <sub>2</sub> O	3.2	UV	MB	5	180	98.2	140
[Ag <sub>2</sub> (4,4'-bpy) <sub>2</sub> ](npdc)]·2H <sub>2</sub> O	3.2	UV	MB	5	180	99.8	140
[Ag <sub>2</sub> (dpe) <sub>1.5</sub> (sbdc) <sub>0.5</sub> (sbdc) <sub>0.5</sub> ]·7H <sub>2</sub> O	3.3	UV	MB	5	180	99.9	140

Note:

<sup>a</sup> MOF-5 = [Zn<sub>4</sub>O(1,4-bdc)<sub>3</sub>](DMF)<sub>6</sub>(C<sub>6</sub>H<sub>5</sub>Cl), (1,4-bdc = 1,4-benzenedicarboxylate; DMF = dimethylformamide; C<sub>6</sub>H<sub>5</sub>Cl = chlorobenzene); emim = 1-ethyl-3-methylimidazolium bromide; btec = 1,2,4,5-benzenetetracarboxylate; btc = 1,3,5-benzenetricarboxylate; tdc = 2,5-thiophenedicarboxylate; 4,4'-bibm = 4,4'-bis(1-imidazolyl)biphenyl; NTU-9 = Ti<sub>2</sub>(dobdc)<sub>3</sub> (H<sub>4</sub>dobdc = 2,5-dihydroxyterephthalic acid); salimcy = N,N'-bis-[(imidazol-4-yl)methylene]cyclohexane-1,2-diamine; Br-ip = 5-bromoisophthalate; bitmb = 1,3-bis(imidazol-1-ylmethyl)-2,4,6-trimethylbenzene; H<sub>2</sub>hfpbb = 4,4'-(hexafluoroisopropylidene)bis(benzoic acid); tpp = tetrphenylphosphonium; 4,4'-obb = 4,4'-oxybis(benzoate); 2,2'-bpy = 2,2'-bipyridine; 4,4'-bpy = 4,4'-bipyridine; pz = pyrazolate; 3,3'-bpy = 2,2'-bipyridine; H<sub>4</sub>tkcomm = tetrakis[4-(carboxyphenyl)-oxamethyl]methane acid; llpd = 4-tolyl-2,2':6',2"-terpyridine; dpbpdca = N<sup>4</sup>,N<sup>4</sup>-di(pyridin-4-yl)biphenyl-4,4'-dicarboxamide; H<sub>3</sub>dcpbp = (3,5-dicarboxyl-phenyl)-(4-(2'-carboxyl-phenyl)-benzyl); ptp = 4'-(4-pyridyl)-4,2':6',4"-terpyridine; pbcpp = (4-phenyl)-2,6-bis(4-carboxyphenyl)pyridine; H<sub>3</sub>tmbtmp = 2,4,6-trimethylbenzene-1,3,5-tris(methylenephosphonic acid); btb = 1,4-bis(1,2,4-triazol-1-yl)butane; bix = 1,4-bis(imidazol-1-ylmethyl)benzene; 2,3-pdc = pyridine-2,3-dicarboxylate; H<sub>3</sub>ttt = 1,3,5-triazine-2,4,6-triyltrithio-triacetic acid; H<sub>2</sub>ox = oxalic acid; H<sub>2</sub>npdyda = naphthalene-1,5-diylldioxy-di-acetic acid; phen = phenanthroline; NH<sub>2</sub>bdcH<sub>2</sub> = 2-amino-1,4-benzene dicarboxylic acid; 4-bpah = N,N'-bis(4-pyridinecarboxamide)-1,2-cyclohexane; 1,3,5-btc = 1,3,5-benzenetricarboxylate; 1,2-bdc = 1,2-benzenedicarboxylate; 1,3-bdc = 1,3-benzenedicarboxylate; 3-bpah = N,N'-bis(3-pyridinecarboxamide)-1,2-cyclohexane; 4,4'-tmbpt = 1-((1H-1,2,4-triazol-1-yl)methyl)-3,5-bis(4-pyridyl)-1,2,4-triazole; cb-iso-p = 5-(4-carboxybenzyloxy)isophthalate; 3,4'-tmbpt = 1-((1H-1,2,4-triazol-1-yl)methyl)-3-(4-pyridyl)-5-(3-pyridyl)-1,2,4-triazole; H<sub>3</sub>dcpbe = (3,5-dicarboxyl-phenyl)-(4-(2'-carboxyl-phenyl)-benzyl)ether; bime = 1,2-bis(imidazol-1-yl)ethane; bet = 1,1'-(2'-oxybis(ethane-2,1-diyl))bis(1,2,4-triazol-1-yl); bpe = 1,2-di(4-pyridyl)ethylene; tkymm = tetrakis(imidazol-1-ylmethyl)methane; sdb = 4,4'-sulfonyldibenzoate; 3-dpsea = N,N'-di(3-pyridyl)sebacidamide; 3-dpyh = N,N'-di(3-pyridinecarboxamide)-1,6-hexane; 1,4-ndc = 1,4-naphthalenedicarboxylate; ptz = 5-(3-pyridyl)tetrazole; Cu/ZIF-67 = copper doped Co-2-methylimidazole framework; dm-bim = 5,6-dimethylbenzimidazole; 2,6-ndc = 2,6-naphthalenedicarboxylate; 4,4'-bimb = 4,4'-bis(1-imidazolyl)biphenyl; 2-mim = 2-imidazole; Hncp = 2-(4-carboxyphenyl)imidazo(4,5-f)(1,10)phenanthroline; H<sub>4</sub>aobtc = azoxybenzene-3,3',5,5'-tetracarboxylic acid; 3,3',4,4'-bptcH<sub>4</sub> = 3,3',4,4'-biphenyltetracarboxylic acid; 3-dpye = N,N'-bis(3-pyridinecarboxamide)-1,2-ethane; 3-dpyb = N,N'-bis(3-pyridinecarboxamide)-1,4-butane; 3-dpyh = N,N'-bis(3-pyridinecarboxamide)-1,6-hexane; 3-H<sub>2</sub>npa = 3-nitrophthalic acid; 3-NO<sub>2</sub>-bdcH<sub>2</sub> = 3-nitro-1,2-benzenedicarboxylic acid; bbi = 1,1'-(1,4-butanediyl)bis(imidazole); 5-H<sub>2</sub>aip = 5-aminoisophthalic acid; 5-H<sub>2</sub>nip = 5-nitroisophthalic acid; 5-H<sub>2</sub>mip = 5-methylisophthalic acid; 5-H<sub>2</sub>AIP = 5-aminoisophthalic acid); bte = 1,2-bis(1,2,4-triazol-1-yl)ethane; sip = 5-sulfoisophthalate; btx = 1,4-bis(1,2,4-triazol-1-ylmethyl)benzene; bip = 5-(benzyloxy)isophthalate; 3-dpyh = N, N'-bis(3-pyridinecarboxamide)-1, 6-hexane; 3-nph = 3-nitrophthalate; 1,4-biyb = 1,4-bis(imidazol-1-ylmethyl)benzene; 2-cmsnH<sub>2</sub> = 2-carboxymethylsulfanyl nicotinic acid; H<sub>2</sub>adtz = 2,5-(s-acetic acid)

dimercapto-1,3,4-thiadiazole; pdmb = 6',6''-(2-phenylpyrimidine-4,6-diyl)bis(6-methyl-2,2'-bipyridine); bhbdh = bis[2-hydroxybenzaldehyde]hydrazone; dpe = 1,2-di(4-pyridyl)ethylene; H<sub>2</sub>ap = 5-aminophthalic acid; H<sub>2</sub>npdc = 2,6-Naphthalenedicarboxylic acid; H<sub>2</sub>sbdc = 4,4'-stilbenedicarboxylic acid.

<sup>b</sup> Cu(ptz) (I) and Cu(ptz) (II) are isomers.

<sup>c</sup>Values estimated from original figures of the references.

---

MOF-5<sup>141</sup> was firstly proposed to behave as a photocatalyst.<sup>68</sup> This MOF is composed of Zn<sub>4</sub>O clusters located at the corners of the cubic framework structure being connected orthogonally by 1,4-bdc ligands. It was found that this MOF has a broad absorption band located in the range from 500 to 840 nm, which can be assigned to delocalized electrons living on the microsecond time scale, and most probably, occupying conduction bands (CB). The actual conduction band energy value was estimated to be 0.2 V versus NHE with a band gap of 3.4 eV, as illustrated in Fig. 1a. It exhibited comparable activity in the degradation of phenol in aqueous solutions, as that of the commercial TiO<sub>2</sub> (Degussa P-25) (Fig. 1b). The charge-separation state with electrons in the conduction band and holes in the valence band (VB) made MOF-5 behave as an efficient photocatalyst. The possible mechanistic proposal as illustrated in Fig. 1c suggested that, just as in the case of TiO<sub>2</sub>, the photodegradation of phenol might occur through a network of reactions including initial formation of radical cation by electron transfer from phenol to MOF-5 hole or the generation of oxygen active species by the reaction of the photoejected electrons with oxygen. The more efficient photocatalytic activity of MOF-5 with respect to the other photocatalysts would probably perform, depending on the light source. In particular, visible irradiation using filtered light (cut-off filter  $\lambda > 380$  nm) would disfavor the activity of TiO<sub>2</sub> and ZnO due to their lack of absorption at wavelength  $> 350$  nm, but the absorption spectrum of MOF-5 extends to 400 nm, which make MOF-5 could achieve more excellent photocatalysis efficiency.

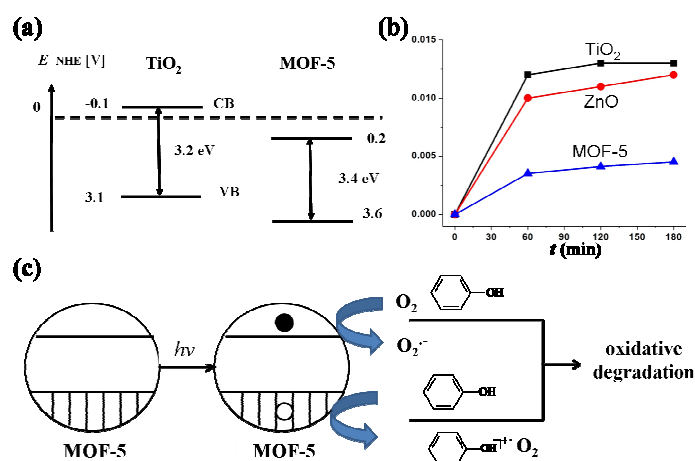


**Fig. 1** (a) Calculated values of the band gap and position of the conduction and valence bands for MOF-5 in comparison with those of TiO<sub>2</sub>. (b) Time conversion plots of phenol disappearance (the y axis represented "mol of phenol degraded/g mol"). (c) A mechanistic proposal for the photodegradation of phenol using MOF-5 as photocatalyst. Reprinted (adapted) with permission from ref. 68. Copyright (2007) Wiley-VCH.

Furthermore, MOF-5 displayed reverse shape-selectivity towards different organic compounds, in which

large phenolic molecules that cannot diffuse freely into the microspores of MOF-5, were degraded significantly faster than those small ones that can access to the interior of MOF-5, as found by Garcia and co-workers<sup>62, 68</sup>. They studied the competitive photodegradation of 2,6-di-tert-butylphenol (DTBP) and phenol (P), in which DTBP was considerably bigger than P molecule. When both compounds were irradiated under UV light in the presence of MOF-5 independently, DTBP was degraded at an initial rate comparable to that of P. The initial rate constants for the two systems (calculated as the slope of the time conversion plots at short irradiation times) gave a  $k(\text{DTBP})_{\text{pure}}/k(\text{P})_{\text{pure}}$  ratio of 1.1. But, when a mixed solution containing both P and DTBP was irradiated in the presence of MOF-5, DTBP was degraded with a rate constant ratio (i.e.,  $k(\text{DTBP})_{\text{mix}}/k(\text{P})_{\text{mix}}$  value) of 4.42 fold higher with respect to P, implying a selective photodegradation of about 82% toward bigger DTBP with respect to P. Furthermore, about 50% phenol and 100% DTBP were decomposed after 180 min of irradiation in the presence of MOF-5, as illustrated in Fig. 2. Clearly, MOF-5 displayed a reverse size-selective photocatalysis. These findings could be explained as that: the smaller molecule P was able to diffuse freely into the interior of MOF-5, resulting in a lower degradation rate, while large molecule DTBP remained on the external surface of the MOF-5, leading to a higher degradation rate. Similar situation could be found in the previous literatures on the titanasilicate ETS-10.<sup>142,143</sup>

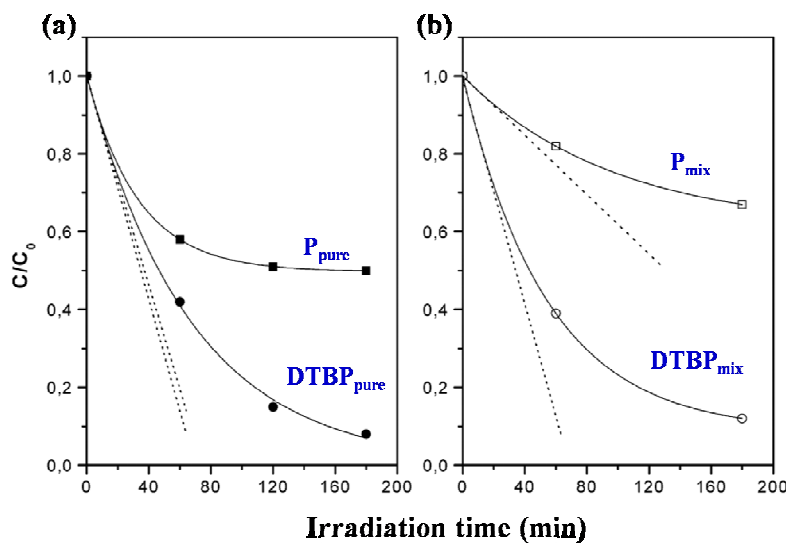


**Fig. 2** Photodegradation curves of phenol (P) and 2,6-di-tert-butylphenol (DTBP) obtained using MOF-5 as a photocatalyst. (a) Curves correspond to photodegradation of 40 mg L<sup>-1</sup> of the pure species; (b) curves correspond to competitive photodegradation (irradiation of a mixture of 20 mg L<sup>-1</sup> of both molecules). Solid lines are the best fit to the experimental data obtained with a first-order exponential decay. Dotted straight lines show the initial degradation rates. Reprinted (adapted) with permission from ref. 62. Copyright (2007) American Chemical Society.

Motivated by the discovery of MOF-5 as an efficient photocatalyst to degrade organic pollutants, Chen and co-workers explored a doubly interpenetrated porous MOF  $[\text{Zn}_4\text{O}(\text{2,6-ndc})_3(\text{DMF})_{1.5}(\text{H}_2\text{O})_{0.5}] \cdot 4\text{DMF} \cdot 7.5\text{H}_2\text{O}$  (UTSA-38), with a band gap of 2.85 eV, which exhibited photocatalytic activity for the degradation of methyl orange (MO) in aqueous solution.<sup>93</sup> It was found that under the irradiation of visible light, the concentration of MO in water gradually decreased as a function of increasing time, suggesting detectable degradation of MO in the presence of the MOF catalyst. When UV light was utilized to initiate such a photocatalytic reaction, the decomposition of MO was significantly faster. MO could be completely decomposed into colorless small molecules in 120 min, indicating clearly that UV light was more efficient for this photocatalytic reaction than visible light, as illustrated in Fig. 3b. Furthermore, the UTSA-38 catalyst could be readily recovered from the reaction mixtures via simple filtration, and showed no obvious decay of catalytic efficiency even after recycling 7 times. The main pathways proposed for MO photodegradation by UTSA-38 under UV or visible light irradiation are shown in Fig. 3a. It was considered that the initial process of photocatalysis was the generation of electron-hole pairs in the UTSA-38. After absorption of energy equal to or greater than the band gap of the UTSA-38 ( $h\nu \geq 2.85$  eV), the electrons ( $e^-$ ) were excited from the valence band (VB) and entered into the conduction band (CB), leaving the holes ( $h^+$ ) in the VB. The electrons and holes migrated to the surface of the UTSA-38, then the photoinduced energy transferred to the adsorbed species: electrons reduced the oxygen ( $\text{O}_2$ ) to oxygen radicals ( $\cdot\text{O}_2^-$ ), and finally they transformed into hydroxyl radicals ( $\cdot\text{OH}$ ); in turn, holes oxidized the hydroxyl ( $\text{H}_2\text{O}$ ) to hydroxyl radicals ( $\cdot\text{OH}$ ). Hydroxyl radicals ( $\cdot\text{OH}$ ) was capable of decomposing MO effectively.<sup>144,145</sup>

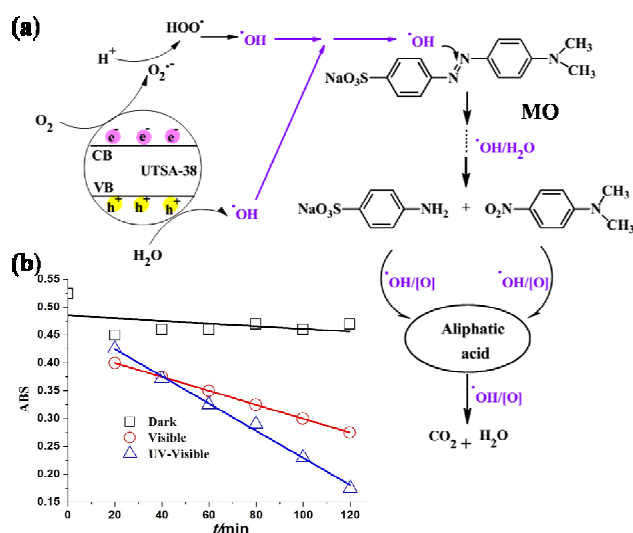


Fig. 3 (a) Main pathways proposed for methyl orange photodegraded by UTSA-38 under UV-visible or visible light irradiation. (b) Curves of

absorbance of the methyl orange solution degraded by UTSA-38 as a function of irradiation time under UV-visible light, visible light and dark.

Reprinted (adapted) with permission from ref. 93. Copyright (2011) The Royal Society of Chemistry.

In order to clarify the relationship between degradation efficiency of different organic dyes and band gap values, Natarajan and co-workers used series of MOFs,  $[\text{Co}_2(4,4'\text{-bpy})](4,4'\text{-obb})_2$ ,  $[\text{Ni}_2(4,4'\text{-bpy})_2](4,4'\text{-obb})_2 \cdot \text{H}_2\text{O}$ , and  $[\text{Zn}_2(4,4'\text{-bpy})](4,4'\text{-obb})_2$  with band gap values of 3.11, 3.89 and 4.02 eV, respectively, to degrade different organic dyes, like orange G (OG), rhodamine B (RhB), remazol brilliant blue R (RBBR), and methylene blue (MB).<sup>63</sup> The Langmuir-Hinshelwood (L-H) kinetic has been successfully used for heterogeneous photocatalytic degradation to determine the relationship between the initial degradation rate and the initial concentration of the organic substrate,<sup>146-148</sup> which could be written as  $r_0 = k_0 C_0 / (1 + K_0 C_0)$ , where  $r_0$  was the initial rate,  $C_0$  was the initial concentration of the dyes,  $k_0$  was the kinetic rate constant, and parameter  $K_0$  represented the equivalent adsorption coefficient. The values of  $k_0$  and  $K_0$  for the photocatalytic degradation of the four dyes in  $[\text{Co}_2(4,4'\text{-bpy})](4,4'\text{-obb})_2$ ,  $[\text{Ni}_2(4,4'\text{-bpy})_2](4,4'\text{-obb})_2 \cdot \text{H}_2\text{O}$ , and  $[\text{Zn}_2(4,4'\text{-bpy})](4,4'\text{-obb})_2$  were listed in Table 3. It was found that all these reactions gave very small  $K_0$  values. As the parameter  $K_0$  represents the adsorption equilibrium coefficient, the low value of  $K_0$  can be attributed to low adsorption. The photocatalytic performances of  $[\text{Co}_2(4,4'\text{-bpy})](4,4'\text{-obb})_2$ ,  $[\text{Ni}_2(4,4'\text{-bpy})_2](4,4'\text{-obb})_2 \cdot \text{H}_2\text{O}$ , and  $[\text{Zn}_2(4,4'\text{-bpy})](4,4'\text{-obb})_2$  were also confirmed to be better than commercial  $\text{TiO}_2$  (Degussa P-25) under the same situations. The band gap values of these MOFs followed a sequence of  $[\text{Co}_2(4,4'\text{-bpy})](4,4'\text{-obb})_2 < [\text{Ni}_2(4,4'\text{-bpy})_2](4,4'\text{-obb})_2 \cdot \text{H}_2\text{O} < [\text{Zn}_2(4,4'\text{-bpy})](4,4'\text{-obb})_2$ , but the kinetic rates and degradation efficiencies of these three MOFs catalysts followed a reverse order with respect to their band gap values.

**Table 3** Kinetic parameters for the degradation of different dyes using  $[\text{Co}_2(4,4'\text{-bpy})](4,4'\text{-obb})_2$ ,

$[\text{Ni}_2(4,4'\text{-bpy})_2](4,4'\text{-obb})_2 \cdot \text{H}_2\text{O}$ , and  $[\text{Zn}_2(4,4'\text{-bpy})](4,4'\text{-obb})_2$ <sup>63</sup>

MOFs	Dyes	$k_0$ (min <sup>-1</sup> )	$K_0$ (mg L <sup>-1</sup> )
$[\text{Co}_2(4,4'\text{-bpy})](4,4'\text{-obb})_2$	OG	0.031	0.0022
$[\text{Co}_2(4,4'\text{-bpy})](4,4'\text{-obb})_2$	RhB	0.013	0.0035
$[\text{Co}_2(4,4'\text{-bpy})](4,4'\text{-obb})_2$	RBBR	0.033	0.0007
$[\text{Co}_2(4,4'\text{-bpy})](4,4'\text{-obb})_2$	MB	0.032	0.0064
$[\text{Ni}_2(4,4'\text{-bpy})_2](4,4'\text{-obb})_2 \cdot \text{H}_2\text{O}$	OG	0.029	0.0049
$[\text{Ni}_2(4,4'\text{-bpy})_2](4,4'\text{-obb})_2 \cdot \text{H}_2\text{O}$	RhB	0.008	0.0023
$[\text{Ni}_2(4,4'\text{-bpy})_2](4,4'\text{-obb})_2 \cdot \text{H}_2\text{O}$	RBBR	0.029	0.0015
$[\text{Ni}_2(4,4'\text{-bpy})_2](4,4'\text{-obb})_2 \cdot \text{H}_2\text{O}$	MB	0.027	0.0027
$[\text{Zn}_2(4,4'\text{-bpy})](4,4'\text{-obb})_2$	OG	0.020	0.0029

$[\text{Zn}_2(4,4'\text{-bpy})](4,4'\text{-obb})_2$	RhB	0.007	0.0020
$[\text{Zn}_2(4,4'\text{-bpy})](4,4'\text{-obb})_2$	RBBR	0.028	0.0069
$[\text{Zn}_2(4,4'\text{-bpy})](4,4'\text{-obb})_2$	MB	0.023	0.0029

In order to further understand the photocatalytic degradation of the organic dyes in  $[\text{Co}_2(4,4'\text{-bpy})](4,4'\text{-obb})_2$ ,  $[\text{Ni}_2(4,4'\text{-bpy})_2](4,4'\text{-obb})_2 \cdot \text{H}_2\text{O}$ , and  $[\text{Zn}_2(4,4'\text{-bpy})](4,4'\text{-obb})_2$ ,<sup>63</sup> a simple mechanism based upon highest occupied molecular orbital (HOMO) and lowest unoccupied molecular orbital (LUMO) was proposed. The HOMO and LUMO of the charge transfer state, in the absence of the UV light, have two electrons in the HOMO, and no electron in the LUMO. Once in the presence of UV light, one electron transfers from the HOMO to LUMO.<sup>149</sup> Generally, the electron of the excited state in the LUMO is easy to be lost, while the HOMO strongly demands one electron to return to its stable state. Generally, the excited  $\text{M}^{2+}$  center decays to its ground state quickly. However, if some molecules are located within a reasonable range and have an appropriate orientation, transitional active complexes could be formed. For example, for RhB in this case one  $\alpha$ -hydrogen atom of the methylene group bonded to the electron-withdrawing nitrogen atom in RhB would give its electron to metal species (MOFs herein), and simultaneously form  $\text{H}^+$ . This finally results in the cleavage of the C-N bond and stepwise N-deethylation of the RhB. Since the HOMO is then reoccupied, the excited electron must remain in the LUMO until it is captured by electronegative substances such as molecular oxygen in solution, which would transform into highly active peroxide anion and subsequently accomplish further oxidation and total degradation of RhB. A similar mechanism had been proposed recently in the degradation of organic dyes in the presence of metal carboxylates.<sup>77,94,95,125</sup>

The selective adsorption and photocatalytic degradation of different dyes with different MOFs have been explored by Natarajan and co-workers in  $\text{Cd}_2(4,4'\text{-bpy})_3(\text{S}_2\text{O}_3)_2$ ,  $\text{Cd}_2(4,4'\text{-bpy})_{2.5}(\text{S}_2\text{O}_3)_2$  and  $[\text{Cd}(4,4'\text{-bpy})(\text{H}_2\text{O})_2(\text{S}_2\text{O}_3)] \cdot 2\text{H}_2\text{O}$  (Table 1).<sup>107</sup> The mechanism of photocatalytic degradation towards anionic and cationic dyes was quite different herein. It was proposed that the hydroxyl radicals played an important role in breaking anthraquinonic anionic dyes like ARS,<sup>150</sup> and azoic anionic dyes such as OG and MO.<sup>151</sup> While, cationic dyes like RBL were involved surface-controlled N-de-ethylation reactions, resulting in forming intermediates that generally compete with the degradation of the original dye in solution<sup>152</sup>. They found that the sulfonated anionic dyes were significantly adsorbed by  $\text{Cd}_2(4,4'\text{-bpy})_3(\text{S}_2\text{O}_3)_2$ ,  $\text{Cd}_2(4,4'\text{-bpy})_{2.5}(\text{S}_2\text{O}_3)_2$ , and  $[\text{Cd}(4,4'\text{-bpy})(\text{H}_2\text{O})_2(\text{S}_2\text{O}_3)] \cdot 2\text{H}_2\text{O}$  in dark, but no apparent adsorption for non-sulfonated cationic dyes. Five non-sulfonated cationic dyes, MB, RBL, MV, MR, and BBR were thus selected to carry out the photocatalytic degradation in presence of the three MOFs, respectively, under UV light. The results revealed that these dyes were

degraded, and the efficiencies are comparable to the Degussa P-25. In these MOFs, the ligand bpy was proposed to donate the electron to Cd center, which helped to decompose the organic dye molecules. The mechanism involved in the photocatalytic degradation of these organic dyes in presence of the three MOFs could be explained by considering the HOMO, filled  $d$ -orbital ( $d^{10}$  in  $\text{Cd}^{2+}$ ), and the lowest LUMO, free  $s$ -orbital. In the presence of UV light, an electron would transfer from the HOMO to the LUMO. The electron in the LUMO could readily lose from the excited state. Simultaneously, the HOMO would accept this electron to return to its stable state, and the excited  $\text{Cd}^{2+}$  center decay to the ground state quickly.<sup>77</sup> When organic molecules presented in a reasonable concentration range with an appropriate orientation, then a transitional activated complex could be formed. The electron-withdrawing group attached to the carbon center of the dye would receive the electron. The hydrogen atom in organic dyes would give one electron and leaves as an  $\text{H}^+$  species. The electron would then be captured by the metal species, resulting in the cleavage of the C–N bond in a stepwise manner, to finish the total degradation of the organic dyes.<sup>77</sup>

The facts that the degradation efficiency of photocatalysts follows a reverse order with respect to their band gap values have also been proved. Two isostructural MOFs,  $[\text{Mn}_3(\text{btc})_2(\text{bimb})_2] \cdot 4\text{H}_2\text{O}$  and  $[\text{Co}_3(\text{btc})_2(\text{bimb})_2] \cdot 4\text{H}_2\text{O}$  were used to degrade an anionic organic dye X3B, by Wen and co-workers.<sup>94</sup> Compared with the control experiments (without photocatalyst), the distinctly shortened degradation time was observed, indicating that both MOFs catalysts are active in the decomposition of X3B in the presence of both UV and visible light irradiations. It was found that the pseudo-first-order kinetics could fit well with the experimental data in both MOFs cases. For  $[\text{Mn}_3(\text{btc})_2(\text{bimb})_2] \cdot 4\text{H}_2\text{O}$  the rate constant under UV light irradiation was found to be  $1.1 \times 10^{-1} \text{ h}^{-1}$ , and that under visible light irradiation was  $7.3 \times 10^{-2} \text{ h}^{-1}$ . While, for  $[\text{Co}_3(\text{btc})_2(\text{bimb})_2] \cdot 4\text{H}_2\text{O}$ , the rate constant under UV light and visible light irradiation was  $2.6 \times 10^{-1}$  and  $1.3 \times 10^{-1} \text{ h}^{-1}$ , respectively. Although the two MOFs have the same topological structures, different central metal ions give distinct bandgap sizes (4.04 and 3.72 eV, respectively), which leads to the discrepancy in their photocatalytic activity. As shown in Fig. 4c, the UV absorption bands of 307 nm for  $[\text{Mn}_3(\text{btc})_2(\text{bimb})_2] \cdot 4\text{H}_2\text{O}$  and 333 nm for  $[\text{Co}_3(\text{btc})_2(\text{bimb})_2] \cdot 4\text{H}_2\text{O}$  can be assigned to the ligand-to-metal charge transfer (LMCT). For the latter MOF, two additional peaks are observed at 547 and 721 nm, which probably originated from the d-d spin-allowed transition of the  $d^7 \text{Co}^{2+}$  ion. While the absorption of the former MOF in the visible region is not as distinct as that of the latter, due to the d-d spin-forbidden transition of the  $d^5 \text{Mn}^{2+}$  ion. Clearly, the band gap energy of  $[\text{Mn}_3(\text{btc})_2(\text{bimb})_2] \cdot 4\text{H}_2\text{O}$  is lower than that of  $[\text{Co}_3(\text{btc})_2(\text{bimb})_2] \cdot 4\text{H}_2\text{O}$ , leading to the degradation rate of X3B follow a reverse order as illustrated in Fig. 4a and 4b. Therefore, the photocatalytic efficiency of  $[\text{Co}_3(\text{btc})_2(\text{bimb})_2] \cdot 4\text{H}_2\text{O}$  under either UV or visible

light was higher than that of  $[\text{Mn}_3(\text{btc})_2(\text{bimb})_2]\cdot 4\text{H}_2\text{O}$ . The former was able to degrade X3B almost completely in 10 h under UV irradiation. In a sense, the difference in the catalytic activity between  $[\text{Mn}_3(\text{btc})_2(\text{bimb})_2]\cdot 4\text{H}_2\text{O}$  and  $[\text{Co}_3(\text{btc})_2(\text{bimb})_2]\cdot 4\text{H}_2\text{O}$  can be attributed to their different UV/vis absorption properties, and further to different central metal atoms of the two MOFs.

In order to study the photocatalytic reaction mechanism in detail, they studied the photodegradation of X3B in the presence of *t*-butyl alcohol (TBA), a widely used  $\bullet\text{OH}$  scavenger.<sup>94</sup> It was found that the presence of TBA greatly depressed the degradation rate of X3B in  $[\text{Mn}_3(\text{btc})_2(\text{bimb})_2]\cdot 4\text{H}_2\text{O}$  and  $[\text{Co}_3(\text{btc})_2(\text{bimb})_2]\cdot 4\text{H}_2\text{O}$ : the relevant rate constants decreased from  $1.1 \times 10^{-1}$  to  $8.0 \times 10^{-3} \text{ h}^{-1}$  and from  $2.6 \times 10^{-1}$  to  $1.4 \times 10^{-2} \text{ h}^{-1}$  under UV light. The  $\bullet\text{OH}$  quenching experiments suggested that the photodegradation of X3B in the two MOFs catalysts was predominately through the attack of  $\bullet\text{OH}$  radicals, rather than a direct hole oxidation. Based on these results, a simplified model of photocatalytic reaction mechanism was proposed as depicted in Fig. 4d, in which the HOMO is mainly contributed by oxygen and (or) nitrogen 2p bonding orbitals (valence band) and the LUMO by empty Mn(Co) orbitals (conduction band). The charge transfer actually took place from oxygen and (or) nitrogen to Mn(Co) on the photoexcitation. In this case, the HOMO strongly demands one electron to return to its stable state. Therefore, one electron was captured from water molecule, which was oxygenated into the  $\bullet\text{OH}$  active species. Meanwhile, the electrons ( $e^-$ ) in LUMO combined with the oxygen adsorbed on the surfaces of MOF to form  $\bullet\text{O}_2^-$ , further transformed to  $\bullet\text{OH}$ . Finally, these formed  $\bullet\text{OH}$  radicals cleaved X3B effectively to finish the photocatalytic process.<sup>94</sup>

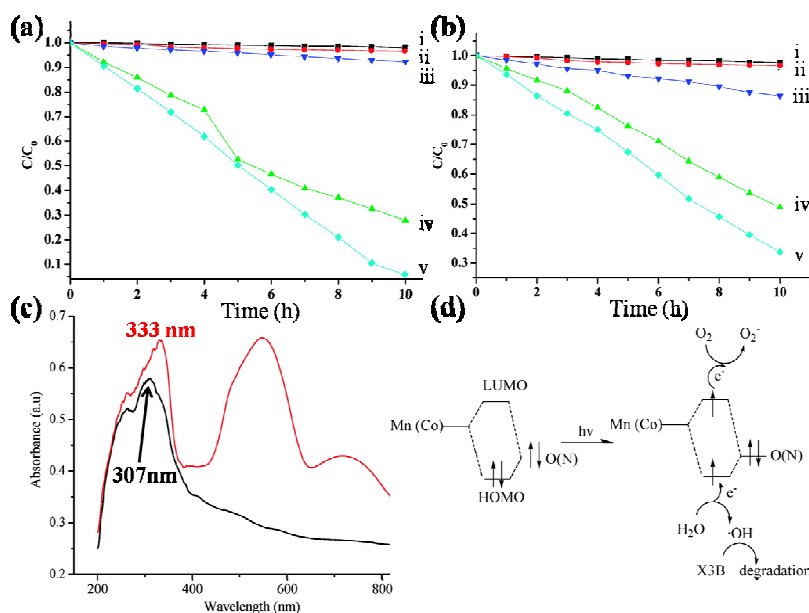


**Fig. 4** (a) Experiments on the photodegradation of X3B: (i) X3B/ $[\text{Mn}_3(\text{btc})_2(\text{bimb})_2]\cdot 4\text{H}_2\text{O}$ /dark; (ii) X3B/UV light (without catalyst); (iii)

X3B/[Mn<sub>3</sub>(btc)<sub>2</sub>(bimb)<sub>2</sub>]-4H<sub>2</sub>O/visible light; (iv) X3B/[Mn<sub>3</sub>(btc)<sub>2</sub>(bimb)<sub>2</sub>]-4H<sub>2</sub>O/*t*-butyl alcohol/UV light; and (v) X3B/[Mn<sub>3</sub>(btc)<sub>2</sub>(bimb)<sub>2</sub>]-4H<sub>2</sub>O/UV light. **(b)** Experiments on the photodegradation of X3B: (i) X3B/[Co<sub>3</sub>(btc)<sub>2</sub>(bimb)<sub>2</sub>]-4H<sub>2</sub>O/dark; (ii) X3B/UV light (without catalyst); (iii) X3B/[Co<sub>3</sub>(btc)<sub>2</sub>(bimb)<sub>2</sub>]-4H<sub>2</sub>O/*tert*-butyl alcohol/UV light; (iv) X3B/[Co<sub>3</sub>(btc)<sub>2</sub>(bimb)<sub>2</sub>]-4H<sub>2</sub>O/visible light; and (v) X3B/[Co<sub>3</sub>(btc)<sub>2</sub>(bimb)<sub>2</sub>]-4H<sub>2</sub>O/UV light. **(c)** UV/vis diffuse-reflectance spectra of [Mn<sub>3</sub>(btc)<sub>2</sub>(bimb)<sub>2</sub>]-4H<sub>2</sub>O (black line) and [Co<sub>3</sub>(btc)<sub>2</sub>(bimb)<sub>2</sub>]-4H<sub>2</sub>O (red line) with BaSO<sub>4</sub> as background. **(d)** A Simplified model of photocatalytic reaction mechanism of X3B on [Mn<sub>3</sub>(btc)<sub>2</sub>(bimb)<sub>2</sub>]-4H<sub>2</sub>O and [Co<sub>3</sub>(btc)<sub>2</sub>(bimb)<sub>2</sub>]-4H<sub>2</sub>O.

Reprinted with permission from ref. 94. Copyright (2009) American Chemical Society.

Wen and co-workers also studied another series of MOFs, Co(btec)<sub>0.5</sub>(bimb), Ni(btec)<sub>0.5</sub>(bimb), and Cd(btec)<sub>0.5</sub>(bimb)<sub>0.5</sub>, which showed good photocatalytic properties to degrade X3B.<sup>95</sup> It was found that compared with [Mn<sub>3</sub>(btc)<sub>2</sub>(bimb)<sub>2</sub>]-4H<sub>2</sub>O and [Co<sub>3</sub>(btc)<sub>2</sub>(bimb)<sub>2</sub>]-4H<sub>2</sub>O,<sup>94</sup> the degradation rates under visible irradiation of these three MOFs on X3B were higher. This might be attributed to the more delocalized  $\pi$  electrons in the ligand 1,2,4,5-benzenetetracarboxylate, which could facilitate the LMCT transitions and decrease electronic band gap of the MOFs, thereby enhanced photocatalytic rate. Thus, it can be concluded that the semiconductor properties of MOFs strongly depend on the resonance effects of their organic linkers.<sup>153</sup>

To investigate active species involved in the photocatalytic process on Cd(btec)<sub>0.5</sub>(bimb)<sub>0.5</sub>, the formation of hydroxyl radicals ( $\bullet$ OH) on the surface of this visible-illuminated MOF was detected by the photoluminescence (PL) technique, using terephthalic acid as a probe molecule.<sup>154,155</sup> With the irradiation time increase, the PL spectra of a  $5 \times 10^{-4}$  M terephthalic acid solution in  $2 \times 10^{-3}$  M NaOH changed in the presence of Cd(btec)<sub>0.5</sub>(bimb)<sub>0.5</sub>. That is, a gradual increase in the PL intensity of photogenerated 2-hydroxyterephthalic acid (from terephthalic acid) at about 425 nm was observed with increasing irradiation time, as illustrated in Fig. 5a. However, no PL intensity increase was observed in the absence of Cd(btec)<sub>0.5</sub>(bimb)<sub>0.5</sub>, implying that the fluorescence was caused by the photocatalytic reaction of terephthalic acid with  $\bullet$ OH formed at the MOF/water interface. It could also deduce that the amount of  $\bullet$ OH radicals formed at the catalyst surface are proportional to the light irradiation time, obeying the zero-order reaction rate kinetics.<sup>156</sup> The formation rate of  $\bullet$ OH radicals could be expressed by the slope of these PL intensity-*vs*-time lines as shown in Fig. 5b. It was found that the formation rate of  $\bullet$ OH radicals on Cd(btec)<sub>0.5</sub>(bimb)<sub>0.5</sub> was much higher than that on Co(btec)<sub>0.5</sub>(bimb) and Ni(btec)<sub>0.5</sub>(bimb), indicating that the formation rate of  $\bullet$ OH radicals was related to the photocatalytic activity of these MOFs. The associated photocatalytic degradation mechanism were thus similar to other reported MOFs.<sup>129,157</sup>

Generally, it is believed that the recombination of photogenerated hole-electron pairs limits the rate of photocatalytic degradation.<sup>158</sup> It had been found that H<sub>2</sub>O<sub>2</sub> could increase the rate of hydroxyl radical formation

via three ways: (i) it acted as an alternative electron acceptor to oxygen (Eq. 1), which inhibited the recombination of the photogenerated electrons and holes; (ii) the reduction of  $\text{H}_2\text{O}_2$  at the conduction band produced hydroxyl radical, or it accepted an electron from superoxide to give rise to hydroxyl radical (Eq. 2); (iii) the self-decomposition by illumination produced hydroxyl radical (Eq. 3).



The synergistic effect of  $\text{H}_2\text{O}_2$  and MOF on the photodegradation of X3B was also investigated by Wen and co-workers<sup>121</sup>. The degradation of X3B in the presence of  $\text{H}_2\text{O}_2$  (10 mL) and  $\text{Cd}(\text{btec})_{0.5}(\text{bimb})_{0.5}$  (50 mg) under different conditions was shown in Fig. 5c. It was found that the degradation of X3B was slow in the dark, with only 23.4% being degraded after 5 h. But, the visible-light irradiation greatly accelerated the photodegradation of X3B to get a 94.1% degradation after 5 h. It is much more interesting that the photocatalytic degradation rate constant of X3B on  $\text{Cd}(\text{btec})_{0.5}(\text{bimb})_{0.5}$  was  $0.56 \text{ h}^{-1}$  in the presence of  $\text{H}_2\text{O}_2$ , being 1.8 times higher than that without  $\text{H}_2\text{O}_2$  ( $0.31 \text{ h}^{-1}$ ) under other similar conditions.

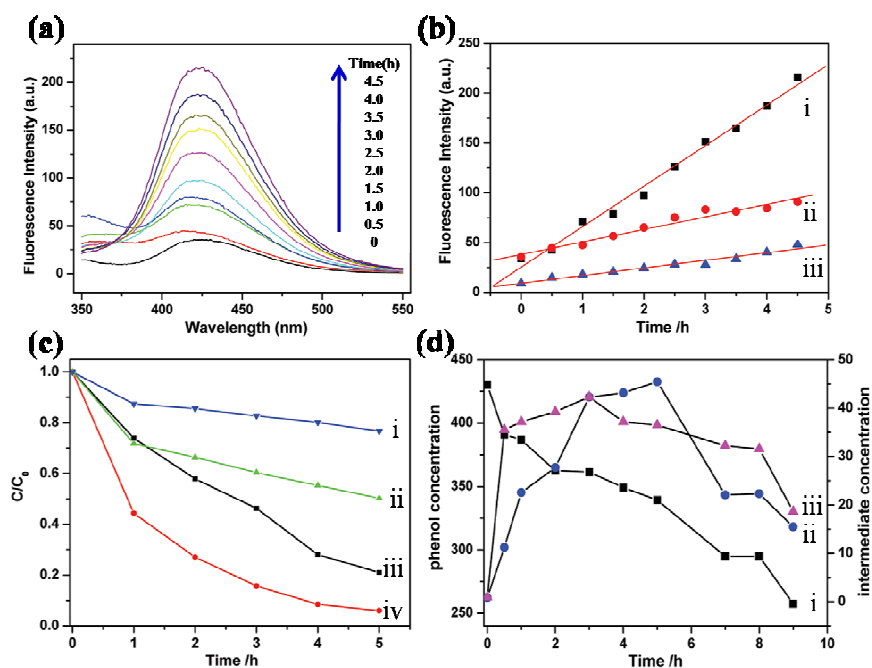
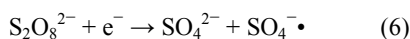
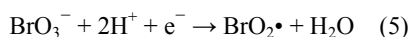
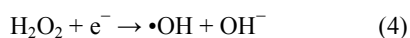


**Fig. 5** (a) PL spectral changes observed during illumination of  $\text{Cd}(\text{btec})_{0.5}(\text{bimb})_{0.5}$  in a  $5 \times 10^{-4} \text{ M}$  basic solution of terephthalic acid (excitation at 315 nm). Each fluorescence spectrum was recorded every 30 min of visible illumination. (b) Comparison of the induced PL intensity at 425 nm for  $\text{Cd}(\text{btec})_{0.5}(\text{bimb})_{0.5}$  (i),  $\text{Co}(\text{btec})_{0.5}(\text{bimb})$  (ii) and  $\text{Ni}(\text{btec})_{0.5}(\text{bimb})$  (iii). (c) Concentration changes of X3B as a function of irradiation time for  $\text{Cd}(\text{btec})_{0.5}(\text{bimb})_{0.5}$  under different conditions: (i)  $\text{H}_2\text{O}_2/\text{Cd}(\text{btec})_{0.5}(\text{bimb})_{0.5}/\text{dark}$ , (ii)  $\text{Cd}(\text{btec})_{0.5}(\text{bimb})_{0.5}/\text{visible light}$ , (iii)  $\text{H}_2\text{O}_2/\text{visible light}$ , and (iv)

$\text{H}_2\text{O}_2/\text{Cd}(\text{btec})_{0.5}(\text{bimb})_{0.5}/\text{visible light}$ . (d) The concentration change of (i) phenol and its (ii) ortho- and (iii) para-intermediates in the presence of  $\text{Cd}(\text{btec})_{0.5}(\text{bimb})_{0.5}$  under simulated solar light. Reprinted (adapted) with permission from ref. 95. Copyright (2011) American Chemical Society.

Considering such a fact that the dyes can also be degraded through photosensitized pathway, Wen and co-workers<sup>95</sup> selected colorless molecule, phenol, acting as model to test the photocatalytic activity of  $\text{Cd}(\text{btec})_{0.5}(\text{bimb})_{0.5}$ . As shown in Fig. 5d, it was found that the concentration of phenol decreased, while its ortho- and para-intermediates increased with increased light irradiation time (the conversion of the phenol was 40.13% and the selectivity for the intermediate catechol was 45.32% after 9 h irradiation). Control experiments (without catalyst or in the dark) showed that no obvious phenol degradation happened. These results demonstrated that  $\text{Cd}(\text{btec})_{0.5}(\text{bimb})_{0.5}$  is quite an efficient visible-responsible photocatalyst.<sup>95</sup>

In addition, Yuan and co-workers used MIL-53(Fe), constructed by  $-\text{Fe}-\text{O}-\text{O}-\text{Fe}-\text{O}-\text{Fe}-$  chains linked by terephthalate linkers (as illustrated in Fig. 6a) as photocatalyst to decompose methylene blue (MB) dye.<sup>27</sup> Just like  $\text{TiO}_2$  semiconductor whose conduction band is constructed by empty Ti 3d orbitals, MIL-53(Fe) containing Fe(III) ions is also expected to be effective as a photocatalyst, based on such a fact that the empty d orbitals in Fe(III) mix with the LUMOs of the organic linkers to form the conduction band.<sup>64</sup> It was proposed that upon light irradiation, electron excitation could take place in the MOF, followed by electron transfer, as illustrated in Fig. 6a. The results showed that MIL-53(Fe) exhibited efficient photocatalytic property for MB degradation under both UV-vis and visible light irradiation, even if the photodegradation rate was not so high (Fig. 6b). This relatively low degradation rate might be attributed to the recombination of photogenerated holes and electrons, which always leads to the reduced holes for the degradation of organic dyes.<sup>159,160</sup> It was also found that the introduction of different inorganic oxidants (as electron acceptors), such as  $\text{H}_2\text{O}_2$ ,  $\text{KBrO}_3$ , and  $(\text{NH}_4)_2\text{S}_2\text{O}_8$  could greatly promote the photocatalytic property of MIL-53(Fe), since these inorganic oxidants could suppress the electron-hole pair recombination according to Eqs. (4)-(6). As shown in Fig. 6b, all these inorganic oxidants had accelerated the rate of MB decolorization both under UV-vis light and visible light irradiation. The enhanced impacts follows the order of  $\text{H}_2\text{O}_2 > (\text{NH}_4)_2\text{S}_2\text{O}_8 > \text{KBrO}_3$  under UV-vis light irradiation, while in the order of  $(\text{NH}_4)_2\text{S}_2\text{O}_8 > \text{H}_2\text{O}_2 > \text{KBrO}_3$  under visible light irradiation (Fig. 6c and 6d).



For the purpose of the practical applications, it is essential to evaluate the long-term stability of a

photocatalyst. MIL-53(Fe) was checked five times as a photocatalyst to degrade MB. The results revealed no apparent loss of the catalytic activity for MB decolorization in MIL-53(Fe) during the five cycles (Fig. 7a). The structure and chemical states of MIL-53(Fe) before and after the MB degradation reaction were identified by PXRD and XPS analysis, which revealed its excellent long-term stability in this case.

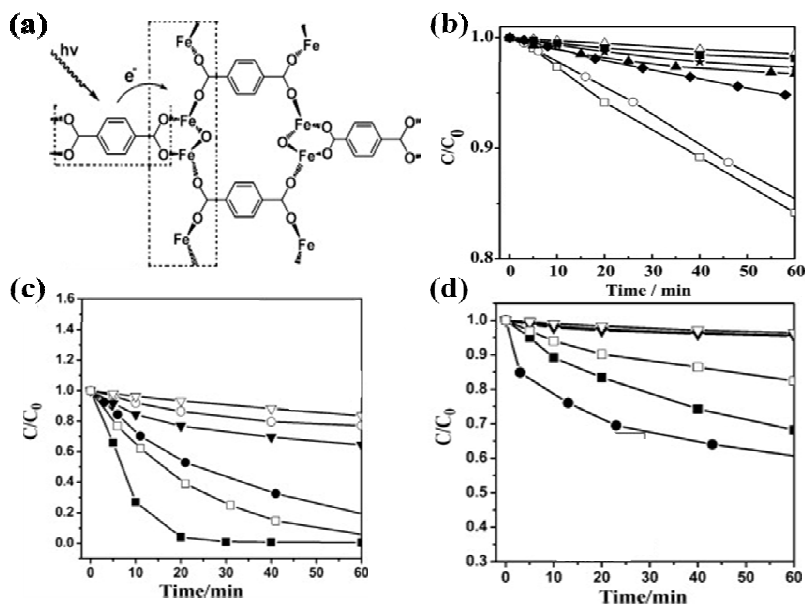


**Fig. 6** (a) The chemical structure of MIL-53(Fe) and the electron transfer processes that occur in MIL-53(Fe) when irradiated by light. (b) MB degradation profile under the irradiation of (■) without light, (△) visible light, (◆) UV-vis light, (▲) visible light with the presence of MIL-53(Fe) photocatalysts, and (□) UV-vis light with the presence of MIL-53(Fe) photocatalyst. (○) UV-vis light with the presence of TiO<sub>2</sub> photocatalysts, (★) visible light with the presence of TiO<sub>2</sub> photocatalyst. (c) and (d) The effect of difference electron acceptor additive on the MB photodegradation under the irradiation of (3) UV-vis light and (4) visible light, (■) with the presence of H<sub>2</sub>O<sub>2</sub> and MIL-53(Fe), (□) with the presence of H<sub>2</sub>O<sub>2</sub> and the absence of MIL-53(Fe), (●) with the presence of (NH<sub>4</sub>)<sub>2</sub>S<sub>2</sub>O<sub>8</sub> and MIL-53(Fe), (○) with the presence of (NH<sub>4</sub>)<sub>2</sub>S<sub>2</sub>O<sub>8</sub> and absence of MIL-53(Fe), (▼) with the presence of KBrO<sub>3</sub> and MIL-53(Fe), (▽) with the presence of KBrO<sub>3</sub> but the absence of MIL-53(Fe). Reprinted (adapted) with permission from ref. 27. Copyright (2011) Elsevier.

Both MIL-53(Al) and MIL-53(Cr) being isostructural to MIL-53(Fe) also displayed photocatalytic activities for the MB decolorization, as illustrated in Fig. 7b. Study on this series of isostructural photocatalysts would provide valuable information in the effect of metal nodes of MOFs on their photocatalytic activities. It was found that after 60 min of UV-vis light irradiation, the MB removals over MIL-53(Al) and MIL-53(Cr) were 30% and 32%, respectively, close to that over MIL-53(Fe). In photocatalysis, it is generally believed that photocatalytic activity increases with the increase of the number of absorbed photons. As altering the metal ions in MIL-53 series,

the amount of the adsorbed photons presumably become more because of the decreased band gaps of 3.87, 3.20, and 2.72 eV for MIL-53(Al), MIL-53(Cr), and MIL-53(Fe), respectively. Then, the MIL-53(Fe) with the narrowest band gap among three MIL-53 photocatalysts was expected to exhibit the highest rate for MB degradation. However, it was found that these MOFs displayed similar rates for MB degradation. The reason is not clear yet. Similar situation has occurred in MIL-88A as photocatalyst to decompose MB.<sup>99</sup>

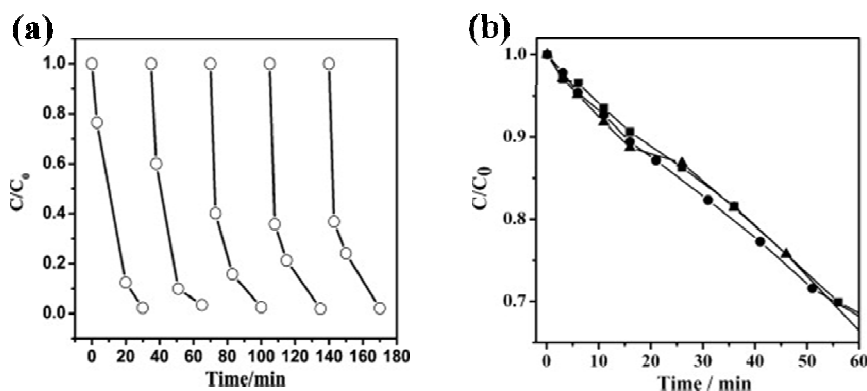


**Fig. 7** (a) Changes of the MB concentration during the five repeated processes over MIL-53(Fe) in the presence of  $\text{H}_2\text{O}_2$  ( $10^{-5} \text{ mol L}^{-1}$ ). (b) MB degradation over MIL-53(Al) (▲), MIL-53(Fe) (●) and MIL-53(Cr) (■) photocatalysts under UV-vis light irradiation. Reprinted (adapted) with permission from ref. 27. Copyright (2011) Elsevier.

In order to understand the mechanism of the synergistic effect in MIL-53(Fe)/visible light/ $\text{H}_2\text{O}_2$  system, Jiang and co-workers evaluated the band position of the MIL-53(Fe), which is intimately close to the redox ability of the photoinduced charge carriers.<sup>88</sup> A typical Mott-Schottky plot of MIL-53(Fe) in the dark was measured at a frequency of 100 Hz, to give a flatband potential of  $-0.60\text{V}$  vs SCE (equivalent to  $-0.36 \text{ V}$  vs NHE). The conduction band (CB) of MIL-53(Fe) was thus estimated to be  $-0.46\text{V}$  vs NHE, which was more negative than the redox potential of  $\text{O}_2/\cdot\text{O}_2^-$  ( $-0.33\text{V}$  vs NHE) (Fig. 8a). This lower potential conduces to the photogenerated electron transfer from catalyst to adsorbed molecular oxygen. The valence band (VB) of MIL-53(Fe) was calculated to be  $2.42 \text{ V}$  vs NHE. As shown in Fig. 8a, MIL-53(Fe) was apparently not effective to oxidize  $\text{OH}^-$  to  $\cdot\text{OH}$  radicals under visible light irradiation, because its VB value was very close to redox potential of  $\cdot\text{OH}/\text{OH}^-$  ( $2.38\text{V}$  vs NHE). The redox potential of RhB is about  $1.43 \text{ V}$  vs NHE,<sup>161</sup> lower than VB level of MIL-53(Fe), implying that the direct hole oxidation process is energetically favorable. The formation of  $\cdot\text{OH}$  radicals in the catalytic system of MIL-53(Fe)/visible light/ $\text{H}_2\text{O}_2$  was indeed detected by photoluminescence (PL) method. For comparison, the MIL-53(Fe)/visible light and MIL-53(Fe)/ $\text{H}_2\text{O}_2$  systems were also investigated under the same

conditions (Fig. 8b). The stronger PL intensity in the MIL-53 (Fe)/visible light/H<sub>2</sub>O<sub>2</sub> suggested that more •OH radicals were generated, which could attribute to the existence of synergistic effects from the combination of MIL-53(Fe) and H<sub>2</sub>O<sub>2</sub>.

To further insight into the synergistic effect in the MIL-53(Fe)/visible light/H<sub>2</sub>O<sub>2</sub> system, the transient photocurrent response of MIL-53(Fe) with H<sub>2</sub>O<sub>2</sub> in solution under visible light irradiation were measured. It was found that both systems were active in generating photocurrent with a reproducible response towards on-off cycles, as shown in Fig. 8c. The photocurrent response of MIL-53(Fe) was greatly reduced with the introduction of H<sub>2</sub>O<sub>2</sub>, which indicated that H<sub>2</sub>O<sub>2</sub> could react with photogenerated electrons to produce •OH radicals. These results are closely consistent with the results from •OH-trapping PL spectra. The proposed mechanism for the activation of H<sub>2</sub>O<sub>2</sub> by MIL-53(Fe) under visible light irradiation was illustrated in Fig. 8d.

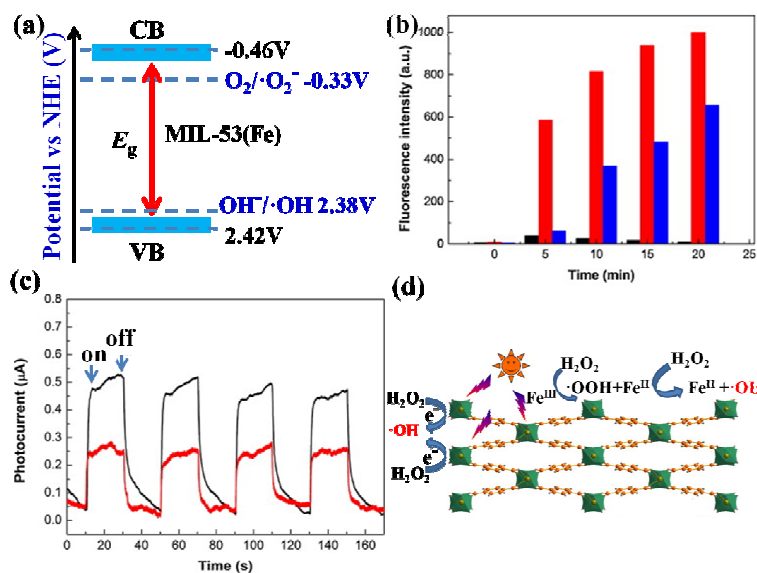


**Fig. 8** (a) Estimated energy level diagram of the MIL-53(Fe). (b) Comparison of the PL intensities recorded every 5min in catalytic systems of MIL-53/visible light (black column) and MIL-53(Fe)/H<sub>2</sub>O<sub>2</sub> (red column) with MIL-53(Fe)/visible light/H<sub>2</sub>O<sub>2</sub> (blue column) catalytic system. (c) Transient photocurrent responses of MIL-53(Fe) (black line) and MIL-53(Fe) with 70mM H<sub>2</sub>O<sub>2</sub> (red line) in 0.5M Na<sub>2</sub>SO<sub>4</sub> aqueous solutions under visible light irradiation. (d) Proposed mechanism for the activation of H<sub>2</sub>O<sub>2</sub> by MIL-53(Fe) under visible light irradiation.

Reprinted (adapted) with permission from ref. 88. Copyright (2014) Elsevier.

In the photocatalytic degradation, a lot of factors affect the degradation efficiency, including pH, the initial concentration of dye, scavenging agents, anions, catalyst dosage, reaction temperature, and so on.<sup>162,163</sup> In order to optimize the design of a process, it was important to identify which factors have the greatest influence. For this purpose, Jiang and co-workers explored the influences of pH, H<sub>2</sub>O<sub>2</sub> dosage, and initial dye concentration on the

degradation of RhB over MIL-53(Fe)/visible light/H<sub>2</sub>O<sub>2</sub> system (Fig. 9a).<sup>88</sup> The results revealed that the MIL-53(Fe) catalyst could work effectively over a wide pH range from 3.0 to 9.0. However, the degradation rate of RhB decreased with the increase of pH from 5.0 to 9.0 (as shown in Fig. 9b), which could be attributed to the fact that H<sub>2</sub>O<sub>2</sub> is not stable in alkaline medium (decompose to form O<sub>2</sub> and H<sub>2</sub>O<sup>164</sup>). As shown in Fig. 9c, the degradation efficiency of RhB was found to strongly depend on the initial dye concentration from 5 to 10 mg L<sup>-1</sup>. As an explanation, the amount of RhB molecules per volume unit in solution increased by increasing the initial dye concentration, which could enhance effectively contact between oxidizing species and dye molecules, resulting in higher degradation efficiency. However, the efficiency was significantly decreased when the concentration of RhB increased from 10 to 25 mg L<sup>-1</sup>. This is because that the more RhB dye in solution the worse permeable of the solution to incident light, which resulted in the low efficiencies of light utilization and low rates of photochemical processes.<sup>165</sup> When H<sub>2</sub>O<sub>2</sub> concentration increased from 5 to 20 mM, the degradation efficiency increased correspondingly from 77 to 98%, because of an increase in •OH radicals with increasing the concentration of H<sub>2</sub>O<sub>2</sub>.<sup>166,167</sup> However, increasing H<sub>2</sub>O<sub>2</sub> concentration from 20 to 40 mM, the degradation efficiency was not further enhanced (as illustrated in Fig. 9d), which could be explained that surplus H<sub>2</sub>O<sub>2</sub> molecules acted as scavenger of •OH radicals to generate perhydroxy radicals with lower potential (see Eqs (7) and (8)).<sup>168</sup>

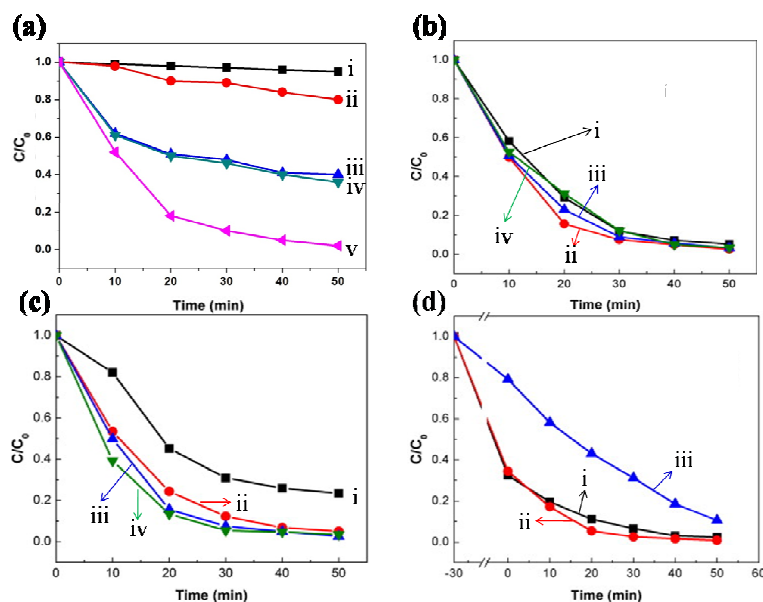
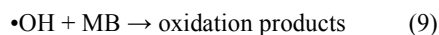


Fig. 9 (a) Degradation of RhB under different conditions: (i) visible light, (ii) visible light with H<sub>2</sub>O<sub>2</sub>, (iii) In presence of MIL-53(Fe) and H<sub>2</sub>O<sub>2</sub> in

dark, (iv) visible light in presence of MIL-53(Fe), and (v) visible light in presence of MIL-53(Fe) and H<sub>2</sub>O<sub>2</sub>. **(b)** Effect of initial pH on the degradation of RhB: (i) pH = 3, (ii) pH = 5, (iii) pH = 7, and (iv) pH = 9. Experimental conditions: RhB, 10 mg L<sup>-1</sup>; H<sub>2</sub>O<sub>2</sub>, 20 mM and MIL-53(Fe), 0.4 g L<sup>-1</sup>. **(c)** Effect of initial dye concentration on the degradation of RhB over MIL-53(Fe)/visible light/H<sub>2</sub>O<sub>2</sub> system: (i) 5 mM, (ii) 10 mM, (iii) 20 mM, and (iv) 40 mM. Experimental conditions: H<sub>2</sub>O<sub>2</sub>, 20 mM; MIL-53(Fe), 0.4 g L<sup>-1</sup>; and initial pH = 5. **(d)** Effect of H<sub>2</sub>O<sub>2</sub> concentration on the degradation of RhB over MIL-53(Fe)/visible light/H<sub>2</sub>O<sub>2</sub> system: (i) 5 mg L<sup>-1</sup>, (ii) 10 mg L<sup>-1</sup>, and (iii) 25 mg L<sup>-1</sup>. Experimental conditions: RhB, 10 mg L<sup>-1</sup>; MIL-53(Fe), 0.4 g L<sup>-1</sup>; and initial pH = 5. Reprinted (adapted) with permission from ref. 88. Copyright (2014) Elsevier.

Etainw and co-worker also studied the effect of dye initial concentration, catalyst amount, pH, and scavenging agent amount on the MB degradation over (Me<sub>3</sub>Sn)<sub>4</sub>Fe(CN)<sub>6</sub> photocatalyst.<sup>92</sup> The initial MB concentrations were set in the range of  $1.0 \times 10^{-6} \sim 1.0 \times 10^{-5}$  M in presence of 0.1 M H<sub>2</sub>O<sub>2</sub> and 0.025 mmol of (Me<sub>3</sub>Sn)<sub>4</sub>Fe(CN)<sub>6</sub> as photocatalyst at pH 5.5. Initially, a large degree of removal was observed, which was due to fast decomposition of H<sub>2</sub>O<sub>2</sub>, producing more •OH radicals. The lifetime of •OH radicals is few nanoseconds, so they only reacted where they are found.<sup>169</sup> As listed in Table 4, increasing the MB concentration led to decrease in the degradation rate. However, even at a higher concentration ( $1.0 \times 10^{-5}$  M), complete decolorization was observed after a longer time of 110 min. This could be explained as that at a higher concentration, the generation of •OH radicals on the surface of catalyst reduced since the active sites were covered by dye molecules. Therefore, as the initial concentration of the dye increased, the catalyst surface needed for the degradation should also be increased. By increasing the amount of catalysts from 0.025 to 0.058 mmol, the rate of degradation thus increased. In this work, the pH effect on the reaction rate was also studied at the constant concentration of the dye and H<sub>2</sub>O<sub>2</sub> as well as a fixed amount of the catalyst at 25 °C. As illustrated in Table 4, in acid media, the deprotonation of H<sub>2</sub>O<sub>2</sub> increased with the increase of pH, which led to an increase in the decomposition rate of H<sub>2</sub>O<sub>2</sub>, therefore leading to facile formation of •OH radicals. But in alkaline medium, the oxidizing species (hydroperoxy anion, HO<sub>2</sub><sup>-</sup>) also formed (as listed in Eqs (9) and (10)), which reacted with the non-dissociated molecules of H<sub>2</sub>O<sub>2</sub>, forming oxygen and water. Furthermore, the deactivation of •OH was more obvious at a higher pH of the solution. The reaction of •OH and HO<sub>2</sub><sup>-</sup> was approximately 100 times faster than its reactions with H<sub>2</sub>O<sub>2</sub>. The effect of the initial H<sub>2</sub>O<sub>2</sub> concentration (10~60 mmol) was investigated in the dye concentration of  $5.0 \times 10^{-6}$  M at pH 6.0. The results showed that the initial H<sub>2</sub>O<sub>2</sub> concentration strongly affected the degradation rate of MB. At low H<sub>2</sub>O<sub>2</sub> concentrations, the formation of the •OH radicals was the kinetic determining step. It was found that an increase in the H<sub>2</sub>O<sub>2</sub> concentration up to 30 mmol led to a dramatic rise in decomposition of the dyes. However, a further increase in the H<sub>2</sub>O<sub>2</sub> concentration partly inhibited the oxidation rate,<sup>88,168</sup> implying the existence of an optimal

dosage in H<sub>2</sub>O<sub>2</sub>. Higher concentration of H<sub>2</sub>O<sub>2</sub> led to produce more •OH radicals, which preferentially reacted with excess H<sub>2</sub>O<sub>2</sub>, which competed with the destruction of the dye chromophores, being undesirable.<sup>170</sup>



**Table 4** Parameters for catalytic degradation rates of MB in presence of (Me<sub>3</sub>Sn)<sub>4</sub>Fe(CN)<sub>6</sub><sup>92</sup>

[MB] (M)	<i>k</i> (min <sup>-1</sup> ) ×10 <sup>2</sup>	<i>R</i> *	[H <sub>2</sub> O <sub>2</sub> ] (M)	<i>k</i> (min <sup>-1</sup> ) ×10 <sup>2</sup>	<i>R</i> *	(Me <sub>3</sub> Sn) <sub>4</sub> Fe(CN) <sub>6</sub> (mM)	<i>k</i> (min <sup>-1</sup> ) ×10 <sup>2</sup>	<i>R</i> *	pH	<i>k</i> (min <sup>-1</sup> ) ×10 <sup>2</sup>	<i>R</i> *
1×10 <sup>-6</sup>	35	0.983	10	15.7	0.988	0.025	28	0.997	4	24.8	0.995
5×10 <sup>-6</sup>	28	0.997	20	19.8	0.990	0.040	36.2	0.996	5	26.3	0.995
7×10 <sup>-6</sup>	21	0.995	30	28	0.997	0.05	48.6	0.989	5.5	27.2	0.998
1×10 <sup>-5</sup>	13.6	0.996	40	21.6	0.992	0.058	57	0.992	6	28	0.972
			60	13.2	0.983				7.5	18.6	0.992

Note: \*correlation coefficient

Ti-based MOFs, MIL-125 and its NH<sub>2</sub>-functionalized isostructure (MIL-125-NH<sub>2</sub>) were also used as photocatalysts to split water or reduce CO<sub>2</sub>.<sup>78,171-175</sup> Zhang and co-workers reported that Ti(IV)-based MOF NTU-9 displayed a strong absorption in the visible region with a bandgap of 1.72 eV and exhibited good photocatalytic activity in the degradation of RhB and MB in aqueous solution under visible light.<sup>101</sup> It was observed that the photocatalytic degradation of RhB (*C*<sub>0</sub> = 47.9 mg L<sup>-1</sup>) and MB (*C*<sub>0</sub> = 31.9 mg L<sup>-1</sup>) were finished after 80 and 20 min, respectively. NTU-9 also showed high photoactivity and good photostability. Ti(IV)-based MOFs are thus promising acting as candidates for the development of efficient visible light photocatalysts.

Inspired by such a fact that some enzymes contain multiple metal-based catalytic units,<sup>176</sup> many efforts have been made to synthesize catalyst materials containing bi-/multi-metallic centers. Li and co-workers prepared a bimetallic MOF, [Cu<sup>II</sup>(salimcy)](Cu<sup>I</sup>)<sub>2</sub>·DMF, containing Cu(II)-salen-based units and Cu(I) iodide clusters, which was used to photocatalytically decompose organic dyes under visible light irradiation.<sup>102</sup> In order to investigate the role of Cu(II) and Cu(I) ions in the decomposition of organic dyes, they performed the degradation of MB in presence of [Cu<sup>II</sup>(salimcy)](Cu<sup>I</sup>)<sub>2</sub>·DMF in dark and under visible light irradiation. The results revealed that 65% and 95% of MB with initial concentration of 12 mg L<sup>-1</sup> were decomposed in the absence of visible-light illumination and under that, respectively. In the former case, the Cu(II) ions in [Cu<sup>II</sup>(salimcy)](Cu<sup>I</sup>)<sub>2</sub>·DMF were crucial in decomposing MB, as confirmed in other study, in which Cu(II) ions were demonstrated to play a key catalytic role in oxidation reactions.<sup>177</sup> While, under visible-light illumination, the degradation of MB was

enhanced by the cooperative decomposition achieved by photoactive Cu(I) entities.<sup>90</sup> Similar situations have been observed in the decomposition of RhB and MO over this MOF.<sup>102</sup>

Similarly, Ru(II)-polypyridine complexes, as metallo-organic ligands, have also been explored in the application of MOF-based multifunctional catalyst and other fields.<sup>178-181</sup> Luo and co-workers synthesized MOF [InRu(dcbpy)<sub>3</sub>](CH<sub>3</sub>)<sub>2</sub>NH<sub>2</sub>·6H<sub>2</sub>O, which showed broad visible-light absorption and strong red luminescence emission based on the photoactive Ru(dcbpy)<sub>3</sub><sup>2+</sup> metalloligand.<sup>182</sup> The photocatalytic activity of this MOF was evaluated by the photodecomposition of methyl orange (MO), one of the most stable azo dyes. The results revealed that about 80% of MO molecules were decomposed in presence of the MOF catalyst upon visible light irradiation for 120 min. The decomposition of MO might attribute to the highly active hydroxyl radicals (•OH) that were generated during the redox cycles of the [Ru(dcbpy)<sub>3</sub>]<sup>4+</sup> metalloligands. This MOF was also confirmed to be stable in the photocatalysis.

On the other hand, one of the difficulties hindering the large-scale application of photocatalysts is their separation from reaction systems. Qiu and co-workers used magnetic Fe<sub>3</sub>O<sub>4</sub> nanoparticles as the core to fabricate Fe<sub>3</sub>O<sub>4</sub>@MIL-100(Fe) core-shell microsphere composite (Fig. 10a-d).<sup>89</sup> The magnetic properties of the material were investigated by vibrating sample magnetometry (VSM) (Fig. 10e), which showed a magnetic hysteresis loop suggesting the strong magnetic response of it to a varying magnetic field. The magnetic separation of the composite was confirmed to be feasible through using an external magnetic field. The optical properties of the material were investigated by UV-vis diffuse reflectance spectroscopy. The result revealed that the main optical absorption band of it was around 485 nm, with strong visible light absorption ability. The photocatalytic degradation of MB dye in aqueous solution using Fe<sub>3</sub>O<sub>4</sub>@MIL-100(Fe) core-shell microspheres as photocatalyst was investigated under UV-vis light and visible light irradiation, respectively. The results showed that this photocatalyst had remarkable photocatalytic activity for MB decolorization both under UV-vis and visible light irradiation, in comparison with typical photocatalysts, such as TiO<sub>2</sub> and C<sub>3</sub>N<sub>4</sub> (Fig. 10f and 10g). It was found that without H<sub>2</sub>O<sub>2</sub> the photodegradation efficiency of MB is very low, with about 35% degradation of MB being observed after 40 min of UV-vis light irradiation. When using H<sub>2</sub>O<sub>2</sub>, the photocatalytic efficiency of this catalyst was obviously improved, up to 99% MB degradation under similar other conditions. This is due to that H<sub>2</sub>O<sub>2</sub> as the electron acceptor could suppress the electron-hole pair recombination, thus enhancing the photodegradation efficiency.

For comparison, the reaction kinetics of the MB degradation catalyzed by various photocatalysts was also studied. The experimental data was fitted by a first-order model as expressed by  $-\ln(C/C_0) = kt$ . As shown in Fig.

10f,  $\text{Fe}_3\text{O}_4@\text{MIL-100}(\text{Fe})$  exhibited a higher rate constant of  $0.1042 \text{ min}^{-1}$  for the MB photodegradation under UV-vis irradiation, nearly three times larger than that of  $\text{TiO}_2$  ( $0.0371 \text{ min}^{-1}$ ) under the same reaction conditions. Under visible light, the rate constant ( $0.01977 \text{ min}^{-1}$ ) in using  $\text{Fe}_3\text{O}_4@\text{MIL-100}(\text{Fe})$  was 33 times more than that in  $\text{C}_3\text{N}_4$  ( $6.074 \times 10^{-4} \text{ min}^{-1}$ , close to that in literature<sup>183</sup>). The recycling reactions were carried out for the photodegradation of MB over  $\text{Fe}_3\text{O}_4@\text{MIL-100}(\text{Fe})$  under visible light irradiation.<sup>89</sup> In five consecutive cycles, the MB photodegradation rate constant values were 0.0164, 0.0162, 0.0157, 0.0151, and  $0.0146 \text{ min}^{-1}$ , respectively, indicating that the  $\text{Fe}_3\text{O}_4@\text{MIL-100}(\text{Fe})$  has a good catalytic stability. The integrality of its structure was also identified by PXRD and UV-vis absorption spectra. A possible mechanism for the photocatalytic degradation of MB over  $\text{Fe}_3\text{O}_4@\text{MIL-100}(\text{Fe})$  was also proposed, as illustrated in Fig. 12d. Just like the  $\text{TiO}_2$  semiconductor whose CB is constructed by empty Ti 3*d* orbitals, MIL-100(Fe) containing transition metals were also expected to be semiconductors since the empty *d* orbitals of metal ions mixed with the LUMOs of the organic linkers to form the CB. In presence of light irradiation, the electron ( $e^-$ ) can be excited from VB of MIL-100(Fe) to enter into its CB and produce holes ( $h^+$ ) in the VB. The photoinduced electrons transfer to  $\text{H}_2\text{O}_2/\text{H}_2\text{O}$  giving rise to more  $\cdot\text{OH}$ , which hindered the recombination of electrons and holes efficiently. The photogenerated holes with strong oxidation ability could directly oxidize adsorbed organic molecules, and the resulting  $\cdot\text{OH}$  could also decompose MB molecules that were adsorbed on the surface of  $\text{Fe}_3\text{O}_4@\text{MIL-100}(\text{Fe})$  particles. Anyway,  $\text{Fe}_3\text{O}_4@\text{MIL-100}(\text{Fe})$  exhibited both excellent photodegradation performances and good magnetic characteristics, making it a good and feasible photocatalyst for the decolorization of organic pollutants in wastewater.

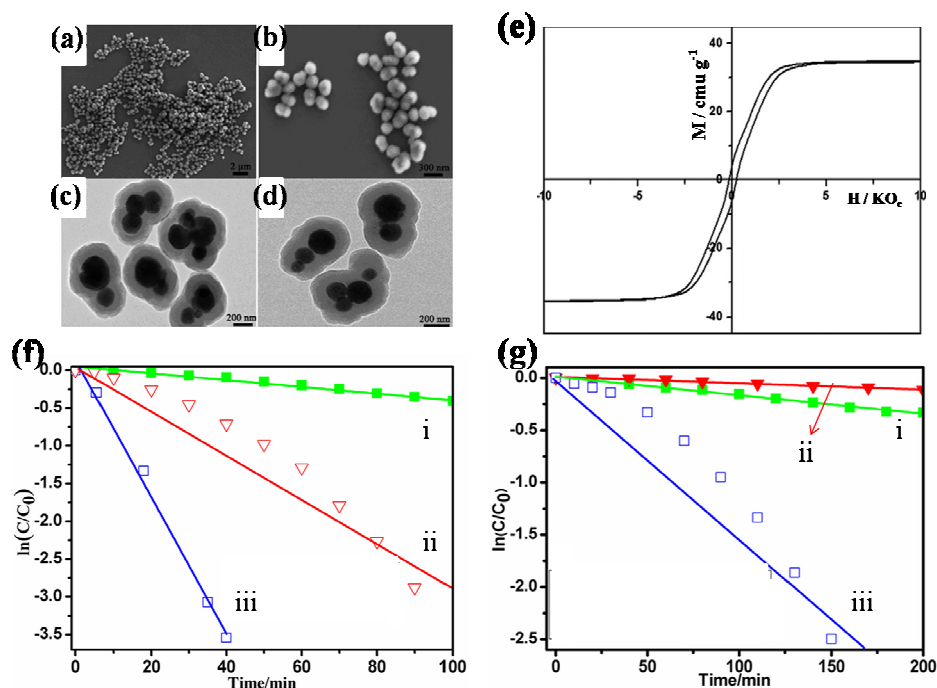


**Fig. 10** (a, b) SEM and (c, d) TEM images of Fe<sub>3</sub>O<sub>4</sub>@MIL-100(Fe) core-shell microspheres obtained at 70°C for 50 layers. (e) Room-temperature magnetization curves of samples of the Fe<sub>3</sub>O<sub>4</sub>@MIL-100(Fe) microspheres at 300 K. (f) First-order kinetics plot for the photodegradation of MB by Fe<sub>3</sub>O<sub>4</sub>@MIL-100(Fe) (i), TiO<sub>2</sub> and H<sub>2</sub>O<sub>2</sub> (ii), and Fe<sub>3</sub>O<sub>4</sub>@MIL-100(Fe) and H<sub>2</sub>O<sub>2</sub> (iii) under the irradiation of UV-vis light. (g) First-order kinetics plot for the photodegradation of MB by Fe<sub>3</sub>O<sub>4</sub>@MIL-100(Fe) (i), C<sub>3</sub>N<sub>4</sub> and H<sub>2</sub>O<sub>2</sub> (ii), and Fe<sub>3</sub>O<sub>4</sub>@MIL-100(Fe) and H<sub>2</sub>O<sub>2</sub> (iii) under the irradiation of visible light. Reprinted (adapted) with permission from ref. 89 Copyright (2013) the Royal Society of Chemistry.

Zeolitic imidazolate frameworks (ZIFs) usually constructed from the tetrahedrally coordinated divalent cations (Zn<sup>2+</sup> or Co<sup>2+</sup>) linked by the imidazolate ligands, are a subclass of MOFs with high thermal and chemical stability, as well as tunable zeotype topologies.<sup>184-186</sup> Zhang and co-workers investigated ZIF-67<sup>187</sup> (with a SOD structural topology as shown in Fig. 11a) and its Cu ions doped composite Cu/ZIF-67 for the photocatalytic degradation of methyl orange under visible-light illumination (MO).<sup>91</sup> It was found that the photocatalytic activity of Cu/ZIF-67 was gradually enhanced with time increasing from 0 to 25 min, as shown in Fig. 11b. After 25 min, the MO in the solution almost disappeared. Moreover, Cu/ZIF-67 was stable in repeated application with a nearly constant photocatalytic degradation rate, which was confirmed by SEM images and PXRD as shown in Fig. 11c-f and Fig. 11g. In contrast, ZIF-67 couldn't achieve such a photocatalytic degradation. These results indicated the importance of Cu-doping in tuning the photocatalytic activity of ZIF-67, although both materials possess the same topological structures and similar band gaps ( $E_g = 1.98$  and 1.95 eV for ZIF-67 and Cu/ZIF-67, respectively). Furthermore, electron paramagnetic resonance (EPR) test indicated that no Cu<sup>2+</sup> signal was observed in the

spectra. Based on the obviously enhanced photocatalytic property on MO, the presence of  $\text{Cu}^+$  ions in the structure of Cu/ZIF-67 was suggested.<sup>188,189</sup> Some reported examples also demonstrated that  $\text{Cu}^{2+}$  ions can be reduced into  $\text{Cu}^+$  ions under solvothermal conditions in the presence of heterocyclic ligands.<sup>190</sup> These  $\text{Cu}^+$  ions with potential tetrahedral coordination geometry might also replace some tetrahedral  $\text{Co}^{2+}$  sites in the host framework of ZIF-67, although the structural details are still unclear. In this work, a doping strategy was thus successfully applied to tune the photocatalytic properties of a ZIF material.

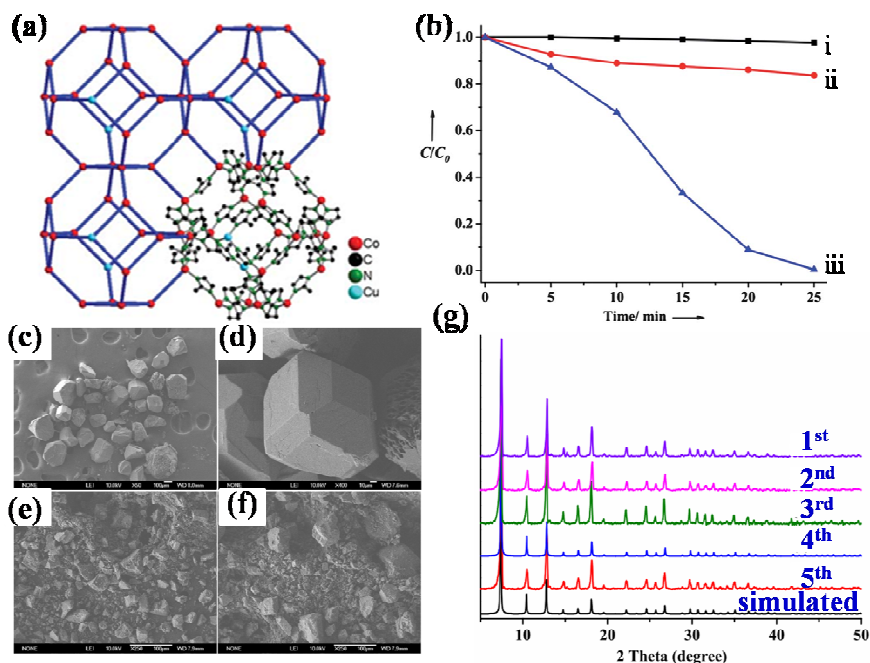


**Fig. 11** (a) The SOD-type framework structure of Cu/ZIF-67. (b) Photodegradation of MO on ZIF-67 and Cu/ZIF-67 under visible-light illumination in the presence of  $\text{H}_2\text{O}_2$  additive: MO- $\text{H}_2\text{O}_2$  solution (i); MO- $\text{H}_2\text{O}_2$  solution with ZIF-67 (ii); and MO- $\text{H}_2\text{O}_2$  solution with Cu/ZIF-67 (iii). (c) and (d) SEM images of Crystals of Cu/ZIF-67; (e) SEM images of powder samples of Cu/ZIF-67 before photocatalytic experiments. (f) SEM images of powder samples of Cu/ZIF-67 after 5 times photocatalytic experiments. (g) The PXRD pattern of Cu/ZIF-67 after photocatalytic experiments. Reprinted (adapted) with permission from ref. 91. Copyright (2012) the Royal Society of Chemistry.

Following that, the same group reported the photocatalytic degradation of methyl orange in two new ZIFs,  $[\text{Zn}_4(2\text{-mim})_6\text{WO}_4] \cdot 1.5(\text{DMF})$  (HZIF-1W) and  $[\text{Zn}_4(2\text{-mim})_6\text{MoO}_4] \cdot 2(\text{DMF})$  (HZIF-1Mo) constructed from two kinds of tetrahedral building blocks, which combined structural features of both zeolites and ZIFs<sup>127</sup>. It is interesting that the  $\text{TO}_4$  ( $T = \text{W}$  or  $\text{Mo}$ ) units used in these HZIFs are not traditional  $\text{SiO}_4$  or  $\text{AlO}_4$  units as in aluminosilicate zeolites, but catalytically active  $\text{MoO}_4$  or  $\text{WO}_4$ . To compare the photocatalytic activities, the commercial  $\text{TiO}_2$  and ZIF-8 were also employed for the degradation of methyl orange under the same conditions.

The bandgap sizes of HZIF-1Mo, HZIF-1W, TiO<sub>2</sub> and ZIF-8 are 1.32, 2.2, 3.2<sup>159</sup> and 4.9 eV<sup>127</sup>, respectively. It was observed that the degradation ratio of methyl orange were 5.9% (nearly comparable to control experiment without catalyst), 19.8, 24.5, and 81.6% with ZIF-8, TiO<sub>2</sub>, HZIF-1W, and HZIF-1Mo as photocatalysts, respectively, after 120 min under visible light irradiation. And, without the MoO<sub>4</sub><sup>2-</sup> or WO<sub>4</sub><sup>2-</sup> anions in the synthesis of HZIF-1Mo and HZIF-1W, the obtained ZIF-8 did not show any catalytic activity under the similar conditions. The commercial TiO<sub>2</sub> showed lower activity than that of HZIF-1W and HZIF-1Mo, which can be attributed to such a fact that TiO<sub>2</sub> has a weak absorption response towards visible light due to its wide band gap.

Because graphene can improve photocatalytic activities of semiconductors via promoting the electron transfer and charge separation processes<sup>191-196</sup>, Li and co-workers explored the photocatalytic degradation of dye in the MOF-graphene composite<sup>197</sup>. They prepared MIL-53(Fe)-rGO (rGO = reduced graphene oxide) hybrids, FeMG-1, FeMG-2 and FeMG-3, with rGO content of ca. 1.3, 2.5, and 3.2 wt%, respectively via a one-step solvothermal reaction. The photocatalytic activities of MIL-53(Fe), FeMG-1, FeMG-2, and FeMG-3 in the degradation of MB under UV light were investigated. The results revealed that FeMG-2 possessed the highest catalytic efficiency, in which 95% MB ( $C_0 = 30 \text{ mg L}^{-1}$ ) was decomposed. While 82% degradation of MB was achieved in presence of MIL-53(Fe) under the same condition. It implied that a suitable increase of rGO content could improve photocatalytic efficiency of this type of composite, but a further increasing rGO might result in decreasing the degradation rate. A possible photocatalytic mechanism was proposed, where in the presence of light irradiation, MIL-53(Fe) absorbed light and was excited, and then the photo-induced electrons were transferred from conduction band of MIL-53(Fe) to rGO sheet. This process could efficiently separate the electrons and suppress electron-hole recombination. The electrons were then trapped by molecular oxygen to generate superoxide radical ( $\bullet\text{O}_2^-$ ). Simultaneously, the holes ( $h^+$ ) reacted with hydroxyl ion (OH<sup>-</sup>) or water molecules to form hydroxyl radical ( $\bullet\text{OH}$ ). The  $\bullet\text{OH}$  and  $\bullet\text{O}_2^-$  have thus strong oxidative ability to degrade MB molecules to form CO<sub>2</sub>, H<sub>2</sub>O, or other products. However, an excessive rGO could decrease photocatalytic activity because of: (i) more rGO has stronger absorption towards light, so that less light was harvested by MIL-53(Fe), resulting in producing less electrons, (ii) an excessive rGO may promote recombination of electrons and holes<sup>198</sup>. Due to specific electrical and surface properties, excellent conductivity, and high surface area of graphene, it is quite interesting to study MOF-rGO hybrids for photocatalysis.<sup>195,196,199-203</sup>

On the other hand, the deposition of MOFs on substrates to fabricate MOF thin films has attracted much attention due to their potential applications in catalysis, sensors, and gas separations.<sup>204-208</sup> Li and co-workers fabricated the Zn<sub>3</sub>(btc)<sub>2</sub> film by *in situ* microwave-assisted solvothermal synthesis.<sup>98</sup> The photocatalytic activity of

this MOF film was evaluated by the photodegradation of MB dye under UV-vis and visible light irradiation. It was found that 99% of MB dye molecules (initial concentration  $10 \text{ mg L}^{-1}$ ) could be degraded within 20 min in the presence of 0.5 mL  $\text{H}_2\text{O}_2$  under UV-vis irradiation, while only 77% and 70% of MB were degraded in using  $\text{TiO}_2$  and  $\text{H}_2\text{O}_2$  under the same condition, respectively. It was also demonstrated that this film has a good stability.

### 3. The organic pollutants degradation in *f*-block metals based MOFs

Compared with transition metal ions, lanthanide ions usually exhibited high coordination number and diverse connectivity, which could facilitate the formation of various and unpredicted structures of MOFs. Lanthanide MOFs are in an intermediate situation between the type of MOFs with photoluminescence localized on the organic linker and those behaving as semiconductors.<sup>61</sup> Lanthanide based MOFs are very promising because the organic linker could act as an antenna producing efficient photosensitization, as listed in Table 5.

**Table 5** Performances of some MOFs constructed with *f*-block metals as photocatalysts for the degradation of organic pollutants in aqueous media

MOF <sup>a</sup>	$E_g$ (eV)	Irrigation	Organic pollutants	Initial concentration (mg L <sup>-1</sup> )	Time (min)	Degradation efficiency (%)	ref
[InRu(dcbpy) <sub>3</sub> ] <sub>3</sub> ·((CH <sub>3</sub> ) <sub>2</sub> NH <sub>2</sub> ) <sub>2</sub> ·6H <sub>2</sub> O	2.19	vis	MO	10	120	80	182
[Gd(5-NO <sub>2</sub> -bdc)(5-NO <sub>2</sub> -bdcH)(bpyo) <sub>0.5</sub> ] <sub>2</sub> ·2H <sub>2</sub> O	-	UV	X3B	3.69	600	70.0 <sup>b</sup>	157
Gd(H <sub>2</sub> O) <sub>3</sub> Co(2,3-pdc) <sub>3</sub>	3.7	UV	RBBR	100	100	-	67
Gd(H <sub>2</sub> O) <sub>3</sub> Co(2,3-pdc) <sub>3</sub>	3.7	UV	OG	100	100	-	67
[Ni <sub>2</sub> (H <sub>2</sub> O) <sub>2</sub> (qa) <sub>2</sub> (4,4'-bpy) <sub>2</sub> U <sub>5</sub> O <sub>14</sub> (H <sub>2</sub> O) <sub>2</sub> (OAc) <sub>2</sub> ] <sub>2</sub> ·2H <sub>2</sub> O	-	UV	MB	35.9	240	100 <sup>b</sup>	76
[Ni <sub>2</sub> (H <sub>2</sub> O) <sub>2</sub> (qa) <sub>2</sub> (4,4'-bpy) <sub>2</sub> U <sub>5</sub> O <sub>14</sub> (H <sub>2</sub> O) <sub>2</sub> (OAc) <sub>2</sub> ] <sub>2</sub> ·2H <sub>2</sub> O	-	vis	MB	35.9	240	80 <sup>b</sup>	76
(UO <sub>2</sub> ) <sub>8</sub> (1,4-ndc) <sub>12</sub> (4,4'-bpyH <sub>2</sub> ) <sub>3</sub> (4,4'-bpyH) <sub>3</sub>	-	UV	RhB	50	80	95 <sup>b</sup>	75
(UO <sub>2</sub> ) <sub>8</sub> (1,4-ndc) <sub>12</sub> (4,4'-bpyH <sub>2</sub> ) <sub>3</sub> (4,4'-bpyH) <sub>3</sub>	-	vis	RhB	50	600	100 <sup>b</sup>	75
(UO <sub>2</sub> ) <sub>3</sub> O[Ag(2,2'-bpy) <sub>2</sub> ] <sub>2</sub> (1,4-ndc) <sub>3</sub>	-	UV	RhB	50	80	100 <sup>b</sup>	75
(UO <sub>2</sub> ) <sub>3</sub> O[Ag(2,2'-bpy) <sub>2</sub> ] <sub>2</sub> (1,4-ndc) <sub>3</sub>	-	vis	RhB	50	600	100 <sup>b</sup>	75
Ag(2,2'-bpy)(UO <sub>2</sub> )(1,4-bdc) <sub>1.5</sub>	-	UV	RhB	47.9	35	100 <sup>b</sup>	77
Ag(2,2'-bpy)(UO <sub>2</sub> )(1,4-bdc) <sub>1.5</sub>	-	vis	RhB	47.9	240	90 <sup>b</sup>	77
Ag <sub>2</sub> (phen) <sub>2</sub> UO <sub>2</sub> (btec)	-	UV	RhB	47.9	120	99 <sup>b</sup>	77
(UO <sub>2</sub> ) <sub>2</sub> (bta)(DMA) <sub>2</sub>	-	UV	RhB	10	130	100	209
[(UO <sub>2</sub> ) <sub>2</sub> (bta)(μ <sub>3</sub> -OH <sub>2</sub> ) <sub>2</sub> ] <sub>2</sub> ·2(HN(CH <sub>3</sub> ) <sub>2</sub> ) <sub>2</sub> ·H <sub>2</sub> O	-	UV	RhB	10	130	50	209
UO <sub>2</sub> (1,4-ndc)((CH <sub>3</sub> ) <sub>2</sub> SO) <sub>2</sub>	-	UV-vis	RhB	479	70	100	210
UO <sub>2</sub> (1,4-ndc)((CH <sub>3</sub> ) <sub>2</sub> SO) <sub>2</sub>	-	Vis	RhB	479	180	100	210
UO <sub>2</sub> (1,4-ndc)(CH <sub>2</sub> OH) <sub>2</sub>	-	UV-vis	RhB	479	70	100	210
UO <sub>2</sub> (1,4-ndc)(CH <sub>2</sub> OH) <sub>2</sub>	-	vis	RhB	479	180	98	210
Gd(H <sub>2</sub> O) <sub>3</sub> Co(2,2-pdc) <sub>3</sub>	-	UV	RBBR	100	90	90 <sup>b</sup>	114
[Sm(H <sub>2</sub> O) <sub>4</sub> (2,6-pdc)] <sub>3</sub> [Sm(H <sub>2</sub> O) <sub>3</sub> (2,6-pdc)](SiM <sub>0.12</sub> O <sub>40</sub> ) <sub>3</sub> ·3H <sub>2</sub> O	-	UV	RhB	9.58	240	85 <sup>b</sup>	211
[La(H <sub>2</sub> O) <sub>4</sub> (2,6-pdc)] <sub>4</sub> (PM <sub>0.12</sub> O <sub>40</sub> ) <sub>4</sub> ·F	-	UV	RhB	9.58	240	85 <sup>b</sup>	211
[Yb(O)(Hbpcdb) <sub>2</sub> (H <sub>2</sub> bpcdb) <sub>0.5</sub> (H <sub>2</sub> O) <sub>3</sub> ](SiM <sub>0.12</sub> O <sub>40</sub> ) <sub>2</sub> ·2.5CH <sub>3</sub> CN·1.5H <sub>2</sub> O	-	UV	RhB	10	90	91.7	212
[Ca(Hbpcdb) <sub>2</sub> (bpcdb) <sub>0.5</sub> (H <sub>2</sub> O) <sub>4</sub> ](SiM <sub>0.12</sub> O <sub>40</sub> ) <sub>5</sub> ·5CH <sub>3</sub> CN·H <sub>2</sub> O	-	UV	RhB	10	90	91.7	212

Note:

<sup>a</sup> dcbpy = 2,2'-bipyridine-4,4'-dicarboxylic acid; 5-NO<sub>2</sub>-bdcH<sub>2</sub> = 5-nitro-1,3-benzenedicarboxylic acid; bpyo = 4,4'-bipyridine-N,N'-dioxide; 2,3-pdc = pyridine-2,3-dicarboxylic acid; H<sub>2</sub>qa = quinolinic acid;

---

4,4'-bpy = 4,4'-bipyridine; 1,4-H<sub>2</sub>ndc = 1,4-naphthalenedicarboxylic acid; 2,2'-bpy = 2,2'-bipyridine; 1,4-bdc = 1,4-benzenedicarboxylate; phen = phenanthroline; btec = 1,2,4,5-benzenetetracarboxylate; H<sub>4</sub>bta = 1,2,4,5-benzenetetracarboxylic acid; 2,3-pdc = pyridine-2,3-dicarboxylic acid; 2,6-pdc = pyridine-2,6-dicarboxylic acid; bpcdb = 1,4-bis(pyridinil-4-carboxylato)-1,4-dimethylbenzene.

<sup>b</sup> Values estimated from original figures of the references.

---

[Gd(5-NO<sub>2</sub>-bdc)(5-NO<sub>2</sub>-bdcH)](bpyo)<sub>0.5</sub>·2H<sub>2</sub>O was one of rare examples of MOFs with a 4f metal ion that exhibited a good photocatalytic activity for the dye degradation under UV light.<sup>157</sup> It was confirmed this MOF was active in the decomposition of X3B under UV light irradiation with a rate constant of 0.1022 h<sup>-1</sup>, while under visible-light the rate was 0.0138 h<sup>-1</sup>. Obviously, the photodegradation rate of X3B under visible light is much slower than that under UV light, implying that the photosensitization degradation reaction could be ignored under UV light.<sup>213-215</sup> It is interesting that TBA could depress the photodegradation rate of X3B in this MOF catalyst, indicating that the photocatalysis was predominately controlled through the attack of •OH radicals, rather than a direct hole oxidation. The corresponding photocatalytic reaction mechanism was depicted in Fig. 12d. The HOMO was mainly contributed by 2p bonding orbitals of oxygen and the LUMO from empty Gd orbitals, charge transfer took place from oxygen to Gd on the photoexcitation. The HOMO demanded one electron to return to its stable state. Thus, one electron was captured from water molecule, which was oxygenated into •OH. Then the •OH radicals cleaved X3B effectively to finish the photocatalytic process.

Previous studies have shown that aqueous solutions of uranyl ions were photocatalytically active in the oxidation of organic substrates in the presence of air, but it was difficult to separate the uranyl ions from the reaction system, which rendered this catalyst system practical applications.<sup>76,216-218</sup> Therefore, it is interesting to synthesize water-insoluble uranyl-containing solid materials for photocatalytic application. In this context, Chen and co-workers reported two uranyl-based MOFs Ag(2,2'-bpy)(UO<sub>2</sub>)(1,4-bdc)<sub>1.5</sub> and Ag<sub>2</sub>(phen)<sub>2</sub>UO<sub>2</sub>(btec), both of which were water-insoluble and active (than nanosized TiO<sub>2</sub> (P-25)) in the photocatalytic degradation of rhodamine B (RhB).<sup>77</sup> Fig. 12a and c showed the rate of RhB degradation in the aqueous solution in the presence of the two MOFs, respectively. After photocatalysis, both MOFs showed PXRD patterns nearly identical to those of the parent MOFs, indicating their stability towards the photocatalysis. More importantly, Ag(2,2'-bpy)(UO<sub>2</sub>)(1,4-bdc)<sub>1.5</sub> showed a remarkable photodegradation activity for RhB when a xenon lamp (wavelength longer than 400 nm) was used as the irradiation source (Fig. 12a and c). For comparison, the visible-light photocatalytic performance of P-25 was also tested, which showed only slight photocatalytic activity under xenon-light irradiation. In contrast, Ag<sub>2</sub>(phen)<sub>2</sub>UO<sub>2</sub>(btec) did not show a photocatalytic activity irradiated under the xenon lamp even for 240 min. The discrepancy in photocatalytic activities of the two MOFs can be attributed to their structural differences. The diffuse-reflectance UV/Vis spectra revealed that Ag(2,2'-bpy)(UO<sub>2</sub>)(1,4-bdc)<sub>1.5</sub> and Ag<sub>2</sub>(phen)<sub>2</sub>UO<sub>2</sub>(btec) had similar absorption features, consisting of absorption components in the UV and Vis regions. The UV component was attributed to the charge-transfer electronic transition of the uranyl group, and the Vis component responsible for the colors of the two MOFs arose from

ligand-to-metal charge transfer (LMCT). In spite of similarities in UV/Vis absorption behaviors, it could be noted that the charge-transfer transition of  $\text{Ag}(2,2'\text{-bpy})(\text{UO}_2)(1,4\text{-bdc})_{1.5}$  occurred in the visible region, while that of  $\text{Ag}_2(\text{phen})_2\text{UO}_2(\text{btec})$  lied in the near-UV region. The UV/Vis absorptions of the two MOFs are clearly related to their structures. First, the uranium atoms are seven-coordinated in  $\text{Ag}(2,2'\text{-bpy})(\text{UO}_2)(1,4\text{-bdc})_{1.5}$  and eight-coordinated in  $\text{Ag}_2(\text{phen})_2\text{UO}_2(\text{btec})$ . The fewer ligands around the uranium center in the former mean less steric hindrance, which allows the access of more dye substrates to the U center. Second, the silver-centered moieties in  $\text{Ag}(2,2'\text{-bpy})(\text{UO}_2)(1,4\text{-bdc})_{1.5}$  were packed almost parallel to the uranyl-organic layers, while in  $\text{Ag}_2(\text{phen})_2\text{UO}_2(\text{btec})$ , they occupied the interlayer spaces. The larger interlayer region in the former makes it easier for the dye molecules accessing the active U centers, whereas the latter has a smaller interlayer region and fully coordinated U centers, which are unfavorable for the access of the dye molecules. For the irradiation under visible light, the difference of photocatalytic activities mainly arose from the difference in visible-light excitations. The dependence of the photocatalytic activity on the structural features have also been demonstrated in other uranyl-containing MOFs  $[\text{Ni}_2(\text{H}_2\text{O})_2(\text{qa})_2(4,4'\text{-bpy})_2\text{U}_5\text{O}_{14}(\text{H}_2\text{O})_2(\text{OAc})_2] \cdot 2\text{H}_2\text{O}$ <sup>71</sup> and  $(\text{ZnO})_2(\text{UO}_2)_3(\text{na})_4(\text{OAc})_2$  (Hna = nicotinic acid).<sup>218</sup>

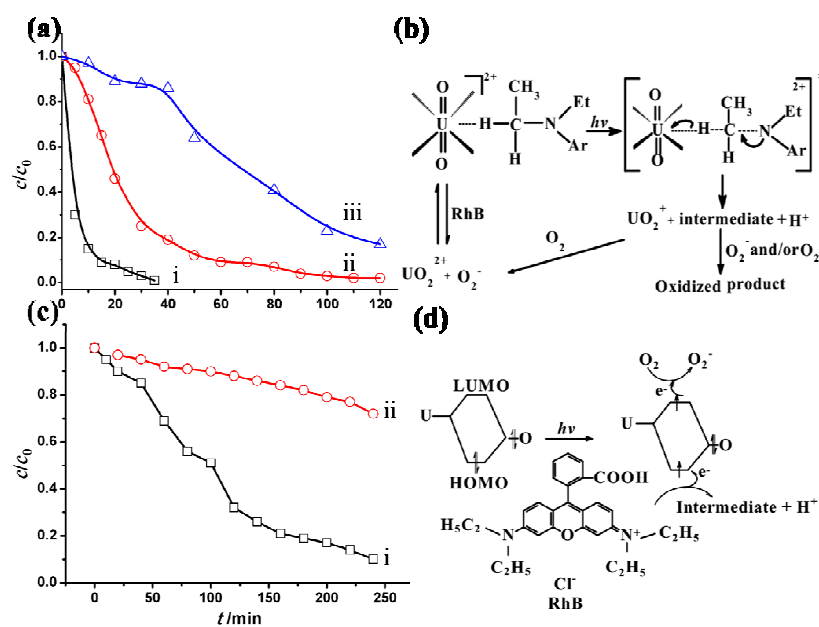


**Fig. 12** (a) Concentration changes of RhB irradiated with UV light as a function of irradiation time  $t_{\text{irr}}$  in the presence of  $\text{Ag}(2,2'\text{-bpy})(\text{UO}_2)(1,4\text{-bdc})_{1.5}$  (i),  $\text{Ag}_2(\text{phen})_2\text{UO}_2(\text{btec})$  (ii), and Degussa P-25 (iii).  $C_1$  and  $C_0$  stand for the RhB concentrations after and before irradiation. (b) Photoexcitation of  $\text{Ag}(2,2'\text{-bpy})(\text{UO}_2)(1,4\text{-bdc})_{1.5}$  or  $\text{Ag}_2(\text{phen})_2\text{UO}_2(\text{btec})$  and oxidation of the RhB substrate. (c) Concentration changes of RhB under irradiation with xenon-lamp light in the presence of  $\text{Ag}(2,2'\text{-bpy})(\text{UO}_2)(1,4\text{-bdc})_{1.5}$  (i) and Degussa P-25 (ii). (d) Proposed

photodegradation pathways of the RhB substrate in the presence of  $\text{Ag}(2,2'\text{-bpy})(\text{UO}_2)(1,4\text{-bdc})_{1.5}$  or  $\text{Ag}_2(\text{phen})_2\text{UO}_2(\text{btec})$ . Reprinted (adapted) with permission from ref. 77. Copyright (2012) Wiley-VCH.

Furthermore, Chen and co-workers analyzed the total organic carbon (TOC) when the color of the solution completely disappeared in the catalysis of  $\text{Ag}(2,2'\text{-bpy})(\text{UO}_2)(1,4\text{-bdc})_{1.5}$  and  $\text{Ag}_2(\text{phen})_2\text{UO}_2(\text{btec})$  under UV irradiation<sup>77</sup>. The results revealed a TOC decrease of 34% and 40%, respectively, which showed that RhB was mineralized to a considerable extent in presence of the two MOFs. The  $\text{NO}_3^-$  ions were detected in the degraded solution, suggesting the conversion of nitrogen in RhB into  $\text{NO}_3^-$ . The percentages of RhB converted into  $\text{NO}_3^-$  ions were about 30% and 34% after 40 min under UV and visible irradiation, respectively in the presence of  $\text{Ag}(2,2'\text{-bpy})(\text{UO}_2)(1,4\text{-bdc})_{1.5}$ , and about 25% after 120 min under UV irradiation in  $\text{Ag}_2(\text{phen})_2\text{UO}_2(\text{btec})$ . Additionally, the formation of formic and acetic acids in the final products of the photocatalytic systems was also confirmed in these catalysis systems.

The intermediate species generated in the degradation of RhB photocatalyzed by  $\text{Ag}(2,2'\text{-bpy})(\text{UO}_2)(1,4\text{-bdc})_{1.5}$  or  $\text{Ag}_2(\text{phen})_2\text{UO}_2(\text{btec})$  were identified by positive-ion ( $M + H$ ) mass spectra. It was found that the specie with a  $m/z$  of 443.2 (RhB) transferred to those of 415.2 (N,N',N''-triethylrhodamine), 387.1 (N,N'-diethylrhodamine), and 359.0 (N-ethylrhodamine), corresponding to stepwise loss of  $\text{C}_2\text{H}_5$  moieties.<sup>219,220</sup> Decarboxylated species were also observed, confirmed by a mass spectral signal at  $m/z = 260.2$ .<sup>220</sup> At the end of the photocatalytic reaction, an apparent decrease was noted in signal intensity of  $m/z = 443.2$ , which indicated that RhB had effectively been photodegraded into other products with lower molecular weight.

Although the photocatalysis in the two MOFs were carried out in heterogeneous systems, it was believed that the uranyl center photocatalytically behaved in a way similar to that in solution. The uranyl center in the two MOFs could be excited by photons, and then one electron in the HOMO jumped to the LUMO. Because the energies of the 5f, 6d, 7p, and 7s orbitals of uranium are comparable, it is quite difficult to determine the electron configuration and orbital combination in uranium compounds. The involved photocatalytic reaction mechanism was proposed in Fig. 12d. Despite the disputable electron configuration and orbital combination, it is clear that the double bonds between uranium and oxygen were involved in the photoexcitation. Because the HOMO is mainly contributed to by oxygen 2p bonding orbitals and the LUMO by empty uranium orbitals, charge transfer actually takes place from oxygen to uranium on photoexcitation to give uranium in +5 and oxygen in -1 oxidation state, respectively. Presumably, the excited  $^*\text{UO}_2^{2+}$  decays easily to its ground state. However, if some molecules locate within a reasonable range and have an appropriate orientation, for example, RhB in this case, transitional active

complexes could thus be formed. Thus, one  $\alpha$ -hydrogen atom of the methylene group bonded to the nitrogen atom in RhB would give an electron and leave as  $H^+$  hole,<sup>221</sup> which is abstracted by uranyl species to result in the cleavage of the C-N bond and stepwise N-deethylation of RhB (Fig. 12b.) Since the HOMO is then reoccupied, the excited electron will remain in the LUMO until it is captured by electronegative substances such as molecular oxygen in solution, which would transform into highly active peroxide anion and subsequently accomplish the further oxidation and total degradation of RhB.<sup>222</sup>

The role of oxygen in this photocatalysis mechanism was also studied by monitoring the photocatalytic activities. When the argon gas was bubbled into the system for 30 min before and during the irradiation, the photocatalytic reaction rate decreased rapidly in  $Ag(2,2'\text{-bpy})(UO_2)(1,4\text{-bdc})_{1.5}$  and quickly dropped to zero in  $Ag_2(\text{phen})_2UO_2(\text{btec})$ . This result revealed that the presence of oxygen was essential for the photocatalytic reaction; otherwise, the  $U^V$  could not be oxidized back to  $U^{VI}$  for a new cycle. The peroxide anion formed from the molecular oxygen was an important intermediate for the further degradation of RhB. Furthermore, spin-trap ESR also demonstrated that no hydroxyl radicals involved in these systems.

In addition, Jie and co-workers reported other two uranyl-based MOFs  $(UO_2)_8(\text{ndc})_{12}(4,4'\text{-bpyH}_2)_3(4,4'\text{-bpyH})_3$ , and  $(UO_2)_3O[Ag(2,2'\text{-bpy})_2](\text{ndc})_3$  with efficient photocatalytic activity towards RhB.<sup>75</sup> Typical UV/vis spectrum of uranyl compounds usually consists of absorptions in both UV region, arising from charge transfer electronic transition within the U=O bonds<sup>223,224</sup> and visible region, resulting from ligand to metal charge transfer (LMCT) between the O (or N) atoms of the coordinating ligands and an empty orbital of the U(VI) ion.<sup>225,226</sup> The former is usually proven to be responsible for photocatalytic activities, in which RhB was degraded almost completely within 80 min under UV irradiation. While under visible light, it was demonstrated that the two MOFs had photocatalytic activities, but complete degradation of RhB can be achieved after 10 h under irradiation. Because the two MOFs have close uranium contents of 33.6% and 30.9%, respectively, and similar structures, the similarity in their photocatalytic performances suggests that the uranyl units are responsible for the catalytic properties, whereas the Ag moieties are of less importance. However, the possibility to tune the catalytic properties of uranyl-containing materials by assembling other metal ions or nonmetal species is not excluded.<sup>227</sup> In this study, the impact of oxygen on the photocatalytic degradation reaction was also addressed. It was found that under visible irradiation, the RhB degraded at a constant rate in the first 3 h in the presence of various oxygen contents, but after that the rate increase lagged behind the oxygen concentration rise.

Mixed-metal MOFs, particularly for *d-f* systems are proposed to be much more effective in the photocatalytic

degradation of dyes, the synthesis of these MOFs is however difficult. Up to now, only a few examples were documented.<sup>76,228,229</sup> Natarajan and co-workers synthesized three *3d-4f* MOFs,  $M(\text{H}_2\text{O})_3\text{Co}(\text{pda})_3$  ( $M = \text{Gd}, \text{Dy},$  and  $\text{Y}$ ), consisting of a network  $\text{MO}_6(\text{H}_2\text{O})_3$  and  $\text{Co}_3\text{N}_3$  polyhedral units, with band gap of 3.7 eV.<sup>67</sup> Comparing to commercial  $\text{TiO}_2$  (Degussa P-25), all these MOFs showed good photocatalytic activity for the decomposition of RBBR and OG. In order to quantify these reactions, the kinetics was determined by the Langmuir-Hinshelwood (L-H) method,  $r_0 = k_0C_0/(1 + K_0C_0)$ . The values of  $k_0$  and  $K_0$  in the degradation of the two dyes in these MOFs are shown in Table 6. For the degradation of RBBR the rate coefficient  $k_0$  varied in the order of  $\text{Y}(\text{H}_2\text{O})_3\text{Co}(\text{pda})_3 > \text{Dy}(\text{H}_2\text{O})_3\text{Co}(\text{pda})_3 > \text{Gd}(\text{H}_2\text{O})_3\text{Co}(\text{pda})_3$ , but for OG, the order was  $\text{Gd}(\text{H}_2\text{O})_3\text{Co}(\text{pda})_3 > \text{Dy}(\text{H}_2\text{O})_3\text{Co}(\text{pda})_3 > \text{Y}(\text{H}_2\text{O})_3\text{Co}(\text{pda})_3$ . It is clear that in spite of having comparable band gaps, the degradation rates of the two dyes are different and depend on the MOFs. Furthermore, the degradation of another two azo dyes (methyl red and methyl orange) was investigated by using these MOFs. The degradation rates followed an order of  $\text{Gd}(\text{H}_2\text{O})_3\text{Co}(\text{pda})_3 > \text{Dy}(\text{H}_2\text{O})_3\text{Co}(\text{pda})_3 > \text{Y}(\text{H}_2\text{O})_3\text{Co}(\text{pda})_3$ , the same as that of OG, confirming the high selectivity of  $\text{Gd}(\text{H}_2\text{O})_3\text{Co}(\text{pda})_3$  for the azo dyes. These results also indicated that these three MOFs are not only photocatalytically active but also selective towards specific organic functional groups. The differences in the activities might be due to the differences in the efficiency of the electron transfers from the organic dyes to the carboxylate radicals of MOFs.

According to previous studies,<sup>160,230,231</sup> the low-spin  $\text{Co}^{3+}$  complexes usually possess ligand-field (LF), intraligand (IL) and charge-transfer (CT) excited states. Among them, the IL and CT states are active when nitrogen containing aromatic ligands are involved in bonding with the  $\text{Co}^{3+}$ . In  $M(\text{H}_2\text{O})_3\text{Co}(\text{pda})_3$ , similar situation existed in  $\text{Co}^{3+}$  species. The room temperature diffuse reflectance UV-vis spectra for these MOFs showed three peaks. The absorption band at 304 nm can be assigned to LMCT; another two peaks at 381 and 516 nm can be assigned to the *d-d* transition of the  $\text{Co}^{3+}$  ions. It is clear that the lanthanide ions in these MOFs do not participate effectively in the electron transfer because their *f* orbitals are well shielded from other ions. The photocatalytic effect of these MOFs thus should originate from  $\text{Co}^{3+}$  ions, even if it is difficult to ascertain precisely the electronic energy levels of them. Of the three types of electronic transfer states observed in these MOFs, the LMCT effect happened in the UV region is thus responsible for the observed photocatalytic activity. Similar mechanism had also been proposed in other *3d-5f* mixed-metal systems for the degradation of organic dyes.<sup>77</sup>

**Table 6** Kinetics parameters for the degradation of dyes using  $M(H_2O)_3Co(pda)_3$  ( $M = Gd, Dy, \text{ and } Y$ )<sup>67</sup>

MOF	Dye	$k_0$ (min <sup>-1</sup> )	$K_0$ (mg L <sup>-1</sup> )
Gd(H <sub>2</sub> O) <sub>3</sub> Co(pda) <sub>3</sub>	RBBR	0.025	0.002
Gd(H <sub>2</sub> O) <sub>3</sub> Co(pda) <sub>3</sub>	OG	0.018	0.003
Dy(H <sub>2</sub> O) <sub>3</sub> Co(pda) <sub>3</sub>	RBBR	0.012	0.015
Dy(H <sub>2</sub> O) <sub>3</sub> Co(pda) <sub>3</sub>	OG	0.009	0.005
Y(H <sub>2</sub> O) <sub>3</sub> Co(pda) <sub>3</sub>	RBBR	0.032	0.018
Y(H <sub>2</sub> O) <sub>3</sub> Co(pda) <sub>3</sub>	OG	0.007	0.003

#### 4. The organic pollutants degradation in polyoxometalates (POMs) based MOFs

Polyoxometalates (POMs), as metal-oxide clusters of early transition metals Mo, W, V, and so on had been widely investigated in various fields.<sup>232-237</sup> One of the attractive properties of POMs was photocatalytic activity,<sup>238-240</sup> which could photocatalytically break down the organic pollutants into non-polluting small molecules.<sup>74,119,241,242</sup> However, there are two main drawbacks slowing down the development of POMs acting as catalysts. (i) High solubility makes them difficult to be recovered and recycled;<sup>243</sup> (ii) Most POMs showed low visible light photocatalytic activity because of high energy gap between the well-defined HOMO and LUMO. It was found only less than 5% of the solar light could usually be utilized, which restrict their application in photocatalysis.<sup>244</sup> In recent years, the introduction of POMs into MOFs has been emerging as one of the most promising strategies for optimizing the performance of POMs in catalysis.<sup>234,235</sup> Some MOFs constructed with POMs and organic ligands indeed showed good photocatalytic activities in the degradation of organic dyes,<sup>238,245-248</sup> as shown in Table 7.

**Table 7** Performances of some MOFs constructed with *d*-block metals as photocatalysts for the degradation of organic pollutants in aqueous media

MOF <sup>a</sup>	$E_g$ (eV)	Irrigation	Organic pollutants	Initial concentration (mg L <sup>-1</sup> )	Time (min)	Degradation efficiency (%)	ref
{[Sm(H <sub>2</sub> O) <sub>4</sub> (2,6-pdc)] <sub>3</sub> } {[Sm(H <sub>2</sub> O) <sub>3</sub> (2,6-pdc)] <sub>3</sub> }(SiMo <sub>12</sub> O <sub>40</sub> )·3H <sub>2</sub> O	-	UV	RhB	9.58	240	85 <sup>b</sup>	134
[La(H <sub>2</sub> O) <sub>4</sub> (2,6-pdc)] <sub>4</sub> (PMo <sub>12</sub> O <sub>40</sub> )F	-	UV	RhB	9.58	240	85 <sup>b</sup>	134
[Yb(O)(Hbpcdb) <sub>2</sub> (H <sub>2</sub> bpcdb) <sub>0.5</sub> (H <sub>2</sub> O) <sub>3</sub> ](SiMo <sub>12</sub> O <sub>40</sub> )·2.5CH <sub>3</sub> CN·1.5H <sub>2</sub> O	-	UV	RhB	10	90	91.7	135
[Ca(Hbpcdb) <sub>2</sub> (bpcdb) <sub>0.5</sub> (H <sub>2</sub> O) <sub>4</sub> ](SiMo <sub>12</sub> O <sub>40</sub> )·5CH <sub>3</sub> CN·H <sub>2</sub> O	-	UV	RhB	10	90	91.7	135
[Ag(4,4'-bpy)] <sub>4</sub> V <sub>4</sub> O <sub>12</sub> ·2H <sub>2</sub> O	2.77	UV	MB	6.0	180	70	73
[Ag(dpa)] <sub>4</sub> V <sub>4</sub> O <sub>12</sub> ·4H <sub>2</sub> O	2.95	UV	MB	6.0	180	65	73
Ag <sub>4</sub> (pzc) <sub>2</sub> V <sub>2</sub> O <sub>6</sub>	2.45	UV	MB	6.0	90	80	73
Ag <sub>4</sub> (pzc) <sub>2</sub> V <sub>2</sub> O <sub>6</sub>	2.45	vis	MB	6.0	180	80	73
[Ag(bbi)][(Ag(bbi)) <sub>4</sub> (Ag <sub>3</sub> (V <sub>4</sub> O <sub>12</sub> ) <sub>2</sub> )]·2H <sub>2</sub> O	-	UV	MB	10.0	90	70	241
Cu <sub>2</sub> <sup>I</sup> (1,3-btp) <sub>2</sub> [Cu <sub>2</sub> <sup>I</sup> (trans-1,3-btp) <sub>2</sub> Mo <sub>6</sub> O <sub>18</sub> (O <sub>3</sub> AsPh) <sub>2</sub>	2.6	UV	MB	17.6	120	76	238
Cu <sub>4</sub> <sup>I</sup> (1,5-btp) <sub>4</sub> Mo <sub>6</sub> O <sub>18</sub> (O <sub>3</sub> AsPh) <sub>2</sub>	2.1	UV	MB	17.6	120	93	238
Cu <sub>4</sub> <sup>I</sup> (1,6-bth) <sub>2</sub> Mo <sub>6</sub> O <sub>18</sub> (O <sub>3</sub> AsPh) <sub>2</sub>	1.9	UV	MB	17.6	120	97	238
[Cu <sub>8</sub> (1,3-btp) <sub>8</sub> [Mo <sub>12</sub> O <sub>46</sub> (AsPh) <sub>4</sub> ] <sub>2</sub> ]·3H <sub>2</sub> O	1.72	vis	MB	17.6	180	70	249
Cu <sub>6</sub> Na <sub>2</sub> (Htrb) <sub>4</sub> (Mo <sub>6</sub> O <sub>19</sub> )(MoO <sub>4</sub> ) <sub>6</sub>	3.13	UV	MB	17.6	120	63	250
[Zn <sub>3</sub> (Htrb)(Mo <sub>10</sub> O <sub>34</sub> )]·8H <sub>2</sub> O	2.87	UV	MB	17.6	120	61	250
[Zn <sub>2</sub> (Htrb)(β-Mo <sub>8</sub> O <sub>26</sub> )(H <sub>2</sub> O) <sub>2</sub> ]·6H <sub>2</sub> O	3.15	UV	MB	17.6	120	60	250
[Co <sub>2</sub> (Htrb)(β-Mo <sub>8</sub> O <sub>26</sub> )(H <sub>2</sub> O) <sub>2</sub> ]·6H <sub>2</sub> O	2.64	UV	MB	17.6	120	56	250
[Co <sub>2</sub> (Htrb)(γ-Mo <sub>8</sub> O <sub>26</sub> )(H <sub>2</sub> O) <sub>6</sub> ]·8H <sub>2</sub> O	2.91	UV	MB	17.6	120	58	250
[Cu <sub>2</sub> (2,4'-tmbpt) <sub>2</sub> (β-Mo <sub>8</sub> O <sub>26</sub> )(H <sub>2</sub> O) <sub>2</sub> ]·7H <sub>2</sub> O	2.88	UV	MB	17.6	120	60	245
[Cu(2,4'-tmbpt)(γ-Mo <sub>8</sub> O <sub>26</sub> ) <sub>0.5</sub> (H <sub>2</sub> O)]·H <sub>2</sub> O	2.13	UV	MB	17.6	120	57	245
Co(2,4'-Htmbpt) <sub>2</sub> (γ-Mo <sub>8</sub> O <sub>26</sub> )(H <sub>2</sub> O) <sub>2</sub>	2.45	UV	MB	17.6	120	52	245
Zn(2,4'-Htmbpt) <sub>2</sub> (γ-Mo <sub>8</sub> O <sub>26</sub> )(H <sub>2</sub> O) <sub>2</sub>	2.94	UV	MB	17.6	120	83	245
[Ni(2,4'-tmbpt)(α-Mo <sub>8</sub> O <sub>26</sub> ) <sub>0.5</sub> (H <sub>2</sub> O)]·2.5H <sub>2</sub> O	2.62	UV	MB	17.6	120	76	245
Ag(2,4'-Htmbpt)(β-Mo <sub>8</sub> O <sub>26</sub> ) <sub>0.5</sub>	2.75	UV	MB	17.6	120	59	245
[Zn <sub>4</sub> (htpmb) <sub>2</sub> (θ-Mo <sub>8</sub> O <sub>26</sub> )(H <sub>2</sub> O) <sub>6.5</sub> ]·0.5H <sub>2</sub> O	2.63	UV	MB	17.6	120	76	246
[Zn <sub>6</sub> (htpmb) <sub>2</sub> (γ-Mo <sub>8</sub> O <sub>26</sub> ) <sub>2</sub> (SO <sub>4</sub> )(H <sub>2</sub> O) <sub>6</sub> ]·6.5H <sub>2</sub> O	3.33	UV	MB	17.6	120	71	246
[Cd <sub>2</sub> (htpmb)(γ-Mo <sub>8</sub> O <sub>26</sub> )(H <sub>2</sub> O) <sub>2</sub> ]·4.5H <sub>2</sub> O	3.20	UV	MB	17.6	120	79	246

[Cu(phen) <sub>2</sub> ] <sub>4</sub> (W <sub>10</sub> O <sub>32</sub> )	-	vis	RRN	11.2	60	19.9	251
[Cu <sub>6</sub> (PO <sub>4</sub> ) <sub>2</sub> (H <sub>2</sub> O) <sub>4</sub> (phen) <sub>6</sub> ](P <sub>2</sub> W <sub>18</sub> O <sub>62</sub> )	-	vis	MO	15	120	98.35	252
[Cu <sup>II</sup> bbi] <sub>4</sub> (SiW <sub>12</sub> O <sub>40</sub> )·H <sub>2</sub> O	-	UV	RhB	8.62	420	100	253
[K <sub>2</sub> (H <sub>2</sub> O) <sub>2</sub> Na <sub>2</sub> (H <sub>2</sub> O) <sub>2</sub> Na <sub>2</sub> (H <sub>2</sub> O) <sub>6</sub> ](P <sub>2</sub> W <sub>18</sub> O <sub>62</sub> )(Me <sub>10</sub> Q <sub>5</sub> ) <sub>2</sub> ·7H <sub>2</sub> O	-	vis	MO	10	180	99.96	21
[K <sub>2</sub> (H <sub>2</sub> O) <sub>2</sub> Na <sub>2</sub> (H <sub>2</sub> O) <sub>2</sub> Na <sub>2</sub> (H <sub>2</sub> O) <sub>6</sub> ](P <sub>2</sub> W <sub>18</sub> O <sub>62</sub> )(Me <sub>10</sub> Q <sub>5</sub> ) <sub>2</sub> ·7H <sub>2</sub> O	-	vis	RhB	10	120	91.32	21
[CoCl <sub>0.5</sub> (H <sub>2</sub> O) <sub>0.5</sub> (Hdppzc) <sub>2</sub> ](PW <sub>12</sub> O <sub>40</sub> ) <sub>0.5</sub> ·3.5H <sub>2</sub> O	-	vis	RhB	10	80	90	254
Cu <sup>I</sup> <sub>3</sub> (1,4-biyb) <sub>2</sub> (tpb)[PMo <sup>VI</sup> <sub>8</sub> V <sup>V</sup> <sub>4</sub> O <sub>40</sub> (V <sup>IV</sup> O) <sub>2</sub> ]·2H <sub>2</sub> O	-	UV	RhB	7.2	300	55	255
CoH(bix) <sub>4</sub> (PMo <sup>VI</sup> <sub>8</sub> V <sup>V</sup> <sub>4</sub> O <sub>40</sub> (V <sup>IV</sup> O) <sub>2</sub> )	-	UV	RhB	9.58	150	55	256
[(H <sub>2</sub> bix) <sub>2</sub> (NaHP <sub>2</sub> Mo <sub>5</sub> O <sub>23</sub> )]·2H <sub>2</sub> O	-	UV	RhB	9.58	150	35	256
H <sub>2</sub> (bix) <sub>4</sub> [Cd(H <sub>2</sub> O) <sub>4</sub> ][Cd(HPO <sub>4</sub> ) <sub>4</sub> (H <sub>2</sub> PO <sub>4</sub> ) <sub>4</sub> (MoO <sub>2</sub> ) <sub>12</sub> (OH) <sub>6</sub> ]·10H <sub>2</sub> O	-	UV	RhB	9.58	150	47	256
(H <sub>2</sub> en) <sub>3</sub> (Co <sub>3</sub> P <sub>4</sub> Mo <sub>4</sub> O <sub>28</sub> )	-	UV	RhB	9.58	150	43	256
(H <sub>2</sub> en) <sub>2</sub> [Cu(pzca) <sub>2</sub> (Mo <sub>8</sub> O <sub>26</sub> )]·4H <sub>2</sub> O	-	UV	MB	17.6	300	73.5	257
[Ni(bix) <sub>2</sub> ](VW <sub>12</sub> O <sub>40</sub> )·(H <sub>2</sub> bix)·H <sub>2</sub> O	-	UV	RhB	10	420	86.7	258
[Co(bix) <sub>2</sub> ](VW <sub>12</sub> O <sub>40</sub> )·(H <sub>2</sub> bix)·2H <sub>2</sub> O	-	UV	RhB	10	420	91.2	258
[Ag <sub>8</sub> (pbpb) <sub>4</sub> (α-Mo <sub>8</sub> O <sub>26</sub> )(β-Mo <sub>8</sub> O <sub>26</sub> )(H <sub>2</sub> O) <sub>3</sub> ]·H <sub>2</sub> O	2.50	UV	MB	3.2	90	75 <sup>c</sup>	259
Cu <sup>I</sup> <sub>4</sub> (btb) <sub>2</sub> (m-OH)(PW <sub>12</sub> O <sub>40</sub> )	-	UV	MB	10	150	87	260
[Cu <sup>II</sup> <sub>2</sub> (btb) <sub>4</sub> (m-Cl)(PW <sub>12</sub> O <sub>40</sub> )]·3H <sub>2</sub> O	-	UV	MB	10	150	85	260
(C <sub>5</sub> H <sub>4</sub> NH)COOH] <sub>3</sub> (PMo <sub>12</sub> O <sub>40</sub> )	-	UV	RhB	9.58	240	85 <sup>b</sup>	211
[Ag <sub>7</sub> (bte) <sub>4</sub> (H <sub>2</sub> O)(HP <sub>2</sub> W <sup>VI</sup> <sub>16</sub> W <sup>V</sup> <sub>2</sub> O <sub>62</sub> )]·2H <sub>2</sub> O	-	UV	MB	17.6	90	74.7	261
[Ag <sub>7</sub> (1,3-btp) <sub>5</sub> (HP <sub>2</sub> W <sup>VI</sup> <sub>16</sub> W <sup>V</sup> <sub>2</sub> O <sub>62</sub> )]·H <sub>2</sub> O	-	UV	MB	17.6	90	83.5	261
[Ag <sub>4</sub> (btb) <sub>3.5</sub> (P <sub>2</sub> W <sub>18</sub> O <sub>62</sub> )](H <sub>2</sub> btb)·2H <sub>2</sub> O	-	UV	MB	17.6	90	85.5	261
[Cu <sub>2</sub> (bpce) <sub>3</sub> (SiMo <sub>12</sub> O <sub>40</sub> )(H <sub>2</sub> O) <sub>6</sub> ]·2H <sub>2</sub> O	-	UV	MB	10	240	82 <sup>b</sup>	261
[Cu <sub>2</sub> (bpcb) <sub>3</sub> (SiMo <sub>12</sub> O <sub>40</sub> )(H <sub>2</sub> O) <sub>6</sub> ]·9H <sub>2</sub> O	-	UV	MB	10	240	90 <sup>b</sup>	262
[Cu <sub>2</sub> (bpcb) <sub>3</sub> (SiW <sub>12</sub> O <sub>40</sub> )(H <sub>2</sub> O) <sub>6</sub> ]·6H <sub>2</sub> O	-	UV	MB	10	240	80 <sup>b</sup>	262
[Cu <sub>2</sub> (bpch) <sub>3</sub> (SiMo <sub>12</sub> O <sub>40</sub> )(H <sub>2</sub> O) <sub>6</sub> ]·4H <sub>2</sub> O	-	UV	MB	10	240	97 <sup>b</sup>	262
[Cu <sub>2</sub> (bpch) <sub>3</sub> (SiW <sub>12</sub> O <sub>40</sub> )(H <sub>2</sub> O) <sub>6</sub> ]·4H <sub>2</sub> O	-	UV	MB	10	240	80	262
[Cu <sub>3</sub> (2-pytz) <sub>2</sub> (4,4'-bpy) <sub>4</sub> (H <sub>2</sub> O) <sub>6</sub> ](H <sub>4</sub> SiW <sub>12</sub> O <sub>40</sub> ) <sub>2</sub> ·6H <sub>2</sub> O	-	UV	RhB	4.79	120	70	263
[Cu <sub>2</sub> (2-pytz)(phen)-(OH)] <sub>2</sub> (SiW <sub>12</sub> O <sub>40</sub> )·H <sub>2</sub> O	-	UV	RhB	4.79	120	61	263
K <sub>2</sub> [Ag <sub>6</sub> (5-pytz) <sub>4</sub> ](PW <sub>12</sub> O <sub>40</sub> )	-	UV	RhB	4.79	360	72	264
[Ag <sub>7</sub> (ptz) <sub>4</sub> (NO <sub>3</sub> )(H <sub>2</sub> O)](H <sub>4</sub> P <sub>2</sub> W <sub>18</sub> O <sub>62</sub> )·5H <sub>2</sub> O	-	UV	MB	0.64	180	86.1	264

$[\text{Ag}_6(\text{ptz})_4(\text{H}_2\text{O})_2](\text{HPMo}_{12}\text{O}_{40}) \cdot 3\text{H}_2\text{O}$	-	UV	MB	0.64	180	42.7	265
$[\text{Ag}_7(\text{ptz})_4](\text{PW}_{12}\text{O}_{40}) \cdot 4\text{H}_2\text{O}$	-	UV	MB	0.64	180	93.7	233,265
$\text{Co}_6(\mu_3\text{-OH})_3(\text{H}_2\text{O})_9(\text{bpyb})(\text{PW}_9\text{O}_{34})$	-	UV	MB	320	90	91.9	266
$[\text{Cu}(\text{II})_2\text{Cu}(\text{I})_3(\text{OH})_4(\text{H}_2\text{O})_2(\text{tp})_4](\text{PW}_{12}\text{O}_{40})$	-	vis	$\text{MO}(\text{H}_2\text{O}_2)$	15	150	91	267
$[\text{Cu}(1,4\text{-bimb})_2(\text{HPW}_{12}\text{O}_{40}) \cdot 3\text{H}_2\text{O}$	-	UV	RhB	10	180	72.6	268
$(1,4\text{-H}_2\text{bimb})_2\text{SiW}_{12}\text{O}_{40}$	-	UV	RhB	10	180	66.8	268
$(1,4\text{-H}_2\text{bimb})_3\text{CoW}_{12}\text{O}_{40}$	-	UV	RhB	10	180	58.9	268
$[\text{Cu}^{\text{I}}_3(\text{bta})_4(\text{Hbta})_8(\text{SiMo}_{12}\text{O}_{40})] \cdot 2\text{H}_2\text{O}$	-	UV	MB	320	140	91.5	269
$[\text{Cu}^{\text{II}}_6(\text{OH})_4(\text{bta})_4(\text{SiW}_{12}\text{O}_{40})(\text{H}_2\text{O})_6] \cdot 6\text{H}_2\text{O}$	-	UV	MB	320	140	96.5	269
$[\text{HMn}^{\text{II}}(\text{bix})_4](\text{PMo}^{\text{VI}}_8\text{V}^{\text{V}}_4\text{O}_{40}(\text{V}^{\text{IV}}\text{O})_2) \cdot 2\text{H}_2\text{O}$	-	UV	RhB	9.58	210	60 <sup>b</sup>	270
$[\text{Zn}(\text{bix})_4](\text{PMo}^{\text{VI}}_9\text{V}^{\text{V}}_3\text{O}_{40}(\text{V}^{\text{IV}}\text{O})_2) \cdot 2\text{H}_2\text{O}$	-	UV	RhB	9.58	210	88 <sup>b</sup>	270
$[\text{Cu}(\text{bix})_4](\text{PMo}^{\text{VI}}_9\text{V}^{\text{V}}_3\text{O}_{40}(\text{V}^{\text{IV}}\text{O})_2) \cdot 4\text{H}_2\text{O}$	-	UV	RhB	9.58	210	88 <sup>b</sup>	270
$[\text{Cu}^{\text{I}}(\text{bix})_2][\text{Cu}^{\text{I}}(\text{bix})(\text{bix})(\text{PMo}_{12}\text{O}_{40}) \cdot 4\text{H}_2\text{O}$	-	UV	RhB	9.58	210	90 <sup>b</sup>	270
$[\text{Mn}(\text{salen})_2(\text{H}_2\text{O})_2](\text{AlMo}_6(\text{OH})_6\text{O}_{18})(\text{arg}) \cdot 16\text{H}_2\text{O}$	-	UV	RhB	9.58	300	100	271
$[\text{Mn}(\text{salen})_2(\text{H}_2\text{O})_2](\text{CrMo}_6(\text{OH})_6\text{O}_{18})(\text{arg}) \cdot 11\text{H}_2\text{O}$	-	UV	RhB	9.58	300	99.6	271
$\text{Cu}^{\text{II}}(\text{bbi})_{1.5}(\text{H}_2\text{bbi})_2(\text{P}_2\text{W}_{18}\text{O}_{62})$	-	UV	RhB	8.6	360	71.6	272
$\text{Cu}^{\text{II}}_{2.5}(\text{mimin})(\text{Hmimin})(\text{bbi})_3(\text{P}_2\text{W}_{18}\text{O}_{62})_3 \cdot \text{H}_2\text{O}$	-	UV	RhB	8.6	360	61.2	272
$\text{Cu}^{\text{II}}(\text{bbtz})(\text{H}_2\text{bbi})(1,3\text{-H}_2\text{btp})(\text{P}_2\text{W}_{18}\text{O}_{62})$	-	UV	RhB	8.6	360	86.2	272
$\text{Ag}_6\text{Cl}_2(\text{mmt})_4(\text{H}_4\text{SiMo}_{12}\text{O}_{40})(\text{H}_2\text{O})_2$	-	UV	MB	10	90	45 <sup>b</sup>	273
$\text{Ag}_4(\text{bmte})_2(\text{H}_2\text{O})_2(\text{SiMo}_{12}\text{O}_{40})$	-	UV	MB	10	90	75 <sup>b</sup>	273
$\text{Ag}_4(\text{bmtr})_2(\text{H}_2\text{O})_2(\text{SiMo}_{12}\text{O}_{40})$	-	UV	MB	10	90	80 <sup>b</sup>	273
$\text{Ag}_4(\text{bmtb})_3(\text{SiMo}_{12}\text{O}_{40})$	-	UV	MB	10	90	72 <sup>b</sup>	273
$[\text{Cu}^{\text{II}}(1,2\text{-bppmb})_2\text{H}(\text{BW}_{12}\text{O}_{40}) \cdot 4\text{H}_2\text{O}$	-	UV	RhB	20	40	91	274
$[\text{Cu}^{\text{I}}(1,2\text{-bppmb})_4(\text{SiW}_{12}\text{O}_{40}) \cdot 5\text{H}_2\text{O}$	-	UV	RhB	20	40	91	274
$[\text{Cu}(1,4\text{-bppmb})_3\text{H}_2(\text{BW}_{12}\text{O}_{40}) \cdot 5\text{H}_2\text{O}$	-	UV	RhB	20	40	91	274
$[\text{Ag}_3(3,3'\text{-tmbpt})_2(\alpha\text{-Mo}_8\text{O}_{26})_{0.5}(\beta\text{-Mo}_8\text{O}_{26})_{0.5}] \cdot 3.5\text{H}_2\text{O}$	2.94	UV	MB	16	90	80	275
$[\text{Ag}_2(3,3'\text{-tmbpt})(\epsilon\text{-Mo}_8\text{O}_{26})_{0.5}] \cdot 1.75\text{H}_2\text{O}$	2.96	UV	MB	16	90	91	275
$[\text{Ag}_2(3,4'\text{-tmbpt})_2(\beta\text{-Mo}_8\text{O}_{26})_{0.5}] \cdot 0.5\text{H}_2\text{O}$	2.78	UV	MB	16	90	84	275
$\text{Ag}(3,4'\text{-Htmbpt})(\beta\text{-Mo}_8\text{O}_{26})_{0.5}$	3.39	UV	MB	16	90	91	275
$[\text{Zn}(\text{phen})_2(\text{H}_2\text{O})_2][\text{VW}_{12}\text{O}_{40}] \cdot 3\text{H}_2\text{O}$	-	UV	MB	10	90	90	276

$[\text{Co}_2(\text{btb})_4(\text{H}_2\text{O})][\text{H}_2\text{P}_2\text{W}_{18}\text{O}_{62}] \cdot 3\text{H}_2\text{O}$	-	UV	MB	10	120	91	277
$[\text{Co}_2(\text{btb})_4(\text{H}_2\text{O})][\text{H}_2\text{As}_2\text{W}_{18}\text{O}_{62}] \cdot 6\text{H}_2\text{O}$	-	UV	MB	10	120	84	277
$(\text{NH}_4)_2[\text{Mn}(\text{salen})(\text{H}_2\text{O})_2]_4[\text{V}_{10}\text{O}_{28}] \cdot 6\text{H}_2\text{O}$	-	UV	RhB	6.7	360	97.4	278
$\text{K}[\text{La}(\text{H}_2\text{O})_4(2,6\text{-pdc})]_4[\text{BW}_{12}\text{O}_{40}] \cdot 2\text{H}_2\text{O}$	3.11	UV	Thiophene	200	720	49	279
$\text{K}[\text{Ce}(\text{H}_2\text{O})_4(2,6\text{-pdc})]_4[\text{BW}_{12}\text{O}_{40}] \cdot 2\text{H}_2\text{O}$	3.11	UV	Thiophene	200	720	97	279
$\text{K}[\text{Tb}(\text{H}_2\text{O})_3(2,6\text{-pdc})]_4[\text{BW}_{12}\text{O}_{40}] \cdot 6\text{H}_2\text{O}$	3.11	UV	Thiophene	200	720	68	279
$\text{K}[\text{Dy}(\text{H}_2\text{O})_3(2,6\text{-pdc})]_4[\text{BW}_{12}\text{O}_{40}] \cdot 6\text{H}_2\text{O}$	3.11	UV	Thiophene	200	720	46	279
$\text{K}[\text{Er}(\text{H}_2\text{O})_3(2,6\text{-pdc})]_4[\text{BW}_{12}\text{O}_{40}] \cdot 6\text{H}_2\text{O}$	3.11	UV	Thiophene	200	720	42	279
$[\text{Cu}_2(2,2'\text{-tmbpt})_2(\text{SiW}_{12}\text{O}_{40})] \cdot 9\text{H}_2\text{O}$	2.62	UV	MB	16	120	41	280
$[\text{Cu}_2(2,3'\text{-tmbpt})_2(\text{SiW}_{12}\text{O}_{40})] \cdot 6\text{H}_2\text{O}$	3.17	UV	MB	16	120	51	280
$[\text{Cu}_2(2,4'\text{-tmbpt})_2(\text{SiW}_{12}\text{O}_{40})(\text{H}_2\text{O})_2] \cdot 6.5\text{H}_2\text{O}$	3.00	UV	MB	16	120	58	280
$[\text{Cu}_2(4,4'\text{-tmbpt})_2(\text{SiW}_{12}\text{O}_{40})(\text{H}_2\text{O})_4] \cdot 13.5\text{H}_2\text{O}$	3.54	UV	MB	16	120	74	280
$[\text{Cu}(4,4'\text{-Htmbpt})(4,4'\text{-tmbpt})(\text{PW}_{12}\text{O}_{40})(\text{H}_2\text{O})_2] \cdot 7\text{H}_2\text{O}$	2.71	UV	MB	16	120	81	280
$[\text{Cu}_2(2,2'\text{-tmbpt})_2(\text{SiW}_{12}\text{O}_{40})] \cdot 9\text{H}_2\text{O}$	2.62	UV	RhB	19.2	120	51	280
$[\text{Cu}_2(2,3'\text{-tmbpt})_2(\text{SiW}_{12}\text{O}_{40})] \cdot 6\text{H}_2\text{O}$	3.17	UV	RhB	19.2	120	-	280
$[\text{Cu}_2(2,4'\text{-tmbpt})_2(\text{SiW}_{12}\text{O}_{40})(\text{H}_2\text{O})_2] \cdot 6.5\text{H}_2\text{O}$	3.00	UV	RhB	19.2	120	55	280
$[\text{Cu}_2(4,4'\text{-tmbpt})_2(\text{SiW}_{12}\text{O}_{40})(\text{H}_2\text{O})_4] \cdot 13.5\text{H}_2\text{O}$	3.54	UV	RhB	19.2	120	56	280
$[\text{Cu}(4,4'\text{-Htmbpt})(4,4'\text{-tmbpt})(\text{PW}_{12}\text{O}_{40})(\text{H}_2\text{O})_2] \cdot 7\text{H}_2\text{O}$	2.71	UV	RhB	19.2	120	74	280
$[\text{Cu}(\text{dap})_2]_{5.5}(\text{Y}(\alpha\text{-PW}_{11}\text{O}_{39}))_2 \cdot 4\text{H}_2\text{O}$	-	UV	RhB	9.58	840	79	281
$\text{Na}_6[\text{Cu}(\text{gly})(\text{H}_2\text{O})]_2[[\text{Cu}(\text{H}_2\text{O})](\text{H}_2\text{W}_{12}\text{O}_{42})] \cdot 21\text{H}_2\text{O}$	-	UV	RhB	8.6	300	75	282
$\text{Na}[\text{Na}(\text{H}_2\text{O})_6][\text{Na}(\text{H}_2\text{O})_4]_3[[\text{Cu}(\text{gly})]_2](\text{H}_5(\text{H}_2\text{W}_{12}\text{O}_{42})) \cdot 8.5\text{H}_2\text{O}$	-	UV	RhB	8.6	300	60	282
$[\text{Cu}_4^{\text{II}}\text{Cu}_2^{\text{I}}(\text{pzca})_6(\text{HPCuMo}_{11}\text{O}_{39})(\text{H}_2\text{O})_6] \cdot 2\text{H}_2\text{O}$	-	UV	MB	10	210	50	283
$\text{H}[(\text{bitdc})\text{Ni}(\text{H}_2\text{O})_3]_2(\text{IMo}_6\text{O}_{24}) \cdot 6\text{H}_2\text{O}$	-	UV	RhB	9.58	660	97.3	284
$[\text{Cd}(\text{Htrz})_3]_2(\text{SiW}_{12}\text{O}_{40}) \cdot 2\text{H}_2\text{O}$	3.16	UV	RhB	4.79	210	71	285
$\text{Co}(\text{bpce})(\text{H}_2\text{Mo}_4\text{O}_{14})(\text{H}_2\text{O})_2$	-	UV	MB	10	210	94.6	286
$\text{Ni}(\text{bpce})(\text{H}_2\text{Mo}_4\text{O}_{14})(\text{H}_2\text{O})_2$	-	UV	MB	10	210	90.5	286
$[\text{Cu}_3(\text{btyb})_3(\text{PMo}_{12}\text{O}_{40})] \cdot 9\text{H}_2\text{O}$	2.70	UV	RhB	4.79	165	94.2	287
$[\text{Cu}_3(\text{btyb})_3(\text{PW}_{12}\text{O}_{40})] \cdot 9\text{H}_2\text{O}$	3.13	UV	RhB	7.19	165	93.7	287
$[\text{Mn}(\text{salen})(\text{CH}_3\text{OH})_2]_3(\text{PMo}_{12}\text{O}_{40})$	-	UV	RhB	4.79	300	94.85	288
$[\text{Mn}(\text{salen})(\text{CH}_3\text{OH})_2]_3(\text{PW}_{12}\text{O}_{40})$	-	UV	RhB	4.79	300	77.08	288

$[\text{Cu}_2(\text{SiW}_{12}\text{O}_{40})(\text{bpce})(\text{phen})_2(\text{H}_2\text{O})] \cdot 3\text{H}_2\text{O}$	-	UV	MB	10	240	84	289
$\text{Cu}_2(\text{SiW}_{12}\text{O}_{40})(\text{bpcb})(\text{phen})_2(\text{H}_2\text{O})_4$	-	UV	MB	10	240	78	289
$[\text{Cu}_2(\text{SiW}_{12}\text{O}_{40})(\text{bpch})(\text{phen})_2(\text{H}_2\text{O})_4] \cdot 6\text{H}_2\text{O}$	-	UV	MB	10	240	83	289
$(\text{H}_4\text{teta})_4[\text{Na}[\text{Mo}^{\text{V}}_{12}(\text{OH})_6(\text{HPO}_4)_7(\text{PO}_4)_7\text{O}_{24}]] \cdot 11\text{H}_2\text{O}$	-	UV	RhB	2	240	28.1	290
$(\text{H}_4\text{teta})_4[\text{Na}[\text{Mo}^{\text{V}}_{12}(\text{OH})_6(\text{HPO}_4)_7(\text{PO}_4)_7\text{O}_{24}]] \cdot 11\text{H}_2\text{O}$	-	sunlight	RhB	2	240	21.2	290
$[\text{Cu}_6^{\text{I}}(\text{ptz})_6](\text{H}_3\text{PMo}_{12}\text{O}_{40}) \cdot 2\text{H}_2\text{O}$	-	UV	MB	10	180	99	291
$[\text{Cu}_6^{\text{I}}(\text{ptz})_6](\text{H}_3\text{PMo}_{12}\text{O}_{40}) \cdot 2\text{H}_2\text{O}$	-	UV	MB	10	180	67	291
$(\text{en})(\text{en})_4\text{Zn}_2\text{Na}[\text{Na}[\text{Mo}_6\text{O}_{16}(\text{HPO}_4)_3(\text{PO}_4)(\text{OH})_3(\text{H}_2\text{O})_2]] \cdot 3\text{H}_2\text{O}$	-	UV	RhB	100	240	82	292
$(\text{SiMo}_{12}\text{O}_{40})(\text{H}_2\text{bipy})_2 \cdot 2\text{H}_2\text{O}$	-	UV	MB	10	60	82	293
$(\text{H}_2\text{bpp})_4[\text{PW}_{11}\text{CuO}_{39}](\text{PW}_{12}\text{O}_{40})$	-	UV	MB	10	90	60	294
$\text{H}_5(\text{bpe})_3(\text{SiW}_{11}\text{CoO}_{39}) \cdot 2\text{H}_2\text{O}$	-	UV	MB	10	90	93	294
$[(\text{H}_2\text{toym})_4(\text{Mo}_8\text{O}_{26})_2] \cdot 15\text{H}_2\text{O}$	2.99	UV	MB	10	120	54.7	295
$[(\text{H}_2\text{toym})_2(\text{SiW}_{12}\text{O}_{40})] \cdot 6\text{H}_2\text{O}$	2.65	UV	MB	10	120	80.4	295

Note:

<sup>a</sup> 4,4'-bpy = 4,4'-bipyridine; dpa = 1,2-bis(4-pyridyl)-ethane; pzc = pyrazinecarboxylate; bbi = 1,1'-(1,4-butanediyl)bis(imidazole); 1,3-btp = 1,3-bis(1,2,4-triazol-1-yl)propane; trans-1,3-btp = trans-1,3-bis(1,2,4-triazol-1-yl)propane; 1,5-btp = 1,5-bis(1,2,4-triazol-1-yl)pentane; 1,6-bth = 1,6-bis(1,2,4-triazol-1-yl)hexane; Htrb = hexakis(1,2,4-triazol-ylmethyl)benzene; 2,4'-tmbpt = 1-((1H-1,2,4-triazol-1-yl)methyl)-3-(2-pyridyl)-5-(4-pyridyl)-1,2,4-triazole; htpmb = hexakis(3-(1,2,4-triazol-4-yl)phenoxy-methyl)benzene; phen = phenanthroline; Hdppzc = dipyrido[3,2-a:2',3'-c]-phenazine-2-carboxylic acid; 1,4-biyb = 1,4-bis(imidazol-1-ylmethyl)benzene; tpb = 1,2,4,5-tetra(4-pyridyl)-benzene; bix = 1,4-bis(imidazol-1-ylmethyl)benzene; en = 1,2-ethylenediamine; Hpzca = 2-pyrazinecarboxylic acid; pbpb = 1,1'-(1,3-propanediyl)-bis[2-(4-pyridyl)benzimidazole]; btb = 1,4-bis(1,2,4-triazol-1-yl)butane; bte = 1,2-bis(1,2,4-triazol-1-yl)ethane; bpce = N,N'-bis(3-pyridinecarboxamide)-1,2-ethane; bpcb = N,N'-bis(3-pyridinecarboxamide)-1,4-butane; bpch = N,N'-bis(3-pyridinecarboxamide)-1,6-hexane; 2-pytz = 2-(pyridyl)tetrazolate; 5-pytz = 5-(pyridyl)tetrazolate; ptz = 5-(3-pyridyl)tetrazole; bpyb = 4,4'-bis(1,2,4-triazol-1-ylmethyl)biphenyl; tpt = tris(4-pyridyl)triazine; 1,4-bimb = 1,4-bis(imidazol-1-ylmethyl)biphenyl; H<sub>4</sub>bta = 1,2,4,5-benzenetetracarboxylic acid; Hbta = 1-H-1,2,3-benzotriazole; salen = N,N'-ethylene-bis(salicylideneimine); mimin = methylimidazol; bbtz = 1,4-bis(triazol-1-ylmethyl)benzene; mmt = 1-methyl-5-mercapto-1,2,3,4-tetrazole; bmte = 1,2-bis(1-methyl-5-mercapto-1,2,3,4-tetrazole)ethane; bmtr = 1,3-bis(1-methyl-5-mercapto-1,2,3,4-tetrazole)propane; bmtb = 1,4-bis(1-methyl-5-mercapto-1,2,3,4-tetrazole)butane; 1,2-bppmb = 1,2-bis(3-(2-pyridyl)pyrazole-1-ylmethyl)benzene; 1,4-bppmb = 1,4-bis(3-(2-pyridyl)pyrazole-1-ylmethyl)benzene; 3,3'-tmbpt = 1-((1H-1,2,4-triazol-1-yl)methyl)-3,5-bis(3-pyridyl)-1,2,4-triazole; 3,4'-tmbpt = 1-((1H-1,2,4-triazol-1-yl)methyl)-3-(4-pyridyl)-5-(3-pyridyl)-1,2,4-triazole; 2,6-pdc = pyridine-2,6-dicarboxylate; 2,2'-tmbpt = 1-((1H-1,2,4-triazol-1-yl)methyl)-3,5-bis(2-pyridyl)-1,2,4-triazole; 2,3'-tmbpt = 1-((1H-1,2,4-triazol-1-yl)methyl)-3-(3-pyridyl)-5-(2-pyridyl)-1,2,4-triazole; 4,4'-tmbpt = 1-((1H-1,2,4-triazol-1-yl)methyl)-3,5-bis(4-pyridyl)-1,2,4-triazole; dap = 1,2-diaminopropane; gly = glycine; bitdc = N,N'-bis(isonicotinoyl)-trans-1,2-diaminocyclohexane; Htrt = 1-H-1,2,4-triazole; btyb = 4-bis(1,2,4-triazol-1-ylmethyl)-benzene; H<sub>4</sub>teta = tetraprotonated triethylenetetramine; bpp = 1,3-di(4-pyridyl)propane; bpe = 1,2-di(4-pyridyl)ethylene; toym = 2,4,6-tris[1-(4-oxidoxypryridinium)-ylmethyl]-mesitylene.

<sup>b</sup> Values estimated from original figures of the references.

Maggard and co-workers reported three silver-vanadate based MOFs,  $[\text{Ag}(4,4'\text{-bpy})]_4\text{V}_4\text{O}_{12}\cdot 2\text{H}_2\text{O}$ ,  $[\text{Ag}(\text{dpa})]_4\text{V}_4\text{O}_{12}\cdot 4\text{H}_2\text{O}$ , and  $\text{Ag}_4(\text{pzc})_2\text{V}_2\text{O}_6$ , which were photocatalytically active in the decomposition of MB under UV/visible light.<sup>74</sup> As shown in Fig. 13a and 13c,  $[\text{Ag}(4,4'\text{-bpy})]_4\text{V}_4\text{O}_{12}\cdot 2\text{H}_2\text{O}$  and  $[\text{Ag}(\text{dpa})]_4\text{V}_4\text{O}_{12}\cdot 4\text{H}_2\text{O}$  are constructed from neutral 2D  $[\text{Ag}_4\text{V}_4\text{O}_{12}]_n$  layers pillared through the 4,4'-bpy ligands through coordinating to the Ag sites in each layer; but  $\text{Ag}_4(\text{pzc})_2\text{V}_2\text{O}_6$  is composed of a 3D  $[\text{Ag}_2(\text{ptz})^+]_n$  network containing  $[\text{VO}_3^-]_n$  chains. As reported previously<sup>296-298</sup>, heterometallic oxides containing both  $d^0$  and  $d^{10}$  transition metals usually showed small optical bandgap with the absorption of visible-light, which could be used to drive photocatalytic reactions. The three MOFs contained either 2D or 3D “ $\text{Ag}_x\text{VO}_3$ ” entities should have photocatalytic reactivity. The UV-vis diffuse reflectance revealed the optical bandgap values of 2.77, 2.95, and 2.45 eV in  $[\text{Ag}(4,4'\text{-bpy})]_4\text{V}_4\text{O}_{12}\cdot 2\text{H}_2\text{O}$ ,  $[\text{Ag}(\text{dpa})]_4\text{V}_4\text{O}_{12}\cdot 4\text{H}_2\text{O}$ , and  $\text{Ag}_4(\text{pzc})_2\text{V}_2\text{O}_6$ , respectively. Photocatalytic studies demonstrated that these MOFs could efficiently decompose MB, with the rates of 1.01, 0.64 and 2.65  $\text{mg L}^{-1} \text{H}^{-1}$ , respectively. It is interesting that the photocatalytic activities of  $[\text{Ag}(4,4'\text{-bpy})]_4\text{V}_4\text{O}_{12}\cdot 2\text{H}_2\text{O}$  and  $[\text{Ag}(\text{dpa})]_4\text{V}_4\text{O}_{12}\cdot 4\text{H}_2\text{O}$  are limited in the UV light region owing to their large bandgaps, while  $\text{Ag}_4(\text{pzc})_2\text{V}_2\text{O}_6$  is active under both UV and visible-light irradiation because of its smaller bandgap (Fig. 13c). It was found that  $\text{Ag}_4(\text{pzc})_2\text{V}_2\text{O}_6$  could achieve a 80% removal of MB after 180 min under visible-light irradiation, with a rate of 1.20  $\text{mg L}^{-1} \text{H}^{-1}$ . It is worthy to notice that the photocatalytic rate of  $\text{Ag}_4(\text{pzc})_2\text{V}_2\text{O}_6$  under either UV or visible light is higher than  $[\text{Ag}(4,4'\text{-bpy})]_4\text{V}_4\text{O}_{12}\cdot 2\text{H}_2\text{O}$  and  $[\text{Ag}(\text{dpa})]_4\text{V}_4\text{O}_{12}\cdot 4\text{H}_2\text{O}$ . These results suggested that the cooperative effect from these complicated vanadate and Ag-oxide/organic chains aided in the transport of excited holes/electrons to the surface to initiate the photocatalytic degradation of MB.

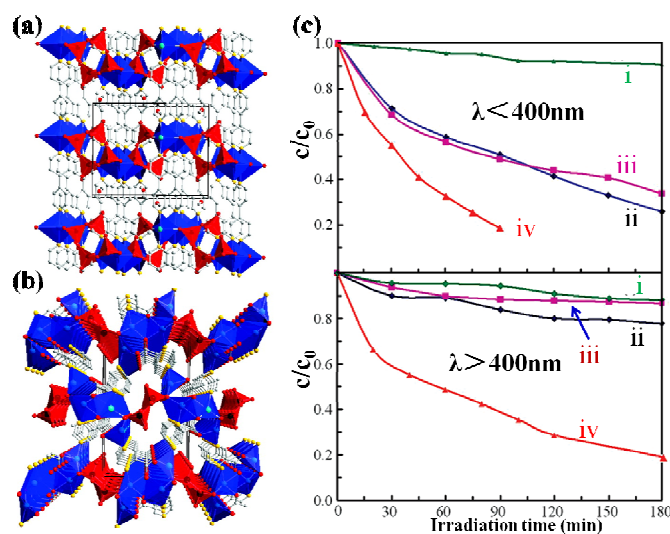
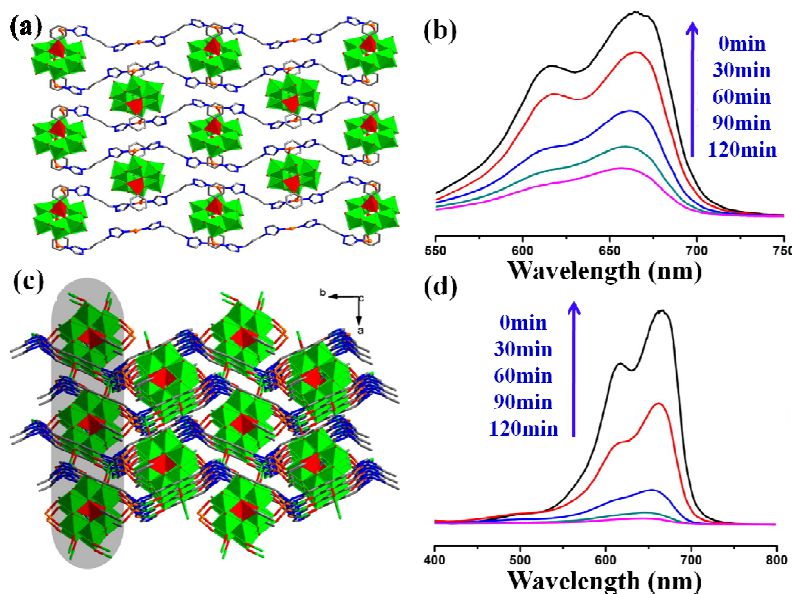


Fig. 13 (a) Structures of  $[\text{Ag}(4,4'\text{-bpy})]_4\text{V}_4\text{O}_{12}\cdot 2\text{H}_2\text{O}$  viewed down the  $[001]$  direction of the unit cells (outlined). Blue polyhedra = Ag-centered

coordination environments, red polyhedra = VO<sub>4</sub>, red spheres = O, yellow spheres = N, white spheres = C, and light-blue spheres = Ag. **(b)** Polyhedral structural view of Ag<sub>4</sub>(pzc)<sub>2</sub>V<sub>2</sub>O<sub>6</sub> down the [100] direction of the unit cell (outlined). Blue polyhedra = Ag-centered coordination environments, red polyhedra = VO<sub>5</sub>, red spheres = O, yellow spheres = N, white spheres = C, and light-blue spheres = Ag. All H atoms are omitted for clarity. **(c)** Photocatalytic decomposition of MB solutions (6.0 mg L<sup>-1</sup>, 50 mL) using 150 mg of the three silver vanadates, either under UV (upper) or under visible-light (lower) irradiation for [Ag(4,4'-bpy)]<sub>4</sub>V<sub>4</sub>O<sub>12</sub>·2H<sub>2</sub>O (ii), [Ag(dpa)]<sub>4</sub>V<sub>4</sub>O<sub>12</sub>·4H<sub>2</sub>O (iii), Ag<sub>4</sub>(pzc)<sub>2</sub>V<sub>2</sub>O<sub>6</sub> (iv). Photolysis of MB without the use of the photocatalysts (i). Reprinted (adapted) with permission from ref. 74. Copyright (2008) American Chemical Society.

Similarly, Ma and co-workers reported four MOFs [Cu<sup>I</sup><sub>2</sub>(1,3-btp)<sub>2</sub>][Cu<sup>I</sup><sub>2</sub>(*trans*-1,3-btp)<sub>2</sub>Mo<sub>6</sub>O<sub>18</sub>(O<sub>3</sub>AsPh)<sub>2</sub>] (**1**), Cu<sup>I</sup><sub>4</sub>(1,4-btp)<sub>4</sub>Mo<sub>6</sub>O<sub>18</sub>(O<sub>3</sub>AsPh)<sub>2</sub> (**2**), Cu<sup>I</sup><sub>4</sub>(1,5-btp)<sub>4</sub>Mo<sub>6</sub>O<sub>18</sub>(O<sub>3</sub>AsPh)<sub>2</sub> (**3**), and Cu<sup>I</sup><sub>4</sub>(1,6-bth)<sub>2</sub>Mo<sub>6</sub>O<sub>18</sub>(O<sub>3</sub>AsPh)<sub>2</sub> (**4**) constructed from [Mo<sub>6</sub>O<sub>18</sub>(O<sub>3</sub>AsPh)<sub>2</sub>]<sup>4-</sup> units and copper-organic fragments, with band gaps (*E<sub>g</sub>*) of 2.6, 2.7, 2.1 and 1.9 eV, respectively.<sup>238</sup> The photocatalytic degradation experiments of MB revealed that the activities of **1**, **3**, and **4** increased from 35% (without catalysts) to 76%, 93%, and 97%, respectively, while **2** did not show an active in the degradation. Notably, although **1**–**3** have an overall 3D structures, the extended As<sub>2</sub>Mo<sub>6</sub>-containing entities in **1** are different from those in **2** and **3**. The former one contained the only 2D [Mo<sub>6</sub>O<sub>18</sub>(O<sub>3</sub>AsPh)<sub>2</sub>]<sup>4-</sup> (as As<sub>2</sub>Mo<sub>6</sub>) layer. However, in **3** and **4**, the As<sub>2</sub>Mo<sub>6</sub><sup>-</sup> containing structures showed the 3D polycatenated framework and the 3D tetranodal (3,4,6)-connected framework, respectively. Obviously, in **3** and **4**, the photocatalytic active As<sub>2</sub>Mo<sub>6</sub> polyoxoanions distributed overall the 3D framework, as shown in Fig. 14a and c. The photocatalytic results of **1**, **3**, and **4** indicated that the more extended 3D As<sub>2</sub>Mo<sub>6</sub>-containing frameworks of the later two had an advantage over the 2D As<sub>2</sub>Mo<sub>6</sub>-containing layer of the former one during the photocatalytic decomposition reaction with MB. In other words, the more extended As<sub>2</sub>Mo<sub>6</sub><sup>-</sup> containing frameworks of **3** and **4** favored the transport of excited holes/electrons to the surfaces to initiate the photocatalytic decomposition reaction with MB,<sup>238</sup> as illustrated in Fig. 14b and d. After the photocatalytic reactions, the PXRD patterns were used in order to evaluate the photostabilities of the MOFs **1**, **3**, and **4**. The PXRD patterns were nearly identical to those of the original MOFs, implying that these three MOFs could be used as stable photocatalysts for the photodegradation of MB. Similar results could be found in other works reported by Ma and co-workers.<sup>245-247,249</sup>



**Fig. 14** (a) 2D highly undulated layer in  $[\text{Cu}_2^{\text{I}}(1,3\text{-btp})_2][\text{Cu}_2^{\text{I}}(\text{trans}\text{-}1,3\text{-btp})_2\text{Mo}_6\text{O}_{18}(\text{O}_3\text{AsPh})_2]$ . (b) UV-vis absorption spectra of the MB solution during the decomposition reaction under UV light irradiation in the presence of  $[\text{Cu}_2^{\text{I}}(1,3\text{-btp})_2][\text{Cu}_2^{\text{I}}(\text{trans}\text{-}1,3\text{-btp})_2\text{Mo}_6\text{O}_{18}(\text{O}_3\text{AsPh})_2]$ . (c) View of the 3D framework of  $\text{Cu}_4^{\text{I}}(1,6\text{-bth})_2\text{Mo}_6\text{O}_{18}(\text{O}_3\text{AsPh})_2$  formed by infinite chains and parallel layers. (d) UV-vis absorption spectra of the MB solution during the decomposition reaction under UV light irradiation in the presence of  $\text{Cu}_4^{\text{I}}(1,6\text{-bth})_2\text{Mo}_6\text{O}_{18}(\text{O}_3\text{AsPh})_2$ . Reprinted (adapted) with permission from ref. 238. Copyright (2013) American Chemical Society.

$[\text{Cu}_6(\text{PO}_4)_2(\text{H}_2\text{O})_4(\text{phen})_6](\text{P}_2\text{W}_{18}\text{O}_{62})$  (CuPW) constructed from Wells-Dawson polyoxometalates and hexacopper phosphates is another POM-based MOF, showing an efficient photocatalytic activity in the degradation of MO, reported by Cao and co-workers<sup>252</sup>. Visible light diffuse reflectance spectrum of CuPW showed a broad band centered at 690 nm, implying that the charge transfer existed between  $[\text{Cu}_6(\text{PO}_4)_2(\text{H}_2\text{O})_4(\text{phen})_6]^{6+}$  and  $(\text{P}_2\text{W}_{18}\text{O}_{62})^{6-}$ . It was proposed that in this MOF  $[\text{Cu}_6(\text{PO}_4)_2(\text{H}_2\text{O})_4(\text{phen})_6]^{6+}$  units can act as a sensitizer (S), being induced by visible light, then the electrons can transmit into the LUMO of  $(\text{P}_2\text{W}_{18}\text{O}_{62})^{6-}$  from them and deposit in its LUMO. The POM core is just like an electron reservoir, which could undergo electron-reduction processes without deforming the whole framework, as illustrated in Fig. 15a and b. In addition, in this system the adsorbed  $\text{H}_2\text{O}_2$  could easily trap an electron in LUMO of the POM anion to yield the oxidizing species  $\bullet\text{OH}$  radicals, which degrade dye molecules.

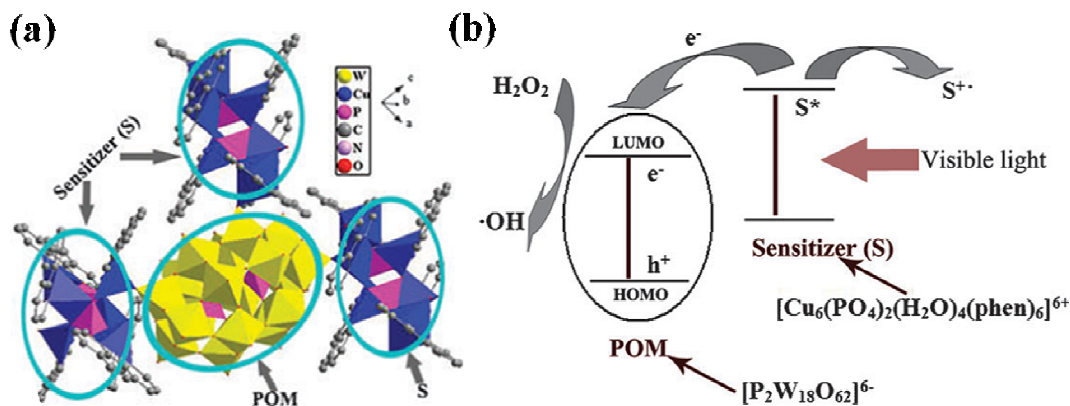


Fig. 15 (a) Relationships between the hexacopper phosphate cluster as sensitizer and the Wells–Dawson polyoxoanions as POM unit in CuPW. (b)

Proposed photodegradation mechanism on CuPM. Reprinted (adapted) with permission from ref. 252. Copyright (2010) The Royal Society of Chemistry.

It is also interesting to combine POM with lanthanide ions due to their unusual coordination characteristics, exceptional optical, and magnetic properties arising from 4*f* electrons.<sup>299-301</sup> It was found that the introduction of Ln(III)-ligand entities could enhance the photocatalytic activity of POMs, being similar to the case that lanthanide ions have the ability to enhance the photocatalytic activity of TiO<sub>2</sub>.<sup>302-304</sup> Chen and co-workers reported three α-Keggin heteropolymolybdates based MOFs, [2,6-pdc]<sub>3</sub>(PMo<sub>12</sub>O<sub>40</sub>), [Sm(H<sub>2</sub>O)<sub>4</sub>(2,6-pdc)]<sub>3</sub>[Sm(H<sub>2</sub>O)<sub>3</sub>(2,6-pdc)]-(SiMo<sub>12</sub>O<sub>40</sub>)·3H<sub>2</sub>O, and [La(H<sub>2</sub>O)<sub>4</sub>(2,6-pdc)]<sub>4</sub>(PMo<sub>12</sub>O<sub>40</sub>)F, which are active in the photocatalytic degradation of RhB.<sup>211</sup> The results revealed that the decomposition efficiencies of RhB over the latter two MOFs were higher than the former one. This result showed that the photocatalytic ability of a POM-based MOF can be enhanced by adding lanthanide ions into its structure being comparable to those in TiO<sub>2</sub> based systems. It is proposed that in the latter two MOFs, lanthanide ions could be used as an electron trapper under UV irradiation, thereby decreasing the recombination rate of photo-generated electron–hole pairs, and increasing the quantum yield of the photocatalytic process.<sup>305</sup> In contrast, Wang and co-workers showed that the lanthanide ions could effectively prohibited the photodegradation of RhB in MOFs [La(2,5-Hpdc)(2,5-pdc)(H<sub>2</sub>O)<sub>6</sub>La(2,5-H<sub>2</sub>pdc)<sub>0.5</sub>(α-PW<sub>11</sub>O<sub>39</sub>H)La(H<sub>2</sub>O)<sub>4</sub>]<sub>2</sub>·8H<sub>2</sub>O, [Ce(2,5-Hpdc)(2,5-pdc)(H<sub>2</sub>O)<sub>6</sub>Ce(2,5-H<sub>2</sub>pdc)<sub>0.5</sub>(α-PW<sub>11</sub>O<sub>39</sub>H)Ce(H<sub>2</sub>O)<sub>4</sub>]<sub>2</sub>·12H<sub>2</sub>O, and [Pr(2,5-Hpdc)(2,5-pdc)(H<sub>2</sub>O)<sub>6</sub>Pr(2,5-H<sub>2</sub>pdc)<sub>0.5</sub>(α-PW<sub>11</sub>O<sub>39</sub>H)Pr(H<sub>2</sub>O)<sub>4</sub>]<sub>2</sub>·8H<sub>2</sub>O.<sup>306</sup> It was explained as: (i) these MOFs can absorb the UV irradiation; and (ii) the hydrogen bonding and weak π–π stacking interactions between RhB and these MOFs can enhance the chemical stability of RhB, finally resulting in its slow photodegradation.<sup>307</sup>

## 5. Conclusion and outlooks

MOFs are a class of new inorganic-organic materials constructed from well-defined molecular building blocks of metal-containing nodes and organic linkers. The ability to design framework structure and incorporate molecular functional components into MOFs has opened the door for their various potential applications. Emerging research has demonstrated MOFs to be a new class of photocatalysts for potential applications in environmental field, such as in organic pollutants degradation. Comparing with conventional semiconductor photocatalytic systems, the photoactive MOF systems have some advantages in degrading organic pollutants: (i) versatile synthetic strategies, including solvothermal, vapor diffusion, emulsion-assistant precipitation, ultrasonication, and even post-synthesis modification, allow a high degree of crystalline quality and morphologies of MOFs photocatalysts; (ii) the well-defined crystalline structures of MOFs are beneficial in the characterization and study of structure-property relationship of these solid photocatalysts; (iii) the modular nature of the MOFs synthesis allows the rational design and fine tuning of these catalysts at the molecular level, making the electronic structure of the MOFs catalysts to be easily tailored; (iv) the structural features of tunable active sites (i.e., metal-oxoclusters and organic linkers) in MOFs lead to solar harnessing more efficiently; (v) the intrinsic porosity and high surface area of MOFs can facilitate the diffusion of the pollutants and products molecules through their open channels, where active catalytic sites located, thereby reaching a high efficiency of the catalytic reaction; (vi) different from typical TiO<sub>2</sub>-based catalysts, the visible light photocatalytic activity can be easily introduced via the linker substitutions of organic chromophores in MOF structures, such as with an amino group,<sup>61, 174, 308-310</sup> (vii) the combination of the photocatalytic properties of TiO<sub>2</sub> with the strong adsorbing properties of some MOFs (like ZIF-8) can generate composite materials with enhanced catalytic efficiency and better visible light response<sup>311</sup>. Further development of these new photocatalysts will require a better understanding of the photochemical mechanisms in MOFs materials and the crucial structural parameters controlling their photocatalytic activity. It should be pointed out that some MOFs were labeled as semiconductors based on their optical transition properties and electrochemical and photochemical activities.<sup>61,312,313</sup> But, recently Gascon and co-workers pointed out that such semiconducting behavior only occurs in a very limited subset of MOFs.<sup>72</sup> In the photocatalysis, MOFs should be treated as molecular catalysts rather than as typical semiconductors.<sup>72,314</sup> To understand the photocatalysis mechanisms of MOFs, they suggested that the terminology of HOMO-LUMO gap should be utilized to describe the discrete character of the light-induced transitions in the MOFs.<sup>72</sup> In all, we believe that the MOFs are promising for use in wastewater treatment, and to this end, they could serve as an ideal choice for light harvesting to achieve photocatalytic degradation of organic pollutants.<sup>311</sup>

Up to now, it is difficult to perform a high-throughput synthesis with amount of kilogram quantities in a matter of hours at ambient pressure, which is an impediment in the achievement of MOFs practical applications. The commonly used solvothermal methods, involving the use of autoclaves and slow-diffusion processes, take days or weeks to complete a MOF synthesis reaction, making difficulty in an industrial preparation of these materials.<sup>1,316</sup> On the other hand, the relatively poor stability is an additional disadvantage of most MOFs. Particularly, many MOFs are known to be unstable in the presence of water,<sup>317</sup> which limit their practical applications in solar energy utilization. Some MOFs based on “hard” metal ions (like  $Zr^{4+}$ ,  $Ti^{4+}$ , and  $Fe^{3+}$ ) linked by organic carboxylate ligands (e.g. UiOs, MIL-140, -125, -101), or soft metal ions (like  $Zn^{2+}$ ) with imidazolate linkers (e.g. ZIFs) have however shown high stability in aqueous solutions. The development of these stable MOFs is thus promising and urgently requisite for their practical applications, such as the photocatalytic pollutants degradation in wastewater treatment. In addition, most of MOFs also suffer from weak mechanical properties, bad processability, and low electric conductivity, all of which hinder the integration of MOFs into functional solar devices.<sup>262</sup> Therefore, to get cheap, stable, and efficient MOFs served as photocatalysts for practical applications is still a challenge.

Availability of the cheap starting materials and the feasibility of obtaining products with high yield and high purity should be considered when designing new MOFs. Simultaneously, the synthetic methods should be developed, so as to obtain low-cost MOFs. Particularly, the choice of ligands and metal salts is significant in designing novel MOFs for the photocatalysis, which determines the efficiency of their applications. Finally, we hope these new materials with high working capacity in photocatalysis can serve as alternatives to replace commercially-available metal oxides and sulfides catalysts. In the future, MOFs might be one of the most powerful photocatalysts for the green environment.

## Acknowledgements

We thank the financial support from the Natural Science Foundation of China (No. 21271015, 21322601), the Program for New Century Excellent Talents in University (No. NCET-13-0647), the Beijing Municipal Natural Science Foundation (No. 2132013), the Beijing Natural Science Foundation & Scientific Research Key Program of Beijing Municipal Commission of Education (KZ201410016018), the Training Program Foundation for the Beijing Municipal Excellent Talents(2013D005017000004), the Importation & Development of High-Caliber Talents Project of Beijing Municipal Institutions (CIT&CD201404076), the China

Postdoctoral Science of Foundation (2013M540831), and Academic Innovation Team of BUCEA.

## References

1. A. A. Adeyemo, I. O. Adeoye and O. S. Bello, *Toxicol. Environ. Chem.*, 2012, **94**, 1846-1863.
2. G. Liu, X. Li, J. Zhao, H. Hidaka and N. Serpone, *Environ. Sci. Technol.*, 2000, **34**, 3982-3990.
3. G. L. Baughman and E. J. Weber, *Environ. Sci. Technol.*, 1994, **28**, 267-276.
4. J. Levec and A. Pintar, *Catal. Today*, 2007, **124**, 172-184.
5. I. Ali, M. Asim and T. A. Khan, *J. Environ. Manage.*, 2012, **113**, 170-183.
6. W.-T. Tsai, H.-C. Hsu, T.-Y. Su, K.-Y. Lin, C.-M. Lin and T.-H. Dai, *J. Hazard. Mater.*, 2007, **147**, 1056-1062.
7. C. Wang, J. Zhang, P. Wang, H. Wang and H. Yan, *Desalin. Water Treat.*, 2014, DOI: 10.1080/19443994.2013.873881.
8. S. Allen and B. Koumanova, *J. Univ. Chem. Technol. Metallurgy*, 2005, **40**, 175-192.
9. D. Wang, T. Silbaugh, R. Pfeffer and Y. Lin, *Powder Technol.*, 2010, **203**, 298-309.
10. D. Lin, Q. Zhao, L. Hu and B. Xing, *Chemosphere*, 2014, **103**, 188-196.
11. P. Padmanabhan, K. Sreekumar, T. Thiagarajan, R. Satpute, K. Bhanumurthy, P. Sengupta, G. Dey and K. Warriar, *Vacuum*, 2006, **80**, 1252-1255.
12. U. I. Gaya and A. H. Abdullah, *J. Photoch. Photobio. C.*, 2008, **9**, 1-12.
13. M. N. Chong, B. Jin, C. W. Chow and C. Saint, *Water Res.*, 2010, **44**, 2997-3027.
14. H. Yang and H. Cheng, *Sep. Purif. Technol.*, 2007, **56**, 392-396.
15. J. Lu, T. Zhang, J. Ma and Z. Chen, *J. Hazard. Mater.*, 2009, **162**, 140-145.
16. H. Coleman, C. Marquis, J. Scott, S.-S. Chin and R. Amal, *Chem. Eng. J.*, 2005, **113**, 55-63.
17. D. H. Bremner, R. Molina, F. Martínez, J. A. Melero and Y. Segura, *Appl. Catal. B-Environ.*, 2009, **90**, 380-388.
18. M. I. Litter, *Appl. Catal. B-Environ.*, 1999, **23**, 89-114.
19. G. Li, Z. Wang, M. Yu, Z. Quan and J. Lin, *J. Solid State Chem.*, 2006, **179**, 2698-2706.
20. G. Li, M. Yu, Z. Wang, J. Lin, R. Wang and J. Fang, *J. Nanosci. Nanotechnol.*, 2006, **6**, 1416-1422.
21. J. Lü, J.-X. Lin, X.-L. Zhao and R. Cao, *Chem. Commun.*, 2012, **48**, 669-671.
22. M. R. Hoffmann, S. T. Martin, W. Choi and D. W. Bahnemann, *Chem. Rev.*, 1995, **95**, 69-96.
23. T. L. Thompson and J. T. Yates, *Chem. Rev.*, 2006, **106**, 4428-4453.
24. A. Mills and S. Le Hunte, *J. Photoch. Photobio. A*, 1997, **108**, 1-35.
25. K. Ayoub, E. D. van Hullebusch, M. Cassir and A. Bermond, *J. Hazard. Mater.*, 2010, **178**, 10-28.

26. U. Akpan and B. Hameed, *J. Hazard. Mater.*, 2009, **170**, 520-529.
27. J. J. Du, Y. P. Yuan, J. X. Sun, F. M. Peng, X. Jiang, L. G. Qiu, A. J. Xie, Y. H. Shen and J. F. Zhu, *J. Hazard. Mater.*, 2011, **190**, 945-951.
28. K. Nakata and A. Fujishima, *J. Photoch. Photobio. C.*, 2012, **13**, 169-189.
29. A. Janczyk, E. Krakowska, G. Stochel and W. Macyk, *J. Am. Chem. Soc.*, 2006, **128**, 15574-15575.
30. A. Y. Nosaka, E. Kojima, T. Fujiwara, H. Yagi, H. Akutsu and Y. Nosaka, *J. Phys. Chem. B*, 2003, **107**, 12042-12044.
31. A. Fujishima, X. Zhang and D. A. Tryk, *Int. J. Hydrogen Energ.*, 2007, **32**, 2664-2672.
32. R. Wang, K. Hashimoto, A. Fujishima, M. Chikuni, E. Kojima, A. Kitamura, M. Shimohigoshi and T. Watanabe, *Nature*, 1997, **388**, 431-432.
33. C. Wang, H.-Y. Li, G.-L. Guo and P. Wang, *Transit. Metal Chem.*, 2013, **38**, 275-282.
34. C. Wang, G.-L. Guo and P. Wang, *Transit. Metal Chem.*, 2013, **38**, 455-462.
35. C. Wang, G. Guo and P. Wang, *J. Mol. Struct.*, 2012, **1032**, 93-99.
36. C. Wang, Z. Wang, F. Gu and G. Guo, *J. Mol. Struct.*, 2011, **1004**, 39-44.
37. C. Wang, P. Wang and G. Guo, *Transit. Metal Chem.*, 2010, **35**, 721-729.
38. C. Wang, Z. Wang, F. Gu and G. Guo, *J. Mol. Struct.*, 2010, **979**, 92-100.
39. J. Lee, O. K. Farha, J. Roberts, K. A. Scheidt, S. T. Nguyen and J. T. Hupp, *Chem. Soc. Rev.*, 2009, **38**, 1450-1459.
40. C.-Y. Sun, S.-X. Liu, D.-D. Liang, K.-Z. Shao, Y.-H. Ren and Z.-M. Su, *J. Am. Chem. Soc.*, 2009, **131**, 1883-1888.
41. R. J. Kuppler, D. J. Timmons, Q.-R. Fang, J.-R. Li, T. A. Makal, M. D. Young, D. Yuan, D. Zhao, W. Zhuang and H.-C. Zhou, *Coord. Chem. Rev.*, 2009, **253**, 3042-3066.
42. X.-S. Wang, S. Ma, D. Sun, S. Parkin and H.-C. Zhou, *J. Am. Chem. Soc.*, 2006, **128**, 16474-16475.
43. J.-R. Li, J. Yu, W. Lu, L.-B. Sun, J. Sculley, P. B. Balbuena and H.-C. Zhou, *Nat. Commun.*, 2013, **4**, 1538.
44. J.-R. Li, J. Sculley and H.-C. Zhou, *Chem. Rev.*, 2011, **112**, 869-932.
45. J.-R. Li and H.-C. Zhou, *Nat. Chem.*, 2010, **2**, 893-898.
46. J.-R. Li, D. J. Timmons and H.-C. Zhou, *J. Am. Chem. Soc.*, 2009, **131**, 6368-6369.
47. J.-R. Li, R. J. Kuppler and H.-C. Zhou, *Chem. Soc. Rev.*, 2009, **38**, 1477-1504.
48. L. Pan, D. H. Olson, L. R. Ciemmolonski, R. Heddy and J. Li, *Angew. Chem. Int. Ed.*, 2006, **118**, 632-635.
49. N. L. Rosi, J. Eckert, M. Eddaoudi, D. T. Vodak, J. Kim, M. O'Keeffe and O. M. Yaghi, *Science*, 2003, **300**, 1127-1129.
50. J. L. Rowsell and O. M. Yaghi, *Angew. Chem. Int. Ed.*, 2005, **44**, 4670-4679.

51. D. J. Collins and H.-C. Zhou, *J. Mater. Chem.*, 2007, **17**, 3154-3160.
52. S. Ma and H.-C. Zhou, *Chem. Commun.*, 2010, **46**, 44-53.
53. K. Sumida, D. L. Rogow, J. A. Mason, T. M. McDonald, E. D. Bloch, Z. R. Herm, T.-H. Bae and J. R. Long, *Chem. Rev.*, 2011, **112**, 724-781.
54. J.-R. Li, Y. Ma, M. C. McCarthy, J. Sculley, J. Yu, H.-K. Jeong, P. B. Balbuena and H.-C. Zhou, *Coord. Chem. Rev.*, 2011, **255**, 1791-1823.
55. A. R. Millward and O. M. Yaghi, *J. Am. Chem. Soc.*, 2005, **127**, 17998-17999.
56. J. M. Simmons, H. Wu, W. Zhou and T. Yildirim, *Energ. Environ. Sci.*, 2011, **4**, 2177-2185.
57. C. Wang, P. Wang and L. Feng, *Transit. Metal Chem.*, 2012, **37**, 225-234.
58. L.-B. Sun, J.-R. Li, W. Lu, Z.-Y. Gu, Z. Luo and H.-C. Zhou, *J. Am. Chem. Soc.*, 2012, **134**, 15923-15928.
59. Y. Xie, H. Yang, Z. U. Wang, Y. Liu, H.-C. Zhou and J.-R. Li, *Chem. Commun.*, 2014, **50**, 563-565.
60. H.-C. Zhou, J. R. Long and O. M. Yaghi, *Chem. Rev.*, 2012, **112**, 673-674.
61. C. G. Silva, A. Corma and H. García, *J. Mater. Chem.*, 2010, **20**, 3141-3156.
62. F. X. Llabrés i Xamena, A. Corma and H. Garcia, *J. Phys. Chem. C*, 2007, **111**, 80-85.
63. P. Mahata, G. Madras and S. Natarajan, *J. Phys. Chem. B*, 2006, **110**, 13759-13768.
64. J. Gascon, M. D. Hernández - Alonso, A. R. Almeida, G. P. van Klink, F. Kapteijn and G. Mul, *ChemSusChem*, 2008, **1**, 981-983.
65. S. Bordiga, C. Lamberti, G. Ricchiardi, L. Regli, F. Bonino, A. Damin, K.-P. Lillerud, M. Bjorgen and A. Zecchina, *Chem. Commun.*, 2004, 2300-2301.
66. T. Tachikawa, J. R. Choi, M. Fujitsuka and T. Majima, *J. Phys. Chem. C*, 2008, **112**, 14090-14101.
67. P. Mahata, G. Madras and S. Natarajan, *Catal. Lett.*, 2007, **115**, 27-32.
68. M. Alvaro, E. Carbonell, B. Ferrer, F. X. Llabrés i Xamena and H. Garcia, *Chem-Eur. J.*, 2007, **13**, 5106-5112.
69. Y. Horiuchi, T. Toyao, M. Takeuchi, M. Matsuoka and M. Anpo, *Phys. Chem. Chem. Phys.*, 2013, **15**, 13243-13253.
70. T. Zhang and W. Lin, *Chem. Soc. Rev.*, 2014, DOI: 10.1039/C4CS00103F.
71. S. Li and Q. Xu, *Energ. Environ. Sci.*, 2013, **6**, 1656-1683.
72. M. A. Nasalevich, M. van der Veen, F. Kapteijn and J. Gascon, *CrystEngComm*, 2014, **16**, 4919-4926.
73. T. Zhang and W. Lin, *Structure and Bonding*, 2014, **157**, 89-104
74. H. Lin and P. A. Maggard, *Inorg. Chem.*, 2008, **47**, 8044-8052.
75. Z.-L. Liao, G.-D. Li, M.-H. Bi and J.-S. Chen, *Inorg. Chem.*, 2008, **47**, 4844-4853.
76. Z.-T. Yu, Z.-L. Liao, Y.-S. Jiang, G.-H. Li, G.-D. Li and J.-S. Chen, *Chem. Commun.*, 2004, 1814-1815.

77. Z. T. Yu, Z. L. Liao, Y. S. Jiang, G. H. Li and J. S. Chen, *Chem-Eur. J.*, 2005, **11**, 2642-2650.
78. T. Toyao, M. Saito, Y. Horiuchi, K. Mochizuki, M. Iwata, H. Higashimura and M. Matsuoka, *Catal. Sci. Technol.*, 2013, **3**, 2092-2097.
79. M. Kurmoo, *Chem. Soc. Rev.*, 2009, **38**, 1353-1379.
80. P. Valvekens, F. Vermoortele and D. De Vos, *Catal. Sci. Technol.*, 2013, **3**, 1435-1445.
81. L. Ma and W. Lin, in *Functional Metal-Organic Frameworks: Gas Storage, Separation and Catalysis*, Springer, 2010, 175-205.
82. P. Horcajada, T. Chalati, C. Serre, B. Gillet, C. Sebrie, T. Baati, J. F. Eubank, D. Heurtaux, P. Clayette and C. Kreuz, *Nat. Mater.*, 2009, **9**, 172-178.
83. P. Horcajada, C. Serre, M. Vallet - Regí, M. Sebban, F. Taulelle and G. Férey, *Angew. Chem. Int. Ed.*, 2006, **118**, 6120-6124.
84. H.-L. Jiang, B. Liu, T. Akita, M. Haruta, H. Sakurai and Q. Xu, *J. Am. Chem. Soc.*, 2009, **131**, 11302-11303.
85. S. L. James, *Chem. Soc. Rev.*, 2003, **32**, 276-288.
86. U. Mueller, M. Schubert, F. Teich, H. Puetter, K. Schierle-Arndt and J. Pastre, *J. Mater. Chem.*, 2006, **16**, 626-636.
87. S.-Y. Song, X.-Z. Song, S.-N. Zhao, C. Qin, S.-Q. Su, M. Zhu, Z.-M. Hao and H.-J. Zhang, *Dalton Trans.*, 2012, **41**, 10412-10421.
88. L. Ai, C. Zhang, L. Li and J. Jiang, *Appl. Catal. B-Environ.*, 2014, **148-149**, 191-200
89. C.-F. Zhang, L.-G. Qiu, F. Ke, Y.-J. Zhu, Y.-P. Yuan, G.-S. Xu and X. Jiang, *J. Mater. Chem. A*, 2013, **1**, 14329-14334.
90. T. Wen and J. Zhang, *Chem. Commun.*, 2013, **49**, 5660-5662.
91. H. Yang, X.-W. He, F. Wang, Y. Kang and J. Zhang, *J. Mater. Chem.*, 2012, **22**, 21849-21851.
92. S. E.-d. H. Etaiw and M. M. El-bendary, *Appl. Catal. B-Environ.*, 2012, **126**, 326-333.
93. M. C. Das, H. Xu, Z. Wang, G. Srinivas, W. Zhou, Y.-F. Yue, V. N. Nesterov, G. Qian and B. Chen, *Chem. Commun.*, 2011, **47**, 11715-11717.
94. L.-L. Wen, F. Wang, J. Feng, K.-L. Lv, C.-G. Wang and D.-F. Li, *Cryst. Growth Des.*, 2009, **9**, 3581-3589.
95. L. Wen, J. Zhao, K. Lv, Y. Wu, K. Deng, X. Leng and D. Li, *Cryst. Growth Des.*, 2012, **12**, 1603-1612.
96. W.-J. Ji, Q.-G. Zhai, S.-N. Li, Y.-C. Jiang and M.-C. Hu, *Inorg. Chem. Commun.*, 2012, **24**, 209-211.
97. W.-J. Ji, Q.-G. Zhai, S.-N. Li, Y.-C. Jiang and M.-C. Hu, *Inorg. Chem. Commun.*, 2013, **28**, 16-19.
98. Z.-Q. Li, M. Zhang, B. Liu, C.-Y. Guo and M. Zhou, *Inorg. Chem. Commun.*, 2013, **36**, 241-244.
99. W.-T. Xu, L. Ma, F. Ke, F.-M. Peng, G.-S. Xu, Y.-H. Shen, J.-F. Zhu, L.-G. Qiu and Y.-P. Yuan, *Dalton Trans.*, 2014,

- 43, 3792-3798.
100. L. Zhou, C. Wang, X. Zheng, Z. Tian, L. Wen, H. Qu and D. Li, *Dalton Trans.*, 2013, **42**, 16375-16386.
101. J. Gao, J. Miao, P.-Z. Li, Y. Zhao and B. Liu, *Chem. Commun.*, 2014, DOI: 10.1039/c1033cc49440c.
102. Y.-L. Hou, R. W.-Y. Sun, X.-P. Zhou, J.-H. Wang and D. Li, *Chem. Commun.*, 2014, **50**, 2295-2297.
103. K. K. Bisht, Y. Rachuri, B. Parmar and E. Suresh, *RSC Adv.*, 2014, **4**, 7352-7360.
104. S.-M. Chen, Y.-F. Chen, R. Lin, X.-P. Lei and J. Zhang, *CrystEngComm*, 2013, **15**, 10423-10426.
105. Y.-P. Wu, D.-S. Li, Y.-P. Duan, L. Bai and J. Zhao, *Inorg. Chem. Commun.*, 2013, **36**, 137-140.
106. X.-P. Zheng, Y. Lu, H. Zhang, Z.-M. Zhang and E.-B. Wang, *Inorg. Chem. Commun.*, 2013, **33**, 29-32.
107. A. K. Paul, G. Madras and S. Natarajan, *Phys. Chem. Chem. Phys.*, 2009, **11**, 11285-11296.
108. J. Guo, J.-F. Ma, J.-J. Li, J. Yang and S.-X. Xing, *Cryst. Growth Des.*, 2012, **12**, 6074-6082.
109. F. Luo, Z.-Z. Yuan, X.-F. Feng, S. R. Batten, J.-Q. Li, M.-B. Luo, S.-J. Liu, W.-Y. Xu, G.-M. Sun and Y.-M. Song, *Cryst. Growth Des.*, 2012, **12**, 3392-3396.
110. P. Du, Y. Yang, Y.-Y. Liu, Y.-C. He, H.-M. Zhang and J.-F. Ma, *Polyhedron*, 2014, **70**, 180-187.
111. Y.-Q. Chen, S.-J. Liu, Y.-W. Li, G.-R. Li, K.-H. He, Y.-K. Qu, T.-L. Hu and X.-H. Bu, *Cryst. Growth Des.*, 2012, **12**, 5426-5431.
112. S. Zhou, Z.-G. Kong, Q.-W. Wang and C.-B. Li, *Inorg. Chem. Commun.*, 2012, **25**, 1-4.
113. C. Y. Zhang, W. X. Ma, M. Y. Wang, X. J. Yang and X. Y. Xu, *Spectrochim. Acta A*, 2014, **118**, 657-662.
114. P. Mahata, G. Sankar, G. Madras and S. Natarajan, *Chem. Commun.*, 2005, 5787-5789.
115. Y. Gong, P.-G. Jiang, Y.-X. Wang, T. Wu and J.-H. Lin, *Dalton Trans.*, 2013, **42**, 7196-7203.
116. Y. Gong, T. Wu and J. Lin, *CrystEngComm*, 2012, **14**, 3727-3736.
117. L. Wen, L. Zhou, B. Zhang, X. Meng, H. Qu and D. Li, *J. Mater. Chem.*, 2012, **22**, 22603-22609.
118. X. Wang, J. Luan, H. Lin, C. Xu, G. Liu, J. Zhang and A. Tian, *CrystEngComm*, 2013, **15**, 9995-10006.
119. W.-Q. Kan, B. Liu, J. Yang, Y.-Y. Liu and J.-F. Ma, *Cryst. Growth Des.*, 2012, **12**, 2288-2298.
120. P. Du, Y. Yang, J. Yang, B.-K. Liu and J.-F. Ma, *Dalton Trans.*, 2013, **42**, 1567-1580.
121. H. Zhang, Y. Lu, Z.-m. Zhang and E.-b. Wang, *Inorg. Chem. Commun.*, 2012, **17**, 9-12.
122. A. K. Paul, R. Karthik and S. Natarajan, *Cryst. Growth Des.*, 2011, **11**, 5741-5749.
123. J. Guo, J. Yang, Y.-Y. Liu and J.-F. Ma, *CrystEngComm*, 2012, **14**, 6609-6617.
124. K. K. Bisht, Y. Rachuri, B. Parmar and E. Suresh, *J. Solid State Chem.*, 2014, **213**, 43-51.
125. X. Wang, J. Luan, F. Sui, H. Lin, G. Liu and C. Xu, *Cryst. Growth Des.*, 2013, **13**, 3561-3576.
126. T. Wen, D.-X. Zhang and J. Zhang, *Inorg. Chem.*, 2012, **52**, 12-14.

127. F. Wang, Z. S. Liu, H. Yang, Y. X. Tan and J. Zhang, *Angew. Chem. Int. Ed.*, 2011, **50**, 450-453.
128. H.-Y. Sun, C.-B. Liu, Y. Cong, M.-H. Yu, H.-Y. Bai and G.-B. Che, *Inorg. Chem. Commun.*, 2013, **35**, 130-134.
129. F. Wang, X. Ke, J. Zhao, K. Deng, X. Leng, Z. Tian, L. Wen and D. Li, *Dalton Trans.*, 2011, **40**, 11856-11865.
130. X. Wang, J. Luan, H. Lin, Q. Lu, C. Xu and G. Liu, *Dalton Trans.*, 2013, **42**, 8375-8386.
131. X.-L. Wang, J. Luan, H.-Y. Lin, G.-C. Liu and M. Le, *Polyhedron*, 2014, **71**, 111-118.
132. H. Qu, L. Qiu, X.-K. Leng, M.-M. Wang, S.-M. Lan, L.-L. Wen and D.-F. Li, *Inorg. Chem. Commun.*, 2011, **14**, 1347-1351.
133. X.-L. Wang, J. Luan, H.-Y. Lin, C. Xu and G.-C. Liu, *Inorg. Chim. Acta*, 2013, **408**, 139-144.
134. X. Zhu, S. Zhao, Y.-F. Peng, B.-L. Li and B. Wu, *CrystEngComm*, 2013, **15**, 9154-9160.
135. G.-H. Cui, C.-H. He, C.-H. Jiao, J.-C. Geng and V. A. Blatov, *CrystEngComm*, 2012, **14**, 4210-4216.
136. X. Li, J. Li, M.-K. Li and Z. Fei, *J. Mol. Struct.*, 2014, **1059**, 294-298.
137. X.-L. Wang, Y. Qu, G.-C. Liu, J. Luan, H.-Y. Lin and X.-M. Kan, *Inorg. Chim. Acta*, 2014, **412**, 104-113.
138. M. Wałęsa-Chorab, V. Patroniak, M. Kubicki, G. Kądziołka, J. Przepiórski and B. Michalkiewicz, *J. Catal.*, 2012, **291**, 1-8.
139. J.-W. Ran, S.-W. Liu, P. Wu and J. Pei, *Chin. Chem. Lett.*, 2013, **24**, 373-375.
140. C. Wang, H. Jing and P. Wang, *J. Mol. Struct.*, 2014, DOI: 10.1016/j.molstruc.2014.05.059.
141. H. Li, M. Eddaoudi, M. O'Keeffe and O. M. Yaghi, *Nature*, 1999, **402**, 276-279.
142. F. X. Llabrés i Xamena, P. Calza, C. Lamberti, C. Prestipino, A. Damin, S. Bordiga, E. Pelizzetti and A. Zecchina, *J. Am. Chem. Soc.*, 2003, **125**, 2264-2271.
143. P. Calza, C. Pazé, E. Pelizzetti and A. Zecchina, *Chem. Commun.*, 2001, 2130-2131.
144. C. Galindo, P. Jacques and A. Kalt, *J. Photoch. Photobio. A*, 2000, **130**, 35-47.
145. J. M. Joseph, H. Destailats, H.-M. Hung and M. R. Hoffmann, *J. Phys. Chem. A*, 2000, **104**, 301-307.
146. J. Saien and S. Khezrianjoo, *J. Hazard. Mater.*, 2008, **157**, 269-276.
147. K. Vasanth Kumar and A. Selvaganapathi, *Dyes Pigments*, 2007, **75**, 246-249.
148. B. Krishnakumar and M. Swaminathan, *Spectrochim. Acta A*, 2011, **81**, 739-744.
149. S. Bhattacharya and S. S. Mandal, *Chem. Commun.*, 1996, 1515-1516.
150. M. Saquib and M. Muneer, *Dyes Pigments*, 2002, **53**, 237-249.
151. M. Stylidi, D. I. Kondarides and X. E. Verykios, *Appl. Catal. B-Environ.*, 2003, **40**, 271-286.
152. T. Watanabe, T. Takizawa and K. Honda, *J. Phys. Chem.*, 1977, **81**, 1845-1851.
153. B. Civalieri, F. Napoli, Y. Noël, C. Roetti and R. Dovesi, *CrystEngComm*, 2006, **8**, 364-371.

154. Q. Xiao, Z. Si, J. Zhang, C. Xiao and X. Tan, *J. Hazard. Mater.*, 2008, **150**, 62-67.
155. J. Yu, W. Wang, B. Cheng and B.-L. Su, *J. Phys. Chem. C*, 2009, **113**, 6743-6750.
156. X. Yu, J. Yu, B. Cheng and M. Jaroniec, *J. Phys. Chem. C*, 2009, **113**, 17527-17535.
157. D.-E. Wang, K.-J. Deng, K.-L. Lv, C.-G. Wang, L.-L. Wen and D.-F. Li, *CrystEngComm*, 2009, **11**, 1442-1450.
158. Z. Sun, Y. Chen, Q. Ke, Y. Yang and J. Yuan, *J. Photoch. Photobio. A*, 2002, **149**, 169-174.
159. Y. Liu and R. O. Claus, *J. Am. Chem. Soc.*, 1997, **119**, 5273-5274.
160. J. K. Barton and A. L. Raphael, *J. Am. Chem. Soc.*, 1984, **106**, 2466-2468.
161. S. Yan, Z. Li and Z. Zou, *Langmuir*, 2010, **26**, 3894-3901.
162. A. Syoufian and K. Nakashima, *J. Colloid Interf. Sci.*, 2008, **317**, 507-512.
163. H.-Y. Shu, M.-C. Chang and H.-J. Fan, *J. Hazard. Mater.*, 2004, **113**, 201-208.
164. S. Zhang, X. Zhao, H. Niu, Y. Shi, Y. Cai and G. Jiang, *J. Hazard. Mater.*, 2009, **167**, 560-566.
165. Q. Jiang, A.-M. Spehar, M. Håkansson, J. Suomi, T. Ala-Kleme and S. Kulmala, *Electrochim. Acta*, 2006, **51**, 2706-2714.
166. R. Idel-aouad, M. Valiente, A. Yaacoubi, B. Tanouti and M. López-Mesas, *J. Hazard. Mater.*, 2011, **186**, 745-750.
167. M. Xia, M. Long, Y. Yang, C. Chen, W. Cai and B. Zhou, *Appl. Catal. B-Environ.*, 2011, **110**, 118-125.
168. Q. Chen, P. Wu, Y. Li, N. Zhu and Z. Dang, *J. Hazard. Mater.*, 2009, **168**, 901-908.
169. C. Galindo, P. Jacques and A. Kalt, *J. Photoch. Photobio. A*, 2001, **141**, 47-56.
170. C. Galindo and A. Kalt, *Dyes Pigments*, 1999, **40**, 27-35.
171. M. Dan-Hardi, C. Serre, T. O. Frot, L. Rozes, G. Maurin, C. M. Sanchez and G. R. Férey, *J. Am. Chem. Soc.*, 2009, **131**, 10857-10859.
172. Y. Horiuchi, T. Toyao, M. Saito, K. Mochizuki, M. Iwata, H. Higashimura, M. Anpo and M. Matsuoka, *J. Phys. Chem. C*, 2012, **116**, 20848-20853.
173. C. H. Hendon, D. Tiana, M. Fontecave, C. Sanchez, L. D'arras, C. Sassoeye, L. Rozes, C. Mellot-Draznieks and A. Walsh, *J. Am. Chem. Soc.*, 2013, **135**, 10942-10945.
174. Y. Fu, D. Sun, Y. Chen, R. Huang, Z. Ding, X. Fu and Z. Li, *Angew. Chem. Int. Ed.*, 2012, **124**, 3420-3423.
175. M. A. Nasalevich, M. G. Goesten, T. J. Savenije, F. Kapteijn and J. Gascon, *Chem. Commun.*, 2013, **49**, 10575-10577.
176. L. Que and W. B. Tolman, *Nature*, 2008, **455**, 333-340.
177. S. Afzal, W. A. Daoud and S. J. Langford, *ACS Appl. Mater. Inter.*, 2013, **5**, 4753-4759
178. Y. Numata, S. P. Singh, A. Islam, M. Iwamura, A. Imai, K. Nozaki and L. Han, *Adv. Funct. Mater.*, 2013, **23**,

- 1817-1823.
179. M. Hussain, A. El-Shafei, A. Islam and L. Han, *Phys. Chem. Chem. Phys.*, 2013, **15**, 8401-8408.
180. Z. Lu, M. Shen and T. P. Yoon, *J. Am. Chem. Soc.*, 2011, **133**, 1162-1164.
181. C.-J. Wallentin, J. D. Nguyen, P. Finkbeiner and C. R. J. Stephenson, *J. Am. Chem. Soc.*, 2012, **134**, 8875-8884.
182. S. Zhang, L. Han, L. Li, J. Cheng, D. Yuan and J. Luo, *Cryst. Growth Des.*, 2013, **13**, 5466-5472.
183. Y. Wang, R. Shi, J. Lin and Y. Zhu, *Energ. Environ. Sci.*, 2011, **4**, 2922-2929.
184. X. C. Huang, Y. Y. Lin, J. P. Zhang and X. M. Chen, *Angew. Chem. Int. Ed.*, 2006, **118**, 1587-1589.
185. Y.-Q. Tian, Y.-M. Zhao, Z.-X. Chen, G.-N. Zhang, L.-H. Weng and D.-Y. Zhao, *Chem-Eur. J.*, 2007, **13**, 4146-4154.
186. A. Phan, C. J. Doonan, F. J. Uribe-Romo, C. B. Knobler, M. O'keeffe and O. M. Yaghi, *Acc. Chem. Res.*, 2010, **43**, 58-67.
187. R. Banerjee, A. Phan, B. Wang, C. Knobler, H. Furukawa, M. O'Keeffe and O. M. Yaghi, *Science*, 2008, **319**, 939-943.
188. L. Zheng, Y. Xu, Y. Song, C. Wu, M. Zhang and Y. Xie, *Inorg. Chem.*, 2009, **48**, 4003-4009.
189. S. L. Castro, S. G. Bailey, R. P. Raffaele, K. K. Banger and A. F. Hepp, *Chem. Mater.*, 2003, **15**, 3142-3147.
190. X.-C. Huang, J.-P. Zhang and X.-M. Chen, *J. Am. Chem. Soc.*, 2004, **126**, 13218-13219.
191. G. Liao, S. Chen, X. Quan, H. Yu and H. Zhao, *J. Mater. Chem.*, 2012, **22**, 2721-2726.
192. V. Štengl, D. Popelková and P. Vláčil, *J. Phys. Chem. C*, 2011, **115**, 25209-25218.
193. Y. Fu and X. Wang, *Ind. Eng. Chem. Res.*, 2011, **50**, 7210-7218.
194. Y. Fu, P. Xiong, H. Chen, X. Sun and X. Wang, *Ind. Eng. Chem. Res.*, 2011, **51**, 725-731.
195. C. Petit and T. J. Bandoz, *Adv. Mater.*, 2009, **21**, 4753-4757.
196. C. Petit and T. J. Bandoz, *Adv. Funct. Mater.*, 2011, **21**, 2108-2117.
197. Y. Zhang, G. Li, H. Lu, Q. Lv and Z. Sun, *RSC Adv.*, 2014, **4**, 7594-7600.
198. 250. H. Ma, J. Shen, M. Shi, X. Lu, Z. Li, Y. Long, N. Li and M. Ye, *Appl. Catal. B-Environ.*, 2012, **121**, 198-205.
199. Z.-H. Huang, G. Liu and F. Kang, *ACS Appl. Mater. Inter.*, 2012, **4**, 4942-4947.
200. R. Kumar, K. Jayaramulu, T. K. Maji and C. Rao, *Chem. Commun.*, 2013, **49**, 4947-4949.
201. Y. Zhao, M. Seredych, Q. Zhong and T. J. Bandoz, *RSC Adv.*, 2013, **3**, 9932-9941.
202. M. Jahan, Q. Bao, J.-X. Yang and K. P. Loh, *J. Am. Chem. Soc.*, 2010, **132**, 14487-14495.
203. C. Petit, B. Levasseur, B. Mendoza and T. J. Bandoz, *Micropor. Mesopor. Mat.*, 2012, **154**, 107-112.
204. R. Jin, Z. Bian, J. Li, M. Ding and L. Gao, *Dalton Trans.*, 2013, **42**, 3936-3940.
205. L. E. Kreno, J. T. Hupp and R. P. Van Duyne, *Anal. Chem.*, 2010, **82**, 8042-8046.

206. S. R. Venna and M. A. Carreon, *J. Am. Chem. Soc.*, 2009, **132**, 76-78.
207. D. Zacher, O. Shekhah, C. Woll and R. A. Fischer, *Chem. Soc. Rev.*, 2009, **38**, 1418-1429.
208. O. Shekhah, J. Liu, R. A. Fischer and C. Woll, *Chem. Soc. Rev.*, 2011, **40**, 1081-1106.
209. Y.-N. Hou, Y.-H. Xing, F.-Y. Bai, Q.-L. Guan, X. Wang, R. Zhang and Z. Shi, *Spectrochim. Acta A*, 2014, **123**, 267-272.
210. Y. Xia, K.-X. Wang and J.-S. Chen, *Inorg. Chem. Commun.*, 2010, **13**, 1542-1547.
211. X.-y. Chen, Y.-p. Chen, Z.-m. Xia, H.-b. Hu, Y.-q. Sun and W.-y. Huang, *Dalton Trans.*, 2012, **41**, 10035-10042.
212. X.-L. Hao, Y.-Y. Ma, Y.-H. Wang, W.-Z. Zhou and Y.-G. Li, *Inorg. Chem. Commun.*, 2014, **41**, 19-24.
213. Y. Xu and C. H. Langford, *Langmuir*, 2001, **17**, 897-902.
214. Z. Xiong, Y. Xu, L. Zhu and J. Zhao, *Environ. Sci. Technol.*, 2005, **39**, 651-657.
215. M. Hu, Y. Xu and J. Zhao, *Langmuir*, 2004, **20**, 6302-6307.
216. A. C. Bean, S. M. Peper and T. E. Albrecht-Schmitt, *Chem. Mater.*, 2001, **13**, 1266-1272.
217. Z.-T. Yu, G.-H. Li, Y.-S. Jiang, J.-J. Xu and J.-S. Chen, *Dalton Trans.*, 2003, 4219-4220.
218. W. Chen, H.-M. Yuan, J.-Y. Wang, Z.-Y. Liu, J.-J. Xu, M. Yang and J.-S. Chen, *J. Am. Chem. Soc.*, 2003, **125**, 9266-9267.
219. S. Horikoshi, A. Saitou, H. Hidaka and N. Serpone, *Environ. Sci. Technol.*, 2003, **37**, 5813-5822.
220. Y. Guo, C. Hu, C. Jiang, Y. Yang, S. Jiang, X. Li and E. Wang, *J. Catal.*, 2003, **217**, 141-151.
221. W. D. Jones, *Acc. Chem. Res.*, 2003, **36**, 140-146.
222. D. A. Nivens, Y. Zhang and S. M. Angel, *J. Photoch. Photobio. A*, 2002, **152**, 167-173.
223. V. A. Volkovich, T. R. Griffiths, D. J. Fray and R. C. Thied, *Phys. Chem. Chem. Phys.*, 2001, **3**, 5182-5191.
224. P. M. Almond and T. E. Albrecht-Schmitt, *Inorg. Chem.*, 2002, **41**, 1177-1183.
225. R. S. Addleman, M. Carrott, C. M. Wai, T. E. Carleson and B. Wenclawiak, *Anal. Chem.*, 2001, **73**, 1112-1119.
226. J. Huang, X. Wang and A. J. Jacobson, *J. Mater. Chem.*, 2003, **13**, 191-196.
227. M. J. Sarsfield and M. Helliwell, *J. Am. Chem. Soc.*, 2004, **126**, 1036-1037.
228. Q.-Y. Chen, Q.-H. Luo, Z.-L. Wang and J.-T. Chen, *Chem. Commun.*, 2000, 1033-1034.
229. B. Zhao, P. Cheng, Y. Dai, C. Cheng, D. Z. Liao, S. P. Yan, Z. H. Jiang and G. L. Wang, *Angew. Chem. Int. Ed.*, 2003, **42**, 934-936.
230. M. B. Fleisher, K. C. Waterman, N. J. Turro and J. K. Barton, *Inorg. Chem.*, 1986, **25**, 3549-3551.
231. S. Moghaddas, P. Hendry, R. J. Geue, C. Qin, A. M. Bygott, A. M. Sargeson and N. E. Dixon, *J. Chem. Soc., Dalton Trans.*, 2000, 2085-2089.

232. J.-L. Wang, C. Wang and W. Lin, *ACS Catal.*, 2012, **2**, 2630-2640.
233. J.-Q. Sha, J.-W. Sun, C. Wang, G.-M. Li, P.-F. Yan, M.-T. Li and M.-Y. Liu, *CrystEngComm*, 2012, **14**, 5053-5064.
234. Y. Liu, X. Lin, G. Liu, J. Ying and A. Tian, *J. Inorg. Organomet. Polym. Mater.*, 2012, **22**, 946-951.
235. C.-H. Li, K.-L. Huang, Y.-N. Chi, X. Liu, Z.-G. Han, L. Shen and C.-W. Hu, *Inorg. Chem.*, 2009, **48**, 2010-2017.
236. X. Zhao, D. Liang, S. Liu, C. Sun, R. Cao, C. Gao, Y. Ren and Z. Su, *Inorg. Chem.*, 2008, **47**, 7133-7138.
237. Y.-Q. Lan, S.-L. Li, X.-L. Wang, K.-Z. Shao, D.-Y. Du, H.-Y. Zang and Z.-M. Su, *Inorg. Chem.*, 2008, **47**, 8179-8187.
238. B. Liu, J. Yang, G. C. Yang and J. F. Ma, *Inorg. Chem.*, 2013, **52**, 84-94.
239. Y. Guo, Y. Wang, C. Hu, Y. Wang, E. Wang, Y. Zhou and S. Feng, *Chem. Mater.*, 2000, **12**, 3501-3508.
240. B. Nohra, H. El Moll, L. M. Rodriguez Albelo, P. Mialane, J. Marrot, C. Mellot-Draznieks, M. O'Keefe, R. Ngo Biboum, J. Lemaire and B. Keita, *J. Am. Chem. Soc.*, 2011, **133**, 13363-13374.
241. Y. Hu, F. Luo and F. Dong, *Chem. Commun.*, 2011, **47**, 761-763.
242. A. Mylonas and E. Papaconstantinou, *J. Photoch. Photobio. A*, 1996, **94**, 77-82.
243. L. Ni, J. Ni, Y. Lv, P. Yang and Y. Cao, *Chem. Commun.*, 2009, 2171-2173.
244. Y.-Q. Lan, S.-L. Li, X.-L. Wang, K.-Z. Shao, D.-Y. Du, H.-Y. Zang and Z.-M. Su, *Inorg. Chem.*, 2008, **47**, 8179-8187.
245. W.-Q. Kan, J. Yang, Y.-Y. Liu and J.-F. Ma, *Dalton Trans.*, 2012, **41**, 11062-11073.
246. W. Wang, J. Yang, W.-Q. Kan and J.-F. Ma, *CrystEngComm*, 2013, **15**, 5844-5852.
247. Z. Zhang, J. Yang, Y.-Y. Liu and J.-F. Ma, *CrystEngComm*, 2013, **15**, 3843-3853.
248. Y. G. Chen, K. Liu, F. X. Meng and Y. Sun, *Synth. React. Inorg. Met-Org. Chem.*, 2007, **37**, 179-184.
249. B. Liu, Z.-T. Yu, J. Yang, W. Hua, Y.-Y. Liu and J.-F. Ma, *Inorg. Chem.*, 2011, **50**, 8967-8972.
250. Z. Zhang, J. Yang, Y.-Y. Liu and J.-F. Ma, *CrystEngComm*, 2013, **15**, 3843.
251. Y.-G. Chen, K. Liu, F.-X. Meng and Y. Sun, *Synth. React. Inorg. Met-Org. Chem.*, 2007, **37**, 179-184.
252. H. Yang, T. Liu, M. Cao, H. Li, S. Gao and R. Cao, *Chem. Commun.*, 2010, **46**, 2429-2431.
253. X. Gan, X. Hu, Z. Shi and Y. Yin, *J. Coord. Chem.* 2013, **66**, 2930-2939.
254. D. Shi, A. Ren, C. Liu, H. Bai, G. Che, H. Sun and R. Cong, *Chin. J. Inorg. Chem.*, 2013, **29**, 2649-2654.
255. J.-X. Meng, Y.-G. Li, H. Fu, X.-L. Wang and E.-B. Wang, *CrystEngComm*, 2011, **13**, 649-655.
256. J.-X. Meng, Y. Lu, Y.-G. Li, H. Fu and E.-B. Wang, *CrystEngComm*, 2011, **13**, 2479-2486.
257. C. Wang, Z. Xie, K. E. deKrafft and W. Lin, *J. Am. Chem. Soc.*, 2011, **133**, 13445-13454.
258. Q. Lan, J. Zhang, Z.-M. Zhang, Y. Lu and E.-B. Wang, *Dalton Trans.*, 2013, **42**, 16602-16607.

259. H.-Y. Liu, L. Bo, J. Yang, Y.-Y. Liu, J.-F. Ma and H. Wu, *Dalton Trans.*, 2011, **40**, 9782-9788.
260. A. Tian, X. Lin, X. Liu, J. Ying and X. Wang, *RSC Adv.*, 2013, **3**, 17188-17194.
261. X. Wang, D. Zhao, A. Tian and J. Ying, *Dalton Trans.*, 2014, **43**, 5211-5220.
262. J.-L. Wang, C. Wang and W. Lin, *ACS Catal.*, 2012, **2**, 2630-2640.
263. J.-Q. Sha, J.-W. Sun, M.-T. Li, C. Wang, G.-M. Li, P.-F. Yan and L.-J. Sun, *Dalton Trans.*, 2013, **42**, 1667-1677.
264. J. Sun, M. Li, J. Sha, P. Yan, C. Wang, S. Li and Y. Pan, *CrystEngComm*, 2013, **15**, 10584-10589.
265. X. Wang, N. Li, A. Tian, J. Ying, G. Liu, H. Lin, J. Zhang and Y. Yang, *Dalton Trans.*, 2013, **42**, 14856-14865.
266. X. Wang, X. Liu, A. Tian, J. Ying, H. Lin, G. Liu and Q. Gao, *Dalton Trans.*, 2012, **41**, 9587-9589.
267. Z. Fu, Y. Zeng, X. Liu, D. Song, S. Liao and J. Dai, *Chem. Commun.*, 2012, **48**, 6154-6156.
268. H.-J. Pang, H.-Y. Ma, J. Peng, C.-J. Zhang, P.-P. Zhang and Z.-M. Su, *CrystEngComm*, 2011, **13**, 7079-7085.
269. X. Wang, Y. Wang, G. Liu, A. Tian, J. Zhang and H. Lin, *Dalton Trans.*, 2011, **40**, 9299-9305.
270. Y. Ding, J.-X. Meng, W.-L. Chen and E.-B. Wang, *CrystEngComm*, 2011, **13**, 2687-2692.
271. Q. Wu, W.-L. Chen, D. Liu, C. Liang, Y.-G. Li, S.-W. Lin and E. Wang, *Dalton Trans.*, 2011, **40**, 56-61.
272. H. Fu, Y. Li, Y. Lu, W. Chen, Q. Wu, J. Meng, X. Wang, Z. Zhang and E. Wang, *Cryst. Growth Des.*, 2011, **11**, 458-465.
273. X.-L. Wang, Q. Gao, A.-X. Tian and G.-C. Liu, *Cryst. Growth Des.*, 2012, **12**, 2346-2354.
274. X. Wang, M.-M. Zhang, X.-L. Hao, Y.-H. Wang, Y. Wei, F.-S. Liang, L.-J. Xu and Y.-G. Li, *Cryst. Growth Des.*, 2013, **13**, 3454-3462.
275. W.-Q. Kan, B. Liu, J. Yang, Y.-Y. Liu and J.-F. Ma, *Cryst. Growth Des.*, 2012, **12**, 2288-2298.
276. Y. Yu, H. Pang, H. Ma, Y. Song and K. Wang, *J. Clust. Sci.*, 2013, **24**, 17-29.
277. X.-L. Wang, D. Zhao and A.-X. Tian, *J. Clust. Sci.*, 2013, **24**, 259-271.
278. S. Lin, Q. Wu, H. Tan and E. Wang, *J. Coord. Chem.* 2011, **64**, 3661-3669.
279. W.-N. Li, F. Lin, X.-X. Li, L.-C. Zhang, W.-S. You and Z.-X. Jiang, *J. Coord. Chem.* 2013, **66**, 2829-2842.
280. W.-Q. Kan, J.-M. Xu, Y.-H. Kan, J. Guo and S.-Z. Wen, *J. Coord. Chem.* 2014, **67**, 195-214.
281. D. Shi, Z. Wang, J. Xing, Y. Li, J. Luo, L. Chen and J. Zhao, *Synth. React. Inorg. Met-Org. Chem.*, 2012, **42**, 30-36.
282. Y. Zhong, H. Fu, J. Meng and E. Wang, *J. Coord. Chem.* 2010, **63**, 26-35.
283. X. Wang, N. Han, H. Lin, J. Luan, A. Tian and D. Liu, *Inorg. Chem. Commun.*, 2014, **42**, 10-14.
284. H. Chen, H. An, X. Liu, H. Wang, Z. Chen, H. Zhang and Y. Hu, *Inorg. Chem. Commun.*, 2012, **21**, 65-68.
285. Y.-Q. Jiao, C. Qin, C.-Y. Sun, K.-Z. Shao, P.-J. Liu, P. Huang, K. Zhou and Z.-M. Su, *Inorg. Chem. Commun.*, 2012,

- 20**, 273-276.
286. H. Lin, C. Xu, X. Wang, Z. Chang, A. Tian, G. Liu and J. Zhang, *Inorg. Chem. Commun.*, 2013, **36**, 81-85.
287. N. Wu, Y. Qin, X.-L. Wang, C. Qin and E.-B. Wang, *Inorg. Chem. Commun.*, 2013, **37**, 174-177.
288. X. Meng, H.-N. Wang, G.-S. Yang, S. Wang, X.-L. Wang, K.-Z. Shao and Z.-M. Su, *Inorg. Chem. Commun.*, 2011, **14**, 1418-1421.
289. X.-L. Wang, Z.-H. Chang, H.-Y. Lin, G.-C. Liu, C. Xu, J. Luan, A.-X. Tian and J.-W. Zhang, *Inorg. Chim. Acta*, 2014, **413**, 16-22.
290. Y. Zhou, L. Zhang, X. Li and W. Ahmad, *J. Mol. Struct.*, 2013, **1049**, 212-219.
291. X.-L. Wang, N. Li, A.-X. Tian, J. Ying, D. Zhao and X.-J. Liu, *Inorg. Chem. Commun.*, 2012, **25**, 60-64.
292. X. Chen, S. Lin, L. Chen, X. Chen, C. Liu, J. Chen and L. Yang, *Inorg. Chem. Commun.*, 2007, **10**, 1285-1288.
293. X.-Y. Yu, X.-B. Cui, J. Lu, Y.-H. Luo, H. Zhang and W.-P. Gao, *J. Solid State Chem.*, 2014, **209**, 97-104.
294. X. Zhao, J. Yan, X. Xue, Z. Han, S. Cui, L. Zong, D. Zheng, C. Shen, H. Yu and X. Zhai, *Inorg. Chim. Acta*, 2014, **414**, 46-52.
295. J. Guo, J. Yang, Y.-Y. Liu and J.-F. Ma, *Inorg. Chim. Acta*, 2013, **400**, 51-58.
296. C.-H. Li, K.-L. Huang, Y.-N. Chi, X. Liu, Z.-G. Han, L. Shen and C.-W. Hu, *Inorg. Chem.*, 2009, **48**, 2010-2017.
297. Y. Guo and C. Hu, *J. Mol. Catal. A-Chem.*, 2007, **262**, 136-148.
298. Z. Zhang, J. Yang, Y.-Y. Liu and J.-F. Ma, *CrystEngComm*, 2013, **15**, 3843-3853.
299. M. A. AlDamen, J. M. Clemente-Juan, E. Coronado, C. Martí-Gastaldo and A. Gaita-Arino, *J. Am. Chem. Soc.*, 2008, **130**, 8874-8875.
300. J. Jing, B. P. Burton-Pye, L. C. Francesconi and M. R. Antonio, *Inorg. Chem.*, 2008, **47**, 6889-6899.
301. T. Devic, C. Serre, N. Audebrand, J. Marrot and G. Férey, *J. Am. Chem. Soc.*, 2005, **127**, 12788-12789.
302. S. Mahapatra, G. Madras and T. G. Row, *J. Phys. Chem. C*, 2007, **111**, 6505-6511.
303. G. Mele, E. Garcia-López, L. Palmisano, G. Dyrda and R. Slota, *J. Phys. Chem. C*, 2007, **111**, 6581-6588.
304. J. Xu, Y. Ao, D. Fu and C. Yuan, *J. Hazard. Mater.*, 2009, **164**, 762-768.
305. A. L. Linsebigler, G. Lu and J. T. Yates Jr, *Chem. Rev.*, 1995, **95**, 735-758.
306. K. Wang, D. Zhang, J. Ma, P. Ma, J. Niu and J. Wang, *CrystEngComm*, 2012, **14**, 3205-3212.
307. J. Niu, S. Zhang, H. Chen, J. Zhao, P. Ma and J. Wang, *Cryst. Growth Des.*, 2011, **11**, 3769-3777.
308. T. Zhou, Y. Du, A. Borgna, J. Hong, Y. Wang, J. Han, W. Zhang and R. Xu, *Energ. Environ. Sci.*, 2013, **6**, 3229-3234.
309. Y. Horiuchi, T. Toyao, M. Saito, K. Mochizuki, M. Iwata, H. Higashimura, M. Anpo and M. Matsuoka, *J. Phys.*

- Chem. C*, 2012, **116**, 20848-20853.
310. K. G. Laurier, F. Vermoortele, R. Ameloot, D. E. De Vos, J. Hofkens and M. B. Roeffaers, *J. Am. Chem. Soc.*, 2013, **135**, 14488-14491.
311. T. T. Isimjan, H. Kazemian, S. Rohani and A. K. Ray, *J. Mater. Chem.*, 2010, **20**, 10241-10245.
312. C. Wang, D. Liu and W. Lin, *J. Am. Chem. Soc.*, 2013, **135**, 13222-13234.
313. F. X. Llabres i Xamena, A. Abad, A. Corma and H. Garcia, *J. Catal.*, 2007, **250**, 294-298.
314. H. A. Lopez, A. Dhakshinamoorthy, B. Ferrer, P. Atienzar, M. Alvaro and H. Garcia, *J. Phys. Chem. C*, 2011, **115**, 22200-22206.
315. A. Pichon, *Nature China*, 2009, DOI: 10.1038/nchina.2009.1124.
316. C. G. Carson, K. Hardcastle, J. Schwartz, X. Liu, C. Hoffmann, R. A. Gerhardt and R. Tannenbaum, *Eur. J. Inorg. Chem.*, 2009, **2009**, 2338-2343.
317. J. J. Low, A. I. Benin, P. Jakubczak, J. F. Abrahamian, S. A. Faheem and R. R. Willis, *J. Am. Chem. Soc.*, 2009, **131**, 15834-15842.

## Broader Context

On account of the ecological and environmental importance, removing organic pollutants with high toxicity and hard degradation properties from the wastewater has been attracting a great deal of attention and becoming a hot research topic nowadays. Traditional methods such as adsorption and coagulation usually suffer from high operating costs and worse still, generating other secondary pollutants in these processes. Alternately, photocatalytic degradation has demonstrated its green implementation and high efficiency, in which the photocatalyst plays a crucial role. Metal-organic frameworks (MOFs), a class of newly-developed functional materials, have given rise to a rapid development in the catalysis field. A number of studies have shown that they are suitable materials for being the photocatalysts that function in the catalytic degradation of organic pollutants. In this review, we summarize research advances with regard to this topic, emphasizing on the related catalytic reaction mechanisms, factors that affect the catalytic performances, and challenges involved in these studies. It is clear that MOFs have a promising future in this regard, and might become one class of the most powerful photocatalysts that could help to generate a green environment, thereby leading to a significant impact on environmental science.